# HYPERSONIC CONTROL EFFECTIVENESS STUDIES ON DELTA WINGS WITH TRAILING-EDGE FLAPS

Dhanvada Madhava Rao

B.Sc., D.I.C., A.F.R.Ae.S.

May 1970

A thesis submitted for the Degree of Doctor of Philosophy in the Faculty of Engineering of the University of London.

# HYPERSONIC CONTROL EFFECTIVENESS STUDIES ON DELTA WINGS WITH TRAILING-EDGE FLAPS


## ABSTRACT

An experimental study of the flow and force characteristics of two delta wings (of 70° and 76° sweepback) with and without full-span trailing-edge flaps was carried out in a Gun Tunnel at Mach 8.2. Force balance, pressure measurements and flow visualisation studies were made at various incidences, flap deflections and Reynold's numbers.

The flow visualisation studies and pressure measurements on the wing and flap surfaces provided a detailed and consistant physical picture of the varying three-dimensional flap-induced separation patterns in the laminar and transitional regimes.

The more extensive separation on the 70° delta, due to the delayed onset of translation produced significant reduction in flap effectiveness in comparison with the 76° delta wing.

Good agreement between simple inviscid calculations of the aerodynamic coefficients and measurements was obtained for the 76° delta with flap deflections of less than 20°. Impingement of the reflected expansion wave from intersection of wing and flap shocks dominated the flap load at higher flap deflections. A simple model was proposed for the three-dimensional shock interaction and used to obtain good prediction of the reflected expansion boundary on the flap surface. When the interaction effect was included in the calculations, satisfactory estimates of the aerodynamic coefficients were obtained for the 76° delta wing up to the highest flap deflection before flap shock detachment.

The balance measurements on the 76° flapped delta wing were in excellent agreement with the results of free-flight tests conducted at the National Physical Laboratory.

ACKNOWLEDGEMENTS

This investigation was supported by a Ministry of Technology contract and monitored by the National Physical Laboratory, represented by Dr. E.W.E. Rogers.

The author is pleased to record his gratitude to -

Mr. J.L. Stollery, the supervisor of this research, for his constant encouragement, advice and critical appraisal throughout the programme of this work,

Mr. J. Cunningham and others in the Workshop for painstaking attention in the manufacture of the models and for ready assistance in numerous ways during the experimental work, and

Mr. J. O'Leary for his advice and help in photography.

Dr. L. Davies and his colleagues of the National Physical Laboratory were extremely co-operative in supplying the details and results of the free-flight tunnel tests.

CONTENTS


| | | Page |
|---|---|---|
| | Abstract | 2 |
| | Acknowledgements | 3 |
| | Contents | 4 |
| | Notation | 6 |
| 1. | Introduction | 8 |
| Part I - General Discussion of Flow over Flapped Wings | | |
| 2. | Two-Dimensional Flow Characteristics | 11 |
| | 2.1 Inviscid Flow | 11 |
| | 2.2 Viscous Flow | 13 |
| | 2.3 Three-dimensional Effects | 17 |
| 3. | Delta Wing Flow | 18 |
| | 3.1 Invdiscid Flow | 19 |
| | 3.2 Viscous Flow | 23 |
| 4. | Review of Some Results on Hypersonic Flap Effectiveness on Delta Wings | 26 |
| Part II - Present Studies and Discussion of Results | | |
| 5. | Experimental Details | 31 |
| | 5.1 Test Programme | 31 |
| | 5.2 Hypersonic Gun Tunnel | 32 |
| | 5.3 Models | 32 |
| | 5.4 Instrumentation | 34 |
| | 5.5 Surface Flow Visualisation Techniques | 36 |
| | 5.6 Flow Conditions | 38 |
| 6. | Two-Dimensional Model | 39 |
| 7. | Delta Wings without Flaps | 40 |
| | 7.1 Balance Data | 40 |
| | 7.2 Shock Angle | 42 |

| | | Page |
|---|---|---|
| | 7.3 Pressures | 42 |
| | 7.4 Transition | 43 |
| 8. | Delta Wings with Flaps | 44 |
| | 8.1 Separation Characteristics | 44 |
| | 8.1.1 Zero or small incidence | 45 |
| | 8.1.2 Increasing incidence | 46 |
| | 8.1.3 Three-dimensional separation patterns | 56 |
| | 8.2 Wave Phenomena | 59 |
| | 8.3 Balance Measurements | 61 |
| 9. | Flow Regimes on 76° Flapped Delta | 67 |
| 10. | Summary of Results | 69 |
| | References | 72 |
| | Appendix | 78 |
| | List of Figures | 81 |

## NOTATION

| | |
|---|---|
| $A$ | Basic wing planform area |
| $C_N$ | Normal force coefficient. (Normal force/$0.5\ \gamma M_\infty^2 \cdot P_\infty \cdot A$) |
| $C_A$ | Axial force coefficient. (Axial force/$0.5\gamma M_\infty^2 \cdot P_\infty \cdot A$) |
| $C_M$ | Pitching-moment coefficient. (Moment/$0.5\gamma M_\infty^2 \cdot P_\infty \cdot A \cdot L'$) |
| $C_{NF}$ | Flap normal force coefficient. (Based on flap area). |
| $C_H$ | Hinge-moment coefficient. (based on flap area and flap chord). |
| $C_P$ | Pressure coefficient $\dfrac{P-P_\infty}{0.5\gamma M_\infty^2 P_\infty}$ |
| $\Delta C_N$ | Incremental normal force due to flap deflection |
| $\Delta C_M$ | Incremental pitching-moment due to flap deflection |
| $L$ | Length from apex to hinge-line |
| $L'$ | Centre-chord length of delta wing |
| $L_F$ | Flap chord |
| $M_\infty$ | Free-stream Mach number |
| $M_w$ | Local Mach number on windward wing surface |
| $P_\infty$ | Free-stream static pressure |
| $P_w$ | Local pressure on windward wing surface |
| $P_{H.L.}$ | Hinge-line pressure on flapped wing |
| $R_\infty$ | Free-stream unit Reynold's no. |
| $R_w$ | Local unit Reynold's no. on windward surface of wing |
| $R_L$ | Local Reynold's no. based on length to hinge-line ($=R_w \times L$) |
| $R_L'$ | Model Reynold's no. based on centre-chord length ($=R_\infty \times L'$) |
| $X$ | Coordinate along balance axis or wing centre, origin at apex (except otherwise defined on figures) |
| $X_S$ | Distance to separation |
| $X_R$ | Distance to re-attachment |
| $X_{C.P.}$ | Distance to centre-of-pressure |
| $Z$ | Spanwise coordinate |

$Z_{H.L.}$ Hinge-line semi-span

$\alpha_o$ Wing incidence angle, measured from balance axis of force models

$\alpha_w$ Windward surface incidence angle

$\alpha_F$ Flap surface incidence angle, measured from free-stream direction

$\delta_F$ Flap deflection angle, measured from windward wing surface

$\delta_{Fi}$ Flap deflection angle for incipient separation

$\theta_1$ Wing shock angle, measured from free-stream direction

$\theta_2$ Flap shock angle, measured from wing surface

$\theta_F$ Flap shock angle, measured from free-stream direction

$\xi_w$ Wing shock stand-off angle, measured from windward surface

$\Lambda$ Leading-edge sweep-back angle

$\varepsilon$ Semi-apex angle $=(\frac{\pi}{2} - \Lambda)$

$\phi$ Ray angle on delta wing surface, measured from centre-line

$\bar{\chi}$ Viscous interaction parameter

## 1. INTRODUCTION

Over the past decade, steady progress has been achieved in the solution of aerodynamic probelms related to the design of hypersonic transport aircraft. Recent developments in space programmes have focussed attention on re-usable boosters and shuttle vehicles for operating between earth orbits and land bases (ref.1) which offer promise for the practical application of hypersonic research. For these roles, an aerodynamically efficient and manouverable vehicle in the hypersonic flight regime will be needed.

The research effort so far has resulted in the optimisation of hypersonic cruise vehicle configurations, which generally appear to favour highly swept wings with sharp leading edges (ref. 2). Some thought has also been given to the feasibility of aerodynamic controls on hypersonic aircraft (ref. 3)*. Preliminary studies have indicated that the trailing-edge flap type of control merits consideration in view of the relative simplicity and because it offers the practical advantage of remaining useful over a wide range of Mach number. Under hypersonic conditions, however, particular aerodynamic problems arise with trailing-edge controls that need consideration.

The prediction of trailing-edge flap effectiveness requires a knowledge of the flow field around the vehicle as well as the characteristics of the boundary layer approaching the control surface. A study of trailing-edge control aerodynamics inevitably leads to the phenomenon of flow separation, which is not only responsible for a deterioration in control effectiveness but also raises secondary problems such as flow unsteadiness, accentuated local heating at re-attachment and the generation of secondary shocks which may adversely interact with other components of the vehicle. Although the control problem has motivated a considerable amount of research on flap-induced separation (e.g. refs. 4-10), the bulk of this work has been restricted to two-dimensional flow. Little attempt

---

* See also a recent review by Rogers, ref. 63.

has so far been made to investigate the validity of this research in the practical three-dimensional design context. Equally, there is a lack of information on three-dimensional separation characteristics at hypersonic speeds.

The experience of separation effects at lower Mach numbers perhaps colours the thinking of the aerodynamicist approaching the problem of hypersonic control effectiveness. The resulting emphasis on the separation phenomena therefore tends to overlook the inviscid effects such as wave interactions,* which are absent at the lower Mach numbers but can produce significant effects on control forces at hypersonic speeds. Here, the results of two-dimensional research while providing some guidance may be of little direct application since the vehicle flow field is not represented.

It is therefore clear that an understanding of the physical nature of three-dimensional separations and their effects on the aerodynamic forces on idealised vehicle shapes incorporating controls will have to come from experimental research. Such experiments will provide the material necessary for an assessment of the validity of two-dimensional ideas and results, and also permit the usefulness of simple prediction methods to be established.

The present study is concerned with the hypersonic aerodynamic characteristics of full-span, positiviely deflected trailing edge flaps on delta wings having sharp leading edges, 'roof-top' upper surfaces and flat bottom. Apart from being a reasonable idealisation of a practical hypersonic vehicle, the chosen geometry is such that quasi-two-dimensional conditions with unseparated (or moderately separated) flow may be reasonably expected on the wind-ward surface and therefore two-dimensional

---

* Viz. between shocks and expansions, as distinct from shock-boundary layer interactions.

concepts may to a first approximation be applicable for the calculation of control effectiveness. However, with increasing severity of separation, significant three-dimensional effects appear and allow the limits of applicability of the simple calculation procedure to be assessed. An equally important part of this investigation was to acquire some understanding of the physical nature of three-dimensional separations likely to be encountered with control surfaces under conditions representative of hypersonic flight.

## Part I - GENERAL DISCUSSION OF THE FLOW OVER FLAPPED WINGS.

### 2. TWO-DIMENSIONAL FLOW CHARACTERISTICS

The purpose of this section is to recall some of the basic aerodynamic features relevant to the present problem. The inviscid and viscous flow phenomena which are believed to significantly influence flap loading are reviewed, and an evaluation of simple prediction methods is attempted. The two-dimensional case is considered first as it provides a logical introduction to the more complex three-dimensional conditions on a delta wing, and also because a strip-type[*] application of two-dimensional results is often made to deal with three-dimensional problems.

#### 2.1 Inviscid Flow

Consider a flat wing at incidence $\alpha_w$ with a trailing-edge flap deflected positively at angle $\delta_F$ relative to the wing. In hypersonic inviscid flow with attached shocks, uniform pressures exist over the windward surfaces, the magnitude of which is given by the oblique-shock theory using appropriate initial flow parameters for the wing and flap shocks (Fig. 1,A).

At higher incidence and/or flap deflection, the wave reflecting from the intersection of the wing and flap shocks impinges on the flap (fig. 1,B). The sign and the strength of the reflected wave is a function of the relative strengths of the interacting shocks. The solution of the reflected wave using exact shock and Prandtl-Meyer relations is straightforward; some results of computation for typical cases are presented in ref. 11.

Such solutions indicate that in the range of parameters ($M_\infty$, $\alpha_w$, $\delta_F$) of present interest, the reflected wave is an expansion. Consequently,

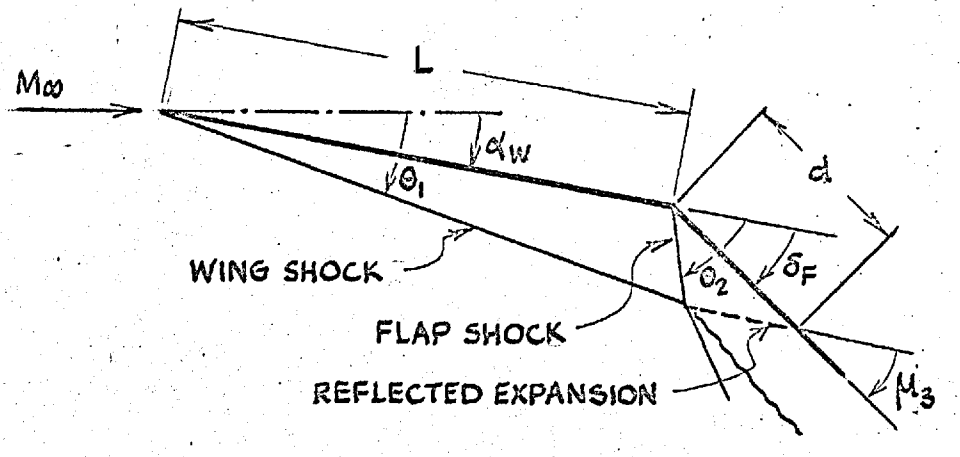
---

[*] The reference is to the streamwise strip theory, in which any longitudinal element of the surface is assumed to behave as though it were part of an unswept two-dimensional plane and independent of the adjoining strips.

a rapid fall of pressure occurs on the flap across the impingement position. Through repeated wave reflections between the flap surface and the slip line originating at the shock intersection, the pressure will eventually attain a constant final value corresponding to the oblique shock compression of the free-stream across a deflection angle $(\alpha_w+\delta_F)$, provided the flap length were sufficient. For practical purposes, however, it is reasonable to assume the total pressure decay to occur at the position of first impingement.

The distance d of the reflected expansion impingement on the flap from the hinge-line obtained from shock-expansion theory is as follows (ref. 11):

$$\frac{d}{L} = \frac{\operatorname{Cot}(\theta_2 - \delta_F) + \operatorname{Cot}\mu_3}{\operatorname{Cot}(\theta_1 - \alpha_w) - \operatorname{Cot}\theta_2} \cdot \frac{\operatorname{Sin}(\theta_2 - \delta_F)}{\operatorname{Sin}\theta_2} \qquad (1)$$




The above solution is no longer valid when the reflected expansion is replaced by a compression, as happens at higher incidence and flap deflection for a given $M_\infty$ . This case occurs outside the range of the present investigation. The reflected shock condition is nevertheless of importance to the control effectiveness problem as shown by previous investigators (see sec. 4).

Under the influence of the reflected expansion therefore, the flap load will reduce below the value predicted by the simple shock theory. Due to the simultaneous upstream movement of the centre of pressure, flap induced moment will also decrease. Such an effect was first noted in investigations on flare-stablisided missiles, where analogous reduction of pressure on the flare across the reflected expansion impingement led to loss of stability (ref. 12). Under two-dimensional or axi-symmetric conditions, this effect is simple to calculate using eq. 1 with appropriate values for the shock angles.

## 2.2 Viscous Flow

### Unseparated flow

When the flap deflection is small, the strength of the flap shock may be insufficient to cause separation of the boundary layer. The maximum flap angle with attached flow, or the incipient separation flap angle ($\delta_{Fi}$), depends on the nature of the flow within the boundary layer at the hinge line. Obviously, it is of practical advantage to operate without flow separation if possible, and thus it is necessary to be able to predict the incipient separation boudary.

Results to date show that incipient separation condition for laminar and turbulent boudary layers can be correlated over a faily wide range of supersonic to hypersonic Mach numbers (ref. 10). The incipient separation flap angle in each case is found to increase with Mach no. (as $\sqrt{M}$). For laminar flow, $\delta_{Fi}$ decreases with increasing Reynold's no. but is relatively little influenced in the turbulent case. Turbulent incipient separation occurs at flap angles 3 to 4 times greater than with laminar boundary layer. Under transitional conditions, $\delta_{Fi}$ varies rapidly between the laminar and turbulent values with changing Reynold's no.

### Flow with separation

A detailed discussion of the two-dimensional flap-induced separated

flow is outside the scope of this thesis. A recent survey of literature will be found in ref. 10. Here, only the major results relevant to simplified engineering estimation of flap heads in the presence of separation will be indicated.

When flap-induced separation is fully established, a simple model of the supersonic separated flow is usually adopted for estimating the main effects on pressure distribution and loads. In this model, the viscous layers are assumed to be infinitesmally thin and the upstream and downstream influence of separation and re-attachment neglected. The effect of separation is simply to create new flow boundary viz. a straight constant-pressure line joining the separation and re-attachment points. Thus the external (inviscid) supersonic flow turns through two shocks (in place of the single flap shock in attached flow) to deflect through the flap angle (Fig. 2,A).

To apply the above model to a particular case, it is necessary to know the flow deflection angle at the separation shock (or alternatively, the bubble pressure) and the scale of separation. The bubble pressure (relative to the upstream pressure) is a function only of the local boundary layer parameters and independent of the agency causing separation for laminar flows (ref. 14). This concept of "free interaction" has enabled correlation of a large number of experimental data on supersonic separated flows, produced on different model configurations over a range of free stream values of M and R. The following equation (with the constant derived from the data of ref. 14) has been found to provide a reasonable good fit of the correlated "plateau" pressure data for laminar separation at Mach numbers up to 15:

$$C_{p_{(PLATEAU)}} \cdot (M^2-1)^{1/4} = 1.74\,(Rx_s)^{-1/4} \qquad (2)$$

The above relation has been found to apply as well to three-dimensional

laminar separations, such as those induced by part-span flaps (ref. 16).

In turbulent separation the pressure in the bubble is not uniform but has a maximum. The peak pressure has been found to correlate to the following empirical equation (ref. 15) in the Mach number range 3.4 to 6.5:

$$C_{p_{(PEAK)}} = 0.13 - \frac{1.5}{M^2} + \frac{9.1}{M^3} \qquad (3)$$

The status of separation length prediction is however far less satisfactory. As one example, Hill (ref. 9) examined the correlations proposed by Erdos and Pallone (ref. 60) and more recently by Needham (ref. 10), against his own measurements and found poor agreement. The difficulty stems partly from the errors in locating the separation and re-attachment points in experiments (very few of which have measured detailed pressure distributions), and is partly due to the uncertainty in some investigations regarding two-dimensionality of the flow. Also, many data believed to have been obtained under fully laminar conditions are probably influenced by transition, which is difficult to detect in the early stages but markedly affects the length of separation (e.g. refs. 7, 9, 10). For a proper assessment of the proposed correlations for separation length, many more data from carefully controlled experiments will be needed.

The basic difficulty of estimating length of separation therefore limits the application of the practical calculation procedures based on elaborations of the simple separation model (in which upstream effect and finite pressure gradients at separation and re-attachment are allowed), such as those set out in refs. 9 and 13. However, when the separation position is known experimentally (e.g. from optical measurements), this simple model can provide a first-order estimate of the effect of separation on the flap load.

The extensive research on two-dimensional flap-induced separation

has been mainly aimed towards the determination of onset and development of separated flow on the wing surface and the flow conditions at separation. Relatively little appears to be known regarding the re-attachment phenomenon and the flow downstream on the flap. From the point of view of control effectiveness, however, the details of the flow and pressure distribution following re-attachment are of primary importance.

The main effect of separation on the flap is to greatly reduce the pressure between the hinge-line and re-attachment. After re-attachment, however, the pressure rises to a higher level than the inviscid value because of a more efficient two-shock compression. For a typical case ($M_\infty = 8$, $\alpha_w = 0$, $\delta_F = 30^\circ$) an increase of about 50 percent over the inviscid level is predicted. In practice, even higher peak values are attained (reaching nearly 60 percent in excess of inviscid pressure in one instance reported by Johnson, ref. 7), due to the quasi-isentropic compression achieved through a series of shocks in the separation and re-attachment zones. A rapid fall-off in pressure follows, evidently as a result of the reflected expansions from the intersection of the separation and re-attachment shocks. Further pressure variations will occur when the effect of interaction between the leading-edge shock and the separation/re-attachment shocks reaches the flap. Complicated and varying pressure distributions must therefore be expected over the flap with changing flow conditions, and it is instructive to see how the flap loads develop in real situations compared with the simple calculations dicussed above.

The flap pressure distributions as measured by Johnson (ref. 7) are illustrative of these effects, and some of his results have been reproduced in fig. 3.A. These distributions show the effect of varying degree of separation at $\delta_F = 30^\circ$ (obtained by changing unit Reynold's number in transitional flow), and also the influence of reflected expansion arising from the inter-section of the separation and re-attachment shocks. Analysis (fig. 3,B) of these measurements shows that while in all cases the integrated normal

load on the flap falls below the inviscid prediction, considerable and unexpected variations occur with changing extent of separation. The effect on integrated hinge moment is particularly marked, in some instances its value actually exceeding that calculated for unseparated flow.

The simple separation model (using experimental re-attachment position) predicts the correct trend of the integrated flap load and moment, although still over-estimating by 15 to 20 percent for this set of data. It should be noted that the incremental normal force produced by the separated flow over the wing was comparatively negligible at this flap deflection.

The above example emphasizes the difficulty of predicting flap effectiveness under conditions of significant separation even in two-dimensional flow. In addition, details of the flow field over the flap must also be considered to identify local peak pressure (and thermal loading problems in practical design.

2.3 Three-Dimensional Effects

In the experimental research on hypersonic two-dimensional separations necessitating the use of finite span models, three-dimensional effects have been observed. These commonly appear in the form of a spanwise venting of the low energy fluid from the higher pressure region in the bubble into the free-stream (fig. 4,A). Similar spanwise outflow in the bubble is observed with part-span flaps (ref. 16).* The most important consequence is a reduction of the centre-line separation length relative to the two-dimensional case.* The centre-line bubble pressure, however, still fairly well follows the two-dimensional free interaction law, a result on which several flat-plate investigations involving three-dimensional separations agree (e.g. ref. 16).

---

* Analogous to the effect of hinge-line suction, ref. 57.

A form of three-dimensionality in a nominally two-dimensional laminar separation is illustrated in fig. 4,B. (based on oil flow visualisation photograph shown on page 115, ref. 13). This is believed to have resulted from a locally trasitional (or turbulent) flow due to an isolated disturbance at or near the leading edge acting as a boundary layer trip, which greatly reduced separation in the middle of the wing. This is an example of the "mixed" laminar-turbulent separation with the resulting complexity of the flow pattern, which is relevant to flap-induced separation on delta wings as will be discussed later.

## 3. DELTA WING FLOW

At hypersonic speeds, the flow over windward surfaces of wings and bodies plays the major role in determining the over-all aerodynamic force characteristics, the contribution from any lee-ward areas being usually small. Also, it is in the wind-ward regions that the most significant heat-transfer problems arise. For these reasons, in most of the high Mach no. delta wing research to date particular attention has been devoted to the calculation and measurement of pressures heat-transfer rates and flow patterns on the wind-ward surface. Although many of the published measurements have been obtained with blunt leading-edge models a number of experimental comparisons have shown the wind-ward flow field on blunt deltas at moderate to large incidence angles to be quite similar to that on sharp edged delta wings with detached leading-edge shock.

The particular relevance of the windward flow to the present study is, of course, that the deflected flap operates in this field. Specifically, knowledge of the wing pressures is needed for the application of the simple methods discussed earlier for calculating the flap load. Also of interest is the shape of the wing shock envelope whose interaction with the flap shock may have to be considered, just as in the two-dimensional case. Further, the boundary layer characteristics must be known in order to

understand the three-dimensional flap induced separation. A brief survey of delta wing literature with regard to these questions is given in the following.

3.1 Inviscid Flow

The wind-ward flow field on a delta will be expected to depend on incidence ($\alpha_w$) and to deviate from two-dimensional conditions progressively with reducing apex angle ($2\varepsilon$). Consequently, it is useful at first to acquire a qualitative picture of the changing flow pattern as a function of these two variables. Chernyi (ref. 17) has considered the general problem of the three-dimensional flow in the shock layer on a planar wing. His solution for conical flows, analysed for the case of delta wings, indicate the different flow regimes in the ($\alpha_w$, $\varepsilon$) plane.

These flow regimes (for $\gamma = 1.4$, $M_\infty = \infty$) are sketched in fig. 5. In region I the shock is attached, and there is a region of uniform flow near the leading edge merging into the central region (or region of apex influence) where the stremlines tend asymptotically to the centre-line. Crossing over to region II causes shock detachment from the leading-edges (though not from the apex). A dividing line appears along a ray, outboard of which the stream-lines flow towards the leading-edge while the inboard flow tends to the centre-line.

In regions I and II the leading edges of the delta can be regarded as aerodynamically independent and, except in the vicinity of the apex, as part of infinite swept wings. Consequently, the leading-edge flow can be formulated in the plane normal to the leading-edge and the wing surface. The transition from I to II is then analogous to the development of transonic flow following shock detachment on a two-dimensional sharp leading edge aerofoil and the appearance of a stagnation (or dividing) point on the lower surface.

As the boundary II-III is approached the dividing line moves to

inboard rays and becomes coincident with the centre-line at the limit of region II. This marks the end of the independent leading-edge flow, and in region III the cross-flow plane formulation must consider the entire wing cross-section. This flow is analogous to that past a two-dimensional plate normal to supersonic free-stream, the wind-ward surface flow on the delta leaving at the leading-edge which aerodynamically is now a trailing-edge.

Chernyi's solution predicts further changes in the nature of the wind-ward surface flow as the incidence approaches $90^{\circ}$, but these lie well outside the range of present interest. These flow regimes have been observed experimentally (refs. 18, 19). Although Chernyi's solution in principle allows the determination of all flow properties on the delta wing in the various regimes, no calculated examples are available for comparison with other theories or with experiment.

Babaev has given an exact numerical solution for flat delta wings with attached shock, based on a method of successive corrections to the shape of an assumed shock surface (ref. 20). He has presented some results which illustrate the main conclusions of his theory. At a given Mach number, increasing sweepback angle causes the pressure in the uniform region near the leading-edge to increase, while the pressure in the apex zone inboard decreases. The relative area of the apex zone increases with increasing sweepback and with incidence. As a result of these pressure variations, the normal force produced by the windward surface varies only slightly with leading-edge sweep angle. A result of particular significance from Babaev's exact theory is that the normal force is closely predicted by the two-dimensional shock theory (assuming the wind-ward surface to be part of a two-dimensional wing), which allows a great simplification in calculating over-all force characteristics of delta wings with attached shock.

Babaev's calculated shock shapes assume an intermediate position between tangent-wedge and tangent-cone solutions in the plane of symmetry, lying closer to the cone value with increasing sweep. All these predictions are generally well supported by experimental results (e.g. ref. 21).

For the case of detached shock, solutions have been offered by Messiter (ref. 22) and Hida (ref. 23) based on a first order correction to Newtonian theory, and by Kennet (ref. 29). These numerical solutions however require excessive computational effort and therefore are not convenient for practical application where less than exact but rapid calculations are desired. Squire, who extended Messiter's theory (ref. 24) has found that for wings with rhombic cross-sections (diamond or caret, with the flat-bottomed roof-top delta as an intermediate case), the solution depended only on two parameters (viz. reduced windward surface anhedral and reduced semi-span), and has presented working charts for calculating surface pressure distribution and shock shape for a range of these parameters (ref. 25). The agreement with experimental pressure distributions on flat delta wings is particularly good (ref. 25).

We may now consider some simple methods suggested in literature for the direct calculation of the normal force (or the average pressure) coefficient on the wind-ward surface of delta wings at hypersonic speeds.

When the leading-edge shocks are attached, the two-dimensional shock (or tangent-wedge) theory is valid (as suggested by Babaev's exact calculation). Balance measurements reported by Opatowski (ref. 21, 58), Bertram and McCauley (ref. 26) and others support the use of the two-dimensional theory in this case.

After shock detachment, the normal force progressively falls short of the two-dimensional shock prediction with increasing incidence (e.g. ref. 26). Such a trend is also predicted by integrated surface pressures obtained from delta wing theories for detached shocks (e.g. Squire).

Based on correlation of measured $C_N$ data for a range of sweep angle and Mach number, a semi-empirical method due to Post (ref. 27) and its modifications by Close (ref. 28) and Fetterman (ref. 38) successfully predict the normal force characteristics of delta wings.

Nagel et al (ref. 30) have suggested another practical approach, based on modification of the exact two-dimensional shock equation

$$C_P = \frac{2 \sin\alpha_w \sin(\alpha_w + \xi_w)}{\cos \xi_w} \qquad (4)$$

The shock "stand-off angle $\xi_w$ (i.e. the difference between the shock angle and the wind-ward surface incidence) is obtained from the solutions of the delta wing flow field with detached shock (e.g. refs. 24 and 29). The use of the delta wing shock angle (rather than the two-dimensional value) in eq. 4 then gives the wind-ward pressure coefficient on the delta wing.

For convenience of calculation, Nagel et al have proposed the following empirical fit to numerical solutions for by the method of Kennet:

$$\xi_w(\text{deg}) = 70 \, (\rho_\infty / \rho_2 \, (\tan\alpha_w / \tan \Lambda)^{0.566} \qquad (5)$$

(the density ratio $\rho_\infty / \rho_2$ across the shock is determined by iteration).

The results for the case of $\Lambda = 76^\circ$, $M_\infty = 8.2$ calculated from the above theories are compared in fig. 6. The tangent-cone and simple Newtonian theories are also shown. It is evident from this comparison that for normal force calculation with detached leading-edge shocks, there is little to choose between the methods reveiwed above. Note that while the simple Newtonian underestimates the normal force in the incidence range considered, the tangent-cone theory yeilds practically the same ($C_N$, $\alpha_w$) curve as the more rational theories.

Finally, a comparison of the shock shape in the plane of symmetry (characterised by the stand-off angle $\xi_w$) calculated by Squire's theory

and by eq. 5 has shown that they both predict rather similar results in the present incidence range. The above theories were also found to compare well with measurements obtained in this investigations (see 7.2).

3.2 Viscous Effects

Unlike the two-dimensional case, where the leading-edge viscous interaction generally does not influence the trailing-edge flap induced separation, on a delta wing such a coupling cannot be ignored particularly in the outboard regions. As will emerge from the following discussion, viscous interaction effect is responsible for important changes in the boundary layer flow even in the inboard areas, which influence the separation characteristics on a delta.

At small incidences significant boundary layer induced pressures are produced near the leading edges. The result is an inward flow of the boundary layer in the direction of the centre-plane, while the streamlines at the edge of the boundary layer are deflected outwards through the leading edge shock (fig. 7,A). This has two consequences. Firstly, as the low energy fluid is swept inwards from both leading edges a greatly thickened boundary layer is formed along the centre-line, leading to reduced skin-friction and heat transfer rates in this region (as shown by the heat-transfer measurements of Dunavant, ref. 18, an example being illustrated in fig. 7,B). Secondly, this cross flow generates longitudinal vorticity in the boundary layer which contributes to instability and a reduction in the transition Reynold's number. (A visualisation of the longitudinal vortex filaments on a delta wing can be seen in fig. 9 of ref. 31).

Even with fully laminar flow over highly swept delta wings, therefore, a considerable change in the boundary layer thickness between the leading edges and the centre chord will exist, over and above that predicted by the two-dimensional strip theory. With the onset of transition (which will occur along fronts parallel to the leading edges, e.g. refs. 40, 51), even greater spanwise variation in the boundary layer

conditions will be encountered. With transition present on the wing, a general spanwise section of the boundary layer will contain laminar flow outboard and transitional or turbulent flow inboard. Flap-induced separation of such a mixed boundary layer will evidently lead to considerable three-dimensionality of the flow (see fig. 37).

An estimate of the viscous interaction-induced pressure on the delta wings may be obtained using the well-known theories for two-dimensional flow (e.g. ref. 32). Comparison with measurements (ref. 33) in the strong-interaction regime has proven inconclusive, while in the weak interaction case agreement with theory was found to be no worse than that with two-dimensional data. In a recent analysis, Davies (ref. 34) found that a strip-wise application of flat plate viscous interaction theories to a $76^{\circ}$ swept delta wing gave a fairly good prediction of the normal force and centre of pressure under conditions of weak interaction. The validity of the strip theory is however considered doubtful in the neighbourhood of the apex, where the mutual interaction of the leading-edges cannot be neglected.

Boundary layer transition is affected by a large number of factors, not all of which are yet properly understood or even indentified. The prediction of transition is hampered by the lack of a theory on the one hand, and the absence of correlated experimental data on the other. At hypersonic speeds, the well-known stretching of the transition process makes it particularly difficult to define a location of transition consistently with respect to the different experimental techniques employed in its detection, such as surface heat transfer, pitot-pressure traverse, acoustic and optical methods. Factors ranging between 1.5 and 2.0 for the Renold's no. at the beginning and at the end of transition are generally quoted, which is also about the order of scatter found in the hypersonic transition data from different sources.

An aspect of transition which is the subject of yet unresolved controversy is the experimentally observed dependency on unit Reynold's no., a dimensional quantity. While a remarkable correlation of numerous tunnel data accomplished by Pate and Schueler (ref. 44) indicates that much of the "unit-R effect" originated from the acoustic radiation from nozzle wall boundary layer, this still leaves unexplained the free-flight range data which are free of the radiated noise influence and yet show a unit Reynold's no. dependency.

On the effect of leading-edge sweep, there is general agreement in the experimental data showing earlier transition with increasing sweep angle.

This effect was analysed by Moeckel (ref. 45), for the case of blunt leading-edges. The delay in transition due to reduced local unit Reynold's number in the entropy layer generated by the detached shock was counteracted by sweeping the leading-edge, and so diminishing the shock strength. This "shock-loss" theory is evidently valid only for supersonic leading-edges, and as Chapman (ref. 47) pointed out, does not fully account for all the reduction in $R_T$ caused by sweep. Chapman showed that the Owen and Randall corssflow instability criterion (ref. 46) remained valid on cylindrical leading-edges from subsonic to $M\infty = 7$ flow and suggested this approach as more appropriate to the leading-edge sweep effect on transition. A simple emirical multiplication factor of $\sqrt{\text{Cos } \Lambda}$ was suggested by Deem and Murphy (ref. 49) to estimate the effect of sweep from the $R_T$ data for unswept flat plates. However, high Mach no. experimental data on delta wing transition are scarce and the available information does not inspire confidence in its use as a reliable guide for prediction. A common example of the problem faced by the experimentalist is to predict the occurrence of transition on a swept-wing model in a particular facility, and the above mentioned theoretical procedures offer some possibility using two-dimensional $R_T$ measured in the same facility for making such a prediction. However, considerably more experimental data are needed to assess the existing theories.

## 4. REVIEW OF SOME RESULTS ON HYPERSONIC DELTA WING FLAP EFFECTIVENESS

Although a moderate amount of published literature is available regarding flap effectiveness on delta-winged vehicles at hypersonic speeds, it is almost exclusively related to re-entry vehicles (typified by the erstwhile 'Dyna-Soar' project). Thus, the studies have been mainly on thick, slab-shaped delta wings with blunt leading edges, operating at angles of incidence up to $90^{\circ}$. Nevertheless, some of the aerodynamic data available is within the scope of our interest, at least in a qualitative sense. The results given in ref. 35 are typical and contain balance data as well as flap pressure measurements on a $60^{\circ}$ delta vehicle at Mach 8. The normal force, axial force and pitching-moment coefficients were found to increase smoothly with incidence angle and flap deflection upto the onset of flap-shock detachment, which caused sudden loss in flap effectiveness (although the authors believed it to be solely the effect of separation). A direct confirmation was provided by the corresponding break in the flap normal force obtained by pressure integration, which occurred when the flap incidence $\alpha_F$ (irrespective of the wing incidence and flap deflection) was approximately equal to two-dimensional shock detachment value.

The flap pressure distributions throw some light on the development of separation with flap deflection and incidence. At zero incidence, the inboard ends of the (part-span) flaps were seen to be quite ineffective, the flap load rapidly increasing in the spawise direction to a maximum near the outboard tips. With increasing incidence the spanwise loading became more uniform except at the highest flap deflections ($30^{\circ}$ and greater). The authors have not discussed these changes in the flap load characteristics in terms of the separated flow phenomenon, although rapid variations in the separation evidently occurred with change of incidance between $0^{\circ}$ and $10^{\circ}$.

A two-dimensional strip application of modified Creager's theory (ref. 36) to allow for viscous interaction and blast wave effects on the wing pressures, in conjunction with two-dimensional compression through the flap shock was used to estimate the flap loads. The theory overestimated in all cases, and this was put down to the effects of separation.

However, such comparisons tend to give an exaggerated impression of the deleterious effects of separation, since the theory used over-estimates the average wing pressure particularly at high incidence and consequently predicts unrealistically magnified flap loads. Also, no account is taken of such inviscid effects as wing-shock/flap shock interaction and three-dimensional relief on flap pressure.

Two other investigations may be quoted where balance data on flapped delta wings have been compared with calculations based on rather different theoretical approaches. Fetterman and Neal (ref. 35) considered the wing flap as isolated panels, and calculated the average pressure on the panels by a semi-empirical theory for delta wings (ref. 37). In one case of positive flap deflection ($\delta_F = 10^\circ$) for which measurements were made, this theory under-estimated the flap load. At all but extreme incidence, this isolated panel assumption is obviously not valid since a considerable area of the flap will be under a flow which has been processed by the wing shock.

Keyes and Ashby (ref. 39) found rather good comparison of the measured pressures with calculations assuming tangent-cone pressure on the wing followed by two-dimensional compression through the flap shock. This is not surprising in view of the observed similarity of the average wind-ward pressure coefficient with tangent-cone theory for delta wings at larger incidence, as pointed out in sec. 3.1.

Some details of the flap-induced separation on sharp edge delta wings have been given by Whitehead and Keyes in a paper (ref. 40) which

appeared during the course of present study. This paper in certain respects parallels the present investigation and offers some useful comparisons which will be referred to in detail when discussing our results, but the broad conclusions may be mentioned here.

Whitehead and Keyes measured pressures and heat transfer rates on the wing and flap surfaces with 70° and 75° delta models at Mach 6. Transitional and fully turbulent flow separations were encountered, the latter achieved by transition fixing. At small incidence and with turbulent separation, two-dimensional calculations gave reasonable estimates of the bubble pressure and the maximum pressure levels over the flap. With free transition, at zero incidence, turbulent separation occurred only in the middle of the wing with more extensive laminar separation outboard. This mixed separation generated a complex flow and highly three-dimensional conditions over the flap (fig.38 ) causing significant loss of flap loading. It will be noted that this mode of separation is consistent with the spanwise variation in the approaching boundary layer on a delta wing discussed in sec. 3.2.

Keyes, in a later paper (ref. 41) presented further results obtained with the 75° delta model with flap. The effects of flap angle and unit Reynold's number variation on pressures and heat transfer rates on the wing and flap surfaces were shown in some detail. It was concluded that although, in general, the wing and flap flows were three-dimensional in nature, centre-line calculations using existing two-dimensional theories gave good indications of the trends over a large incidence range and, in some cases, predicted the maximum levels of local pressure and heat transfer. For calculations at incidence greater than zero, Keyes used tangent-cone pressures on the wing. Two-dimensional shock compression was assumed through the separation and re-attachment shocks (i.e. separation model described in sec. 2.2) to obtain the maximum pressure

level on the flap.

The effect of wing shock/flap shock interaction at high incidence ($\alpha_w > 20^o$), when a strong reflected shock impinges on the flap, were also noted. The sudden reversal of the hinge-moment curve slope with incidence (as observed in the measurements of ref. 35) was recognised by Whitehead and Keyes to be essentially caused by the reflected shock. (This phenomenon is distinct from the reflected expansion impingement (sec. 2.1) which also causes a loss of flap effectiveness but as a more gradual effect, and occurs at smaller incidence angles.)

The work of Whitehead and Keyes was primarily concerned with the turbulent flow case, regarded by them as more representative of the full-scale flight. The limited extent of separation under these conditions allowed reasonably uniform flow to develop over most of the flap surface even at large deflections, and from the evidence of pressure measurements, simple two-dimensional calculations appeared to provide a good estimate of the flap load characteristics, except when reflected shock effects were present.

It is thought that the prolonged transition process at hypersonic speeds, the swept transition front on delta planforms and the small incidence angles corresponding to flight at $(L/D)_{max.}$ are factors more likely to promote transitional rather than fully turbulent flow conditions near the trailing-edge of hypersonic delta-winged vehicles. Consequently, sepration will not only be more extensive but also uneven across the span and sensitive to relatively small variations in incidence, leading to complicated effects on control loads. This appears to constitute a significant gap in the present knowledge of hypersonic control aerodynamics on delta wings.

Due to lack of measurements in the range of small incidence of interest to curise vehicles (as opposed to large incidence operation typical

of re-entry configurations which have been more thoroughly studied), the phenomenon of reflected expansion impingement on the flap has largely escaped the attention of investigators. In this context, the results obtained recently by Mukherjee (ref. 42) who carried out a test programme suggested by this author in parallel with the present study, are illustrative. Mukherjee measured the loads on a $70^{\circ}$ delta wing with part-span flap configuration at Mach 8.2. It was found that, even under conditions of negligible separation (due to the small aspect-ratio of the flaps), significant loss in flap effectiveness occurred which could be traced to the reflected-expansion effect.

These results have shown that while the importance of separation studies cannot be over-stressed, a more complete examination of the inviscid influences on hypersonic control loads is also needed, and that on both scores the available information is meagre.

## Part II - PRESENT STUDIES AND DISCUSSION OF RESULTS

# 5. EXPERIMENTAL DETAILS

## 5.1 Test Programme

A consideration of the various aerodynamic features discussed in the preceding sections shows that the trailing-edge flap on a delta wing at hypersonic speeds would be subject to complicated and changing viscous as well inviscid effects with varying incidence, flap angle and Reynold's number. In general, highly three-dimensional conditions would prevail on the flap surface and therefore balance measurement was the only accurate method of obtaining overall aerodynamic characterisitics. A programme of balance tests therefore comprised the first phase of this study. It was thought desirable initially to measure the forces on a two-dimensional wing/flap configuration, to test the balance performance under conditions typical of the present programme and also to acquire some preliminary indications regarding the overall effects of separation in a flow field which was basically well understood.

In order to check the balance measurements on the delta models for any sting interference effects, a collaborative programme was subsequently arranged with the Aerodynamics Division, National Physical Laboratory, to obtain free-flight shock tunnel data on one delta wing ($76^{\circ}$) over a portion of the incidence and flap angle range. The results of these tests, reported in detail elsewhere, (ref. 43), are compared with the present measurements.

The second phase of this investigation was devoted to pressure measurements on the delta wing and flap surfaces in some test configurations common with the force measurement programme. This included the no-flap case, in order to obtain data on hypersonic delta wing pressures which are reltaively scarce in the literature. The object of this phase was to acquire pressure measurements in sufficient detail to enable an

assessment of the surface flow visualisation interpretations regarding the three-dimensional separation patterns, as well as to provide basic data on pressure levels particularly over the flap in order to judge the validity of the theoretical methods for predicting control effectiveness.

5.2 Hypersonic Gun Tunnel

A description of the design, operation and performance of the Imperial College 8-inch Gun Tunnel has been given elsewhere (e.g. ref. 61). For the present tests, the tunnel was fitted with a contoured nozzle producing a uniform airflow at M = 8.2. A detailed flow survey in the test section with this nozzle (ref. 21) showed that the Mach no. in the jet was constant to within $\pm$1.5% about a mean value of 8.25, while the flow inclination did not exceed 0.1°.

5.3 Models

Force models

The two-dimensional model (fig. 8 ) was a conventional flat plate configuration with provision for attachment to the balance. A set of four interchangeable wedge blocks, suitably hollowed to minimise weight, were provided to give flap deflection angles of 10°, 20°, 30° and 40°. The projected chord of the flaps in the plane of the plate length, was kept maintained constant at about 30% of the total plate length, so that the actual flap chord increased with wedge angle.

The two delta wing models (fig. 9 ) were selected from the series tested previously by Opatowski (ref. 21). The basic wing configuration consisted of flat bottom, inverted-V top (with the upper ridge line inclined at 6° with respect to the bottom plane) and blunt base. The apex and leading-edges were nominally sharp. The actual leading-edge thickness of the models (measured at several stages during the test programme) varied from .002" to .005" approximately. In this range, the leading-edge bluntness effect on the aerodynamic characteristics of the

flapped delta wings was considered to be negligible because of the large sweep angle.

As for the two-dimensional model, wedge-shaped inter-changeable blocks were provided for each delta wing to represent deflected flaps ($\delta_F$ = 10°, 20° and 30°). The flap chord in this case was maintained constant at 20% of the wing centre-chord, as was the hinge-line position at 80% of the centre-chord. In planform, the flaps for each wing were identical with the portion of the wing downstream of the hinge-line.

The choice of the flap area (about 36% of the total wing area in each case) was based mainly on the need for obtaining well-defined load measurements at the smallest flap angle, for which unseparated flow could be expected. It is believed that the flap size selected in these studies is not unrepresentative of actual hypersonic vehicle designs (see, for example, ref. 35).

All force models were machined from light alloy in order to minimise the total weight, to avoid undue oscillations of the balance arising from transient starting loads.

Pressure models (figs. 10 and 11)

These stainless steel delta wing models were designed to measure static pressures over the flat windward surfaces with and without flaps. The instrumented surface of each model was ground to a high degree of flatness (better that .001" over a length of 8 inches). The opposite (i.e. lee-ward) surfaces were left relatively rough and used for leading out the pressure tubes, and also for supporting the model. The sharp leading edges were levelled on the rough side, the included angle being small enough to prevent shock detachment at $\alpha_w$ = 0°.

Because of its larger area, the 70° delta model had the tips cropped streamwise behind the hinge-line to avoid tunnel blockage in tests at incidence with highly deflected flap. It is believed that this

modification did not materially alter the flow characteristics over the instrumented portion of the wing. Also, when fitted with flaps with streamwise tips, the flow separation on this delta is unlikely to differ qualitatively from that caused by flaps with raked tips, (ref. 42).

As before, a series of wedge-shaped blocks representing deflected flaps were provided for both the delta models, with pressure tappings incorporated as shown in fig. 10 and 11 .

The pressure models were mounted on a variable-incidence support (fig. 12 ) which could be set to give $\alpha_w = 0^\circ$ to $20^\circ$ in steps of $1^\circ$.

5.4 Instrumentation

Balance

This was a three-component strain gauge sting balance, the design and use of which has been described in detail by Opatowski (ref. 21). The design features of special interest are the possibility of locating the moment sensor inside the model close to the estimated C.P. for increased accuracy of normal force and C.P. measurements, and the use of high- sensitivity semi-conductor (Silicon) gauges which allowed a considerable increase in stiffness. This balance was well proved in a previous experimental programme described in ref. 21. However, in the present investigation, where it was impractical to position the balance moment station close enough to the C.P. with highly deflected flaps, its performance had to be independently established.

As will be seen in the comparison of the present measurements with the N.P.L. free flight tunnel results on the $76^\circ$ flapped delta (fig. 56 ), this balance was proved to be sufficiently accurate instrument for the purpose of the present investigation.

The balance was used in four series of tests in this programme, with a time gap ranging between two to four months between series. On each occasion, calibration was carried out (with the balance in the tunnel)

before and after the test series. The calibration factors remained constant within about 5%; however, the factors used for data reduction in each series were those obtained from the calibrations made for that series.

Further, before the start of each series of experiments, a "standard" configuration, i.e. 76° delta with 30° flap at zero incidence, was tested to provide a check on the overall repeatability. Additional measurements were made on the standard configuration with the model rolled 180°. The mean deviation in these check data were as follows:

Normal force: 2%

Axial force: 4%

Pitching moment: 2.5%

The estimated overall accuracy of balance results presented here are as follows:

Normal force: ±6%

Axial force: ±7.5%

Pitching moment: ±4.5%

Pressure transducers

Pressure measurements were carried out using four unbonded strain gauge diaphragm transducers (C.E.C. 4-326) of 0 to 10 PSIA range. These transducers have a full range output of about 40 mV with an excitation voltage of 10V. The range of pressures to be measured was from about 0.3 PSI (over wing surface) to nearly 5 PSI (on the flap), and in this range the overall accuracy of measurement was about 2%. The transducers were calibrated in-situ inside the tunnel against a McLeod gauge in the range 0.1 to 10 mm Hg, and a linear and repeatable calibration was obtained within the accuracy of the recording system.

The transducers were placed at the base of the model support outside the flow, keeping the pressure leads (of 1/16 inch bore) as short as

possible to minimise the response time.

The balance and pressure transducer outputs were displayed on Tektronix type 502 double-beam oscilloscopes and recorded using Land-Polaroid cameras and film.

Optical system

A conventional single-pass optical arrangement, with a short duration spark source, was used to obtain schlieren and shadowgraph pictures. For schlieren, both knife-edge and graded filters were employed. A Land-Polaroid camera back was adapted to provide an alternative photographic facility, which was found particularly useful for a quick look at the flow pattern on Polaroid film immediately after each run. More permanent records of selected tests were obtained on normal photographic plates (Illford fast, blue-sensitive).

### 5.5 Surface Flow Visualisation Techniques

Since the optical studies provided only one view of the three-dimensional flow phenomena, surface flow visualisation was obviously necessary to obtain a more complete description of the flow pattern, especially of the flap induced separation. Unfortunately, the short running time available posed an obstacle to the successful use of conventional oil flow techniques which have been found so valuable in other studies of three-dimensional flows. Attempts with the well-known oil-dot method (using silicone high-vacuum oil) were successful in the relatively high shear regions on the models, such as the flap surface in attached flow. In this instance, this method was found useful for locating re-attachment boundaries as well as reflected wave impingement.

To visualise the separation regions on the wing surface, a fair amount of effort was devoted to the powder technique. Here, a fine powder (talcum or, as in the present case, Titianium di-oxide) is lightly dusted on the dry surface of the model. After the run, the region of

separated flow becomes visible as areas of powder residue, in contrast with attached flow regions where the powder has been swept away. This method has been used before by several investigators but mainly to observe departures from two-dimensionality. To this author's knowledge, little attempt has been made to exploit the technique for studying details of three-dimensional flows. In the absence of alternative means of surface flow visualisation suitable for conditions of this investigation, the powder method was pursued and some understanding of its promise and limitations obtained.

From initial experiments on the two-dimensional model, where a direct comparison with optical results could be made, it was established that the powder pattern gave a fairly accurate position of separation (fig. 13). Additionally, some details of the flow in the separation bubble were indicated, such as the spanwise outflow and evidence of a secondary eddy in the flap corner at large deflections. The powder method was found sensitive enough to show up clearly the longitudinal vortices on the $10^{\circ}$ flap which are characterisitc of supersonic reattaching laminar flows (ref. 31).

On the flapped delta models, it was found that although meaningful and repeatable patterns could be obtained, they were less straightforward to read. In some cases the patterns were diffused, and others showed multiple boundaries (see fig.37 ). These appeared to correspond to transitional separation, where a rapid oscillation of the separation position has been observed (ref. 59). In general, the powder residue boundary was consistently found to extend somewhat upstream of separation as determined from schlieren photographs (this tendency had also been noted in two-dimensional tests, but there the difference was usually within the error of locating separation optically). From a large number of studies carried out during the balance test programme, it was concluded

that the powder patterns responded sensitively to local shear levels and directions, and these appeared to have complex distributions depending on the geometry of the three-dimensional separation. In particular, it appeared that the powder residue boundaries extended to the region of upstream influence of the pressure rise due to the flap, with or without separation, and this was important to bear in mind when attempting to deduce separation regions from the powder patterns. A detailed discussion of the interpretation of typical patterns is best done along with the results and will be deferred to sec. 8.1.

5.6 Flow Conditions

All tests in this investigation were carried out at a free stream Mach no. of 8,2.

In the bulk of the tests, the free-stream Reynold's no. was $0.17 \times 10^6$ per inch, and the free-stream stagnation temperature approximately 1000°K (corresponding to a driver pressure of 1000 p.s.i. with initially atmospheric barrel). The tests with varying unit Reynold's were carried out by suitably varying the barrel and driver pressures so as to keep the variation in flow temperature to a minimum. Since the model essentially remained at room temperature during the run, the present results may be regarded as relating to "cold wall" conditions.

The local flow conditions at the model surface at incidence are different from the free-stream. On the windward surface, the local Reynold's no. was calculated from the following relation (ref. 21):

$$R_{w/R_\infty} = \left(\frac{P_\infty}{P_w}\right)^n \left[\frac{P_\infty/P_w + 6}{6\,P_\infty/P_w + 1}\right]^{1+n} \qquad (6)$$

where n = 0.84 for the present tunnel conditions.

As pointed out in section 3.1 the windward pressure on a delta wing varies from two-dimensional value with attached leading-edge shock to a

level approaching the tangent-cone with increasing indidence beyond shock detachment. The range of local Reynold's number can thus be obtained from the curves calculated from eq. 6, shown in fig. 14,A .

Similarly, the local mean Mach no. on the windward surface will range between two-dimensional and tangent-cone values, as indicated by the curves corresponding to the two theories plotted in fig. 14,B . It will be noted that in the range of incidence of interest, there is little to choose between the two.

## 6. TWO-DIMENSIONAL MODEL:

Normal force, axial force and pitching-moment data were obtained at zero incidence with flap deflection angles of $10^{\circ}$, $20^{\circ}$, $30^{\circ}$ and $40^{\circ}$. All balance measurements and flow visualisation tests were carried out at a Reynold's number ($R_L$) of $0.41 \times 10^6$ (based on length to hinge-line).

Fig. 15 shows separation and re-attachment positions measured from schlierenphotographs, plotted versus flap deflection. Also shown are other separation data at Mach 8 for about the same Reynold's no. as the present experiments the agreement, with the exception of Johnson's data, is quite good except in the neighbourhood of incipient separation (where the accuracy of locating separation is relatively poor). Johnson's model had a much shorter flap than in the other studies and his results are believed to be influenced by the flap length.

The incipient separation flap angle obtained by extrapolating the present schlieren data to zero separation lies close to the value of $8.4^{\circ}$ predicted by Needham's correlation for laminar boundary layer (ref. 10). The separation length increases almost linearly with flap angle, but beyond $\delta_F = 30^{\circ}$ appears to asymptote to a limiting separation (i.e. close to the leading edge) which is probably reached at $\delta_F = 40^{\circ}$. On the other hand, the re-attachment position on the flap is found to

change little with flap angle, as also noted in other investigations (e.g. ref. 7).

The incremental normal force and pitching-moment are compared with inviscid (two-dimensional shock) theory in fig. 16 . The normal force is progressively over-estimated by the inviscid theory as a result of increasing separation with flap deflection. The results of $\Delta C_N$ calculations from the simple separated flow model using separation data from schlieren photographs are also shown. While the empirical calculations still lie above the experimental data, they are better than the inviscid prediction. For $\delta_F = 40^\circ$, where a pronounced reflected-expansion influence on the flap was observed, calculation based on the appropriate flow model provides a value which fortuitously agrees with the inviscid prediction, evidently due to the compensating factors as pointed out in section 2.2.

The incremental pitching-moment measurements generally appear to be in good agreement with the inviscid theory up to $30^\circ$ flap deflection. This agreement is attributable to a fortuitous combination of the normal force and centre-of-pressure variations induced by separation. At the largest flap angle, the reflected expansion effect is evidently responsible for a higher pitching-moment than predicted by the calculations, a trend similar to that already noted in the analysis of Johnson's pressure measurements under similar conditions (fig. 3 ).

## 7. DELTA WINGS WITHOUT FLAP

### 7.1 Balance Measurements

Three-component measurements on the delta models without flap were carried out at incidence angles $\alpha_o = 0^\circ$ to $20^\circ$ ($\alpha_w = 3^\circ$ to $23^\circ$) and Reynold's number $R_L = 0.85 \times 10^6$ (based on centre-chord)*. The purpose of these measurements was to check the balance performance by comparing the results with those obtained by Opatowski (ref. 21) under identical

* Tabulated in Appendix

test conditions, and also to extend the no-flap data to higher angles of incidence.

The force coefficients and the centre-of-pressure positions derived from the balance readings are shown in figs. 17 and 18 . The normal force measurements agree well with Opatowski's results, and also with the two-dimensional shock theory up to the respective shock-detachment incidence on the two wings. At higher incidence, the departure from the two-dimensional theory is relatively slow, On the 76° delta, where the shock is detached over most of the incidence range, the $C_N$ is reasonably well predicted by eq. 4 (which, as already shown in fig. 6 is representative of the calculations from other theories). In these estimates, the leeward pressure coefficient was taken as $-1/M^2$ as suggested in ref. 62.

The axial force measurements on the 76° delta are generally higher than Opatowski's results, which is believed to be largely due to an increase in apex bluntness suffered by this model since the original tests. To a lesser extent, this is also the case with the 70° delta. The increased axial force relative to the inviscid two-dimensional shock theory mainly indicates the magnitude of the skin friction contribution. However, the accuracy of drag data on these models is probably inadequate to properly assess the viscous drag.

The shock tunnel free-flight results of N.P.L. for the 76° delta are in excellent agreement with the balance measurements of $C_N$, and also compare well with $C_A$ data.

The centre of pressure position (distance from the apex along the balance axis) on both the wings was generally found to lie a little upstream of the 2/3 chord point (centroid) at low incidence, but moving towards it with increasing incidence. This trend is predicted by the viscous interaction effect, and the present measurements (having an

accuracy of about $\pm$0.5% of the wing centre-chord) are in good agreement with calculations based on ref. 34. However, the total movement of the present C.P. data in the incidence range is contained within 1% of the centre-chord, as also the maximum deviation from the centroid.

7.2 Shock Angle

Wing shock measurements (in terms of stand-off angle $\xi_w$) from schlieren photographs are compared in fig. 19 with other experimental data and also with calculations. The measurements are accurate to $\pm$0.25%. The data for $\alpha_w < 5^\circ$ are evidently influence by viscous interaction on the present models, particularly on the 70° delta. The results for 76° delta compare well with N.P.L. data. Opatowski's measurements (ref. 58), which relate to a thicker model (i.e. upper ridge line inclined at 10° to the bottom surface as against 5° in the present case) are also in good agreement, suggesting negligible influence of the leeward surfaces on the windward shock shape even with detached shock. The calculations from eq. 5 as well as from Squire's theory give reasonably good predictions of the centre- line shock angle in the detached shock regime.

7.3 Pressures

The centre-line pressures on the 76° delta at various incidence angles $\alpha_w = 3^\circ$ to 18° are presented in fig. 20 and compared with two-dimensional shock, tangent-cone and Squire's theories.

The data for $\alpha_w = 3^\circ$ show the effect of viscous interaction, which increases the pressure level roughly as indicated by the two-dimensional weak interaction theory (ref. 32). At $\alpha_w = 8^\circ$, the predicted viscous interaction is negligible. Here, Squire's inviscid theory gives a fair mean value of the centre-line pressures. The limited data at the higher incidence angles are also found to be in good agreement with Squire's theory.

A cross-plot of this data with incidence is given in fig.21 The incidence range of viscous interaction effect on pressures appears to agree with the shock angle data at the same Reynold's no. (fig.19 ). The interaction influence according to the present data vanishes at $\bar{\chi}_L = M_w^3/\sqrt{R_L} = 0.3$ approximately, which may be compared with the criterion $\bar{\chi}_L > 0.22$ for significant viscous interaction on delta surfaces suggested by Cook (ref. 56).

An alternative presentation, shown in fig. 22 , permits a comparison of the present results with other hypersonic pressure measurements on a 76° delta at comparable Mach numbers. The available data in the Mach no. range 6.8 to 9.6 are found to agree fairly well in the mean with the tangent-cone theory, outside the domain of viscous interaction influence.

The pressure distribution normal to leading edge on the delta wings at two incidence angles ($\alpha_w = 3°$ and $8°$) is shown in fig. 23 . At the higher incidence, in the absence of significant viscous effects, the characteristic distribution with higher pressure towards the leading edge is obtained. Here, again, Squire's theory for the 76° delta gives a reasonably good mean through the measured data.

7.4 Transition

Some data on boundary layer transition on the delta wings were obtained in tests at zero incidence and varying unit Reynold's number. Transition was identified as a disruption of the sharp line in the schlieren photographs denoting the edge of the boudnary layer on the upper surface ridge line. It has been suggested that the position so measured lies towards the end of the transition process (ref. 10). The present measurements are compared with available data from the literature in fig. 24 .

In view of the remarks already made regarding the effect of facility-induced disturbances on transition measurements (sec. 3.2), it would perhaps be unwise to draw any conclusions from this comparison

except to note that the present transition data lie well within the overall trend. The two-dimensional transition measurements obtained in the same facility by Richards (ref. 54) are also indicated in fig. 24, and the relative postion of the present data in this comparison at least confirms the known effect of leading-edge sweep in hastening transition (sec. 3.2). There appears no support in the present results for the opposite conclusion (viz. earlier transition on the delta wing of smaller sweep angle) reached by Opatowski on the basis of axial force measurements (ref. 21).

The present results are of relevance insofar as they can provide an indication of the onset of transitional condition which is known to strongly affect separated flows. This information will be found useful in later sections in explaining the differences between the flap-induced separation characteristics of the two delta wings.

## 8. DELTA WINGS WITH FLAP

### 8.1 Separation Characteristics

The flap-induced separation on the delta wings was studied using optical and surface flow visualisation and pressure measurements. While the schlieren photographs provide an overall indication of the extent of separation, the surface flow patterns and pressure data fill in some details of the three-dimensional separations. Although both the $70^{\circ}$ and $76^{\circ}$ delta wing configurations were investigated, the coverage in each case had to be necessarily limited in a practical test programme. In the total, however, sufficient evidence has been obtained to permit discussion of the essential physical aspects of the separated flow phenomena on delta wings in general terms, as well as to provide a comparison between the two wings in specific configurations.

For the purposes of the present discussion, two basic configura-

tions have been identified. The first case of zero (or small) incidence is when, at the lowest Reynold's numbers of the present tests, viscous interaction effect is present in the boundary layer flow over the wing, which is essentially laminar across the hinge line. In the second case, the wing is at incidence and the separated flow phenomena are primarily influence by the onset of transition. This classification is merely one of convenience for presenting the results of this investigation. It is not to be construed that the basic flow conditions mentioned above cannot arise at other incidence angles, under free-stream conditions different from the present tests. Indeed, at higher Reynold's numbers, transitional separations have been found even at zero incidence in the present studies.

8.1.1 Zero or small incidence

A series of schlieren photographs with increasing flap deflection is shown in fig.25 .

With $\delta_F = 10^\circ$, the flow appeared unseparated on the $76^\circ$ delta, while marginal separation could be noticed on the $70^\circ$ wing. The predicted flap angle for two-dimensional laminar incipient separation (corresponding to the prevailing local flow conditions on the wing centre-chord) is about $7^\circ$. Assuming that the two-dimensional criterion is valid here, it would appear that the boundary layer on the centre-chord is on the verge of transition near the hinge-line on the $76^\circ$ delta. (This corresponds to $R_T = 0.85 \times 10^6$ for a local unit Reynold's number of $0.22 \times 10^6$ per inch, which is not inconsistent with the transition data for delta wings shown in fig. 24 ). On the $70^\circ$ delta, transition has evidently not yet reached the hinge-line and a small laminar separation bubble exists.

The separation and re-attachment positions from the schlieren of fig. 25 (taken as the points on the model surface directly below

the feet of the separation and re-attachment shocks respectively) have been plotted in fig. 26 . This shows an almost linear increase of the separation distance from the hinge-line with flap deflection up to $30^{\circ}$, and also a consistently larger separation on the $70^{\circ}$ delta. The difference between the separation lengths on the two wings is almost certainly due to an earlier onset of transition on the $76^{\circ}$ delta (in accordance with the well-known effect of leading-edge sweep angle, as already discussed in 7.4).

This is confirmed by a measurement at a slightly lower Reynold's number with $\delta_F = 30^{\circ}$ on the $76^{\circ}$ delta (flagged symbol) which is evidently for laminar flow and compares well with the separation length for the $70^{\circ}$ delta wing. Fig. 26 also shows a remarkable agreement of the delta wing centre-chord separation length (particularly for $70^{\circ}$ sweep) with two-dimensional laminar separation data.

The centre-chord pressure distribution for a typical case ($\delta_F = 30^{\circ}$) given in fig. 27 also shows more extensive separation on the $70^{\circ}$ wing in comparison with the $76^{\circ}$ delta. Due to the higher Reynold's number of the pressure models, separation is transitional on both the wings and therefore the separated lengths are less than the corresponding laminar data for the force models shown in fig. 26 . The pressure over the flap after re-attachment are found to agree well with inviscid predictions.

Surface flow visualisation

Powder patterns generated at $\alpha_o = 0^{\circ}$ (i.e. $\alpha_w = 3^{\circ}$) with increasing flap deflections on the $70^{\circ}$ delta (fig. 28 ). These serve to illustrate some features of flap-induced separation in the presence of viscous interaction effects on the delta wing boundary layer.

With $\delta_F = 10^{\circ}$, the effect of separation is seen to reach further

upstream on the centre-chord than outboard. This is evidently the result of reduced shear locally due to the piling up of the boundary layer flow on the centre-chord, under a pressure gradient induced by viscous interaction as explained in section 3.2.

The flow with $10^{\circ}$ flap deflection is evidently unseparated in the outboard regions. Such a separation pattern conforms to the strip-theory viewpoint using two-dimensional laminar incipient separation criterion which predicts separation to appear first on the centre-chord (where $\bar{\chi}_L$ is minimum). With further flap deflection, separation will spread spanwise towards the hinge-line extremeties.

At $\delta_F = 20^{\circ}$, separation has clearly spread over the whole span of the hinge-line as well as upstream. The region close behind the leading-edge is however free of any powder residue, indicating a relatively high shear in these areas under viscous interaction. There is evidence of the secondary corner eddy which scrubs the powder away from the hinge-line due to relatively high local velocity (as found on the two-dimensional model, fig. 13 ). The re-attachment boundary is also distinctly shown.

The powder pattern for $\delta_F = 30^{\circ}$ conveys the impression of a greatly extended separation covering nearly the whole of the wing surface. A limiting condition has evidently been reached, with separation occuring parallel to and close behind the leading edges. According to the schlieren photograph for this case, actual separation did not reach as close to the apex, possibly inhibited by the favourable pressure gradient associated with strong viscous interaction in the vicinity of the apex. Nevertheless, the overall pattern is auggestive of a "conical" bubble, which intuitively fits the picture of limiting flap-induced laminar separation on a delta wing. A similar pattern was also obtained for the $76^{\circ}$ delta.

A distinctive feature common to the surface patterns in this series is the streak appearing along the flap centre-chord. This represents a low-shear trail, and was also noted in the oil-dot visualisations (and particularly well shown up in the oil flow pattern obtained by Keyes, see fig. 8a of ref. 41). It is believed that this is associated with a retarded pressure rise locally on the flap following the re-attachment of a much thicker viscous layer generated on the wing centre-chord at low incidence (sec. 3.2). Note that this characteristic disappears when the incidehce is increased, as found in the series of powder patterns shown in fig. 37 .

Pressure contours

An example of the pressure distribution obtained with flap-induced separation in the presence of viscous interaction effect on the 70° delta wing boundary layer ($R_L = 1.17 \times 10^6$) is presented in fig. 29 . Notable features are the spike-shaped contours on the wing and flap centre-lines. These characteristics well illustrate the highly localised upstream propagation of the separation pressure rise along the wing centre-chord, as well as the delayed pressure rise over the flap centre consequent to the re-attachment of a singularly thickened viscous flow, as explained in the preceding section. The interpretations of the powder flow visualisation are thus corroborated by these pressure measurements. For comparison, pressure contours obtained at a slightly higher Reynold's number ($R_L = 1.43 \times 10^6$) are shown alongside. A remarkable transformation in the shape of the isobars along the centre-line is noted, in particular the disappearance of the "spikes" on the wing and flap centre-chord (compared with powder patterns, fig 28 and 37 ). A general trend towards two-dimensionality of the flap pressure field with the disappearance of the viscous interaction influence is indicated.

The effect of Reynold's number increase on the flap pressure field

on the 76° delta is shown in fig. 30 . A "conical" type deep separation was observed at $R_L = 0.85 \times 10^6$, which collapsed with a very small increment in Reynold's no. to $0.90 \times 10^6$.

The pressure distribution is highly three-dimensional with "conical" separation, with a low pressure "valley" along the centre-line dividing the flap pressure field into two symmetrical halves. Just after the collapse of "conical" separation, the pressure contours reveal a remarkably two-dimensional flow over most of the flap surface. When $R_L$ was raised further to $1.1 \times 10^6$, the isobars were found to distort once again. This is evidently due to separation becoming transitional and receding in the inboard region, and consequently assuming the characteristic two-lobed shape (as visualised in the powder pattern in fig. 37 ). The suggested separation patterns corresponding to these cases are sketched in fig. 30 .

8.1.2 Increasing indicence

Schlieren data

A typical series of schlieren photographs with increasing incidence at constant flap deflection (30°) is shown in fig. 31 . Separation and re-attachment positions measured from such photographs have been plotted in fig. 32 against incidence for each of the three flap deflections. It is seen that more extensive separation occurs over the 70° delta throughout the incidence range.

The variation of separation length with incidence with 10° flap is found to be quite different from that at higher flap deflections. Bearing in mind that the local Reynold's number increases with incidence (fig. 14) the growth of separation with $\delta_F = 10°$ is indicative of laminar separation, whereas at higher flap angles separation is evidently transitional.

The powder flow visualisation results also suggest laminar separation with $10^{\circ}$ of flap. A fine pattern of closely-spacedlongitudinal streaks over the flap surface, which are believed to be produced by Goertler-type votices characteristics of re-attaching laminar flows (ref. 31) were repeatedly obtained in this case (but were conspicously absent at the higher flap angles). For $\delta_F = 20^{\circ}$ and $30^{\circ}$ the separated length reached a minimum between $10^{\circ}$ and $15^{\circ}$ incidence and thereafter increased with further rise in incidence. This point of reversal corresponds to the incidence angle at which the local Reynold's no. reaches a peak and then falls (fig. 14 ), which is consistent with the behaviour of transitional separation.

The re-attachment position data shown in fig. 32 logically follow the variations in the position of separation with incidence. The relatively small effect of flap deflection on re-attachment length is in keeping with the trend already noted on the two-dimensional model.

Assuming that the separation length is mainly governed by Reynold's number, an attempt has been made to correlate the present results (for $\alpha_o < 15^{\circ}$) with other available data for flap induced separation on $76^{\circ}$ delta on the basis of local Reynold's number ($R_L$). The data used correspond to varying incidence as well as model scale. As shown in fig. 33 , a reasonable agreement is obtained between the present measurements and those of Keyes (ref. 41) and N.P.L. (free-flight tunnel tests). The trends apparent in this figure for the different flap angles are in conformity with the known effect of Reynold's number on laminar and transitional separations.

The above observations of the Reynold's no. effect on separation confirm that, at the relatively low unit Reynold's no. of the force tests in the present investigation, the flow conditions on the $76^{\circ}$ delta

wing were already transitional at $\alpha_o = 0^\circ$, and became so on the $70^\circ$ delta at a small angles of incidence. Thus, the more extensive separation found on the $70^\circ$ wing was mainly a consequence of transition on this wing lagging behind in comparison with the $76^\circ$ delta.

Centre-line pressures

At $\alpha_w = 8^\circ$ and $13^\circ$ (figs. 34 and 35 ) separation is quite limited on the $76^\circ$ delta and the wing centre-line pressure upstream of separation approaches closely the tangent-cone value (compare with fig. 20 ). The pressures over flap become more uniform. The flap pressures are progressively better predicted by "cone-wedge" estimates. (Note that at these incidence angles when the leading-edge shock on the $76^\circ$ delta is detached, the "cone-wedge" calculations are practically identical with those based on Squire's theory or eq. 4). The onset of the reflected expansion impingement is clearly seen as a sudden fall in pressure towards the flap trailing edge, at a position which agrees well with calculation based on eq. 1 using $\xi_w$ from Squire's theory.

A feature of note in the centre-line pressure distributions is the continuously rising pressure on the wing in a region where separation is indicated on the schlieren pictures unlike the 2-D case where a plateaux exists. The pressure on the hinge-line (which must correspond to the bubble pressure in separated flow) is always found to be significantly higher than the value at the nearest upstream ( $\Delta x = 0.5$ in.) point of measurement. This feature of gradually rising pressure on the wing centre-line within what is indicated to be a separated zone is also to be found in the measurements presented in refs. 40 and 41. While in two-dimensional separations a rising pressure in the bubble is generally associated with the occurence of transition in the shear layer close to re-attachment (ref. 14), in the present instance three-dimensional effects in the separation bubble are believed to be mainly responsible.

Incipient separation

The flap angle for incipient separation on the 76° delta (obtained by extrapolation at constant $\delta_F$ or $R_L$ from separation length data of this and other investigations) are compared with the correlated two-dimensional results for laminar, transitional and turbulent flow, in fig.36 . Although the delta wing results are few, two significant points of departure from two-dimensional characteristics are apparent.

Firstly, the flap angle for laminar incipient separation is increased on the delta wing. This is believed to be the result of spanwise outflow in the boundary layer at the hinge-line in a three-dimensional configuration, analogous to the case of part-span flaps (ref. 16) where a similar increase in $\delta_{Fi}$ for laminar flow was found. A theoretical justification for this behaviour is provided by the results of an analysis by Libby et al (ref. 55), who show that an outflow in the laminar boundary layer from the plane of symmetry in an adverse pressure gradient leads to a reduction in boundary layer thickness which tends to inhibit separation.

Secondly, a rise in the incipient separation flap angle with $R_L$ which is characteristic of transitional flow occurs sooner on the delta. This merely confirms the earlier onset of transition on the delta wing in comparison with two-dimensional flow.

On the other hand, the turbulent incipient separation on the 76° delta is seen to agree well with the two-dimensional characteristics.

Sufficient data is not available to deduce incipient separation on the 70° flapped delta. However, from the above trends, it appears reasonable to assume that the characteristics of this wing will lie somewhere between the 76° delta and two-dimensional for laminar as well as transitional cases.

Surface flow visualisation

The notable feature in the patterns with increasing incidence (fig. 37 ) is the initial spread of separation in the outborad regions at the expense of separated flow in the middle of the wing ($\alpha_o = 5^o$). This is evidently due to increased local Reynold's no. causing extension of laminar separation outboard, while onset of transition leads to diminishing separation inboard. This pattern is regarded as an early stage in the development of "mixed" separation reported by Whitehead and Keyes (ref. 40), who found turbulent separation (at a higher Reynold's no. than the present tests) in the middle of a $70^o$ delta with $40^o$ flap together with laminar separation outboard. This flow pattern (based on the oil flow visualisation presented in ref. 40) is reproduced in fig. 38 .(Note tha general similarity with the flow sketched in fig.4,B).

When the incidence is raised further to $10^o$, a more regular separation boundary is produced, as the flow becomes transitional over most of the span. This change of separation pattern can also be identified in the corresponding schlieren photographs, as a double separation shock system (associated with mixed separation) gives way to a single separation shock (fig.31 ). It may be pointed out that with an attached leading edge shock the separation length must be zero at the extremeties of the hinge-line. With increasing incidence (at fixed flap deflection) the local wing flow conditions in the vicinity of the hinge-line ends approach incipient separation and will cause a local shock detachment with the onset of separation. However, on highly swept delta wings as in the present study, with increasing incidence the leading edge shock detaches before separation spreads to the hinge-line extremity. With the opening out of the bubble at the sides, spanwise venting occurs and the separation pattern then will resemble the flow sketched in fig. 4,A. This case is illustrated in the oil-dot

visualisation shown in fig. 39 .

Pressure contours

A comparison of the 76° delta wing pressure field with and without 30° deflected flap at $\alpha_w = 8°$ is shown in fig. 40 . It is noted that although centre-line separation is quite limited in this case, the upstream effect is still considerable along the centre-chord. It would appear that even outside the regime of viscous interaction influence, a relatively low energy boundary layer flow results on the centre-chord, presumably arising from the inward pressure gradient predicted (and found experimentally, fig. 23 ) on the delta wing even for the inviscid case. At incidence angles much higher than for leading-edge shock detachment, such a pressure gradient is not found (ref. 18) and consequently this particular characteristic of the boundary layer on the centre-chord will also disappear.

The pressure contours on the 70° and 76° delta wings under identical condtions are compared in fig. 41 . Apart from greater scale of separation on the 70° delta, the pressure field produced by flap-induced separation is seen to be very similar over both the wing and flap surfaces. The shape of the separation front indicated by the contours on the wing is remarkably consistent with the surface flow visualisation of mixed separation obtained by Whitehead and Keyes (fig. 38 ), and is further confirmed by the oil-dot picture shown in fig. 42 , obtained in the present tests. The relatively even spacing of the isobars in the three-dimensional separated flow explains the lack of clarity of the powder patterns.

Hinge-line pressure distribution

The variation of pressure along the hinge-line provides an independent means for checking the spanwise variation of separated flow on the flapped delta. These measurements, (figs. 43 and 44 )

were obtained at points on the wing just upstream of the hinge-line.

With unseparated flow, the hinge-line pressure would be expected to lie close tc the wing pressure, while separation would result in significant pressure increase. The hinge-line pressure with separation should at least equal the laminar bubble pressure (as estimated from two-dimensional empirical theory, eq. 2, which has been found to be valid for three-dimensional separations also), and will exceed this level under transitional conditions (although an estimate in this case is not possible). Applying these simple criteria to the data in fig. 43 leads to the following conclusions:

i) With $\delta_F = 10^\circ$ the flow is unseparated at $\alpha_w = 3^\circ$. With incidence raised to $8^\circ$, laminar separation appears outboard ($Z/Zh.l. > 0.2$) while the flow appears to remain attached in the central region where the approaching boundary layer is probably turbulent.

ii) With the flap deflected to $20^\circ$, laminar separation is produced over the whole instrumented span of the hinge-line at $\alpha_w = 3^\circ$. At the higher incidence when the boundary layer on the centre-chord undergoes transition, separation collapses in the central region while the flow outboard remains separated.

iii) At $\delta_F = 30^\circ$, the hinge-line is largely under transitional separation. A pressure gradient favourable to an inward flow in the bubble exists. A pressure peak appearing on the centre-line may signify a local interruption of the separation bubble, most likely associated with unseparated turbulent flow along the centre chord (the local pressure peak was found to lie well below the estimated bubble pressure for turbulent separation).

The hinge-line pressures with $\delta_F = 20^\circ$ were investigated over a larger range of incidence, with the results as shown in fig. 44. The characteristic pressure distribution with a "bucket" in the region

of the centre-chord (associated with locally attached transitional or turbulent flow) persists up to $\alpha_w = 15^\circ$. A sudden change in the pressure distribution occurs at $\alpha_w = 16^\circ$ which now indicates separated flow over the whole of the hinge-line span. (A discontinuous increase in the separation length was noted in the corresponding schlieren photographs).

Estimates based on the transition data from fig. 24 indicated that in the above incidence range separation always occurred downstream of transition on the wing centre-chord. It is suggested that the change-over in the hinge line pressure distribution is associated with change from attached to separated flow of the transitional (or turbulent) boundary layer on the centre-chord, as the local flow conditions (i.e. M and R) move across the incipient separation boundary for the given flap angle. Support for this conjecture is provided by the incipient separation data for 76° delta discussed in sec. 8.1.1. The local conditions at the change-over are $\delta_{Fi}/M_L = 0.86$; $R_L = 2.0 \times 10^6$, which correspond very closely with the transitional incipient separation boundary for the delta wing indicated in fig.

A consequence of the change-over in the separation pattern is the appearance of a hinge-line pressure gradient favouring a spanwise outward flow in the separation bubble. An oil flow pattern was shown in fig. 39 .

8.1.3 Three-dimensional separation patterns

From the experimental evidence based on schlieren, surface flow fisualisation and pressure measurements presented in the preceding sections, it is possible to build up a consistent physical picture of the three-dimensional separations induced by the trailing-edge flap on delta wings at hypersonic speeds.

When the wing surface is streamwise or at small positive incidence

(i.e. when the local conditions are such as to promote viscous interaction effects), the wing boundary layer approaching the flap develops a characteristic peculiarity along the centre-chord viz, a greatly increased thickening and reduction of skin friction relative to the adjacent regions. The boundary layer flow over the rest of the wing contains a spanwise variation arising simply from the decreasing length of run (or $R_x$) due to the delta geometry. The response of this boundary layer to the adverse pressure field imposed by the flap will accordingly vary in the spanwise direction.

From the incipient separation condition for two-dimensional flow, separation would be anticipated first on the centre-chord (where $\bar{\chi}_L$ is a minimum) and spread tip-wards with increasing flap deflection. As separation develops, the upstream influence in the boundary layer (or interaction distance) will extend much farther upstream along the centre-chord because of the local thickening of the boundary layer along the centre-line. On the other hand, the upstream influence might be inhibited by the viscous interaction induced pressure gradient in the outboard regions due to the proximity of the leading edge.

These ideas were found helpful toward a proper appraisal of the powder patterns such as those shown in fig. 28 and 37 , and in the deduction of separated regions from such visualisation studies.

From the geometry, it is evident that separation will soon attain a limiting condition near the hinge-line extremities and, as the flap is further deflected, this condition will continuously progress upstream along the leading edges until the separated flow from the two sides merge near the apex. When this happens, a "conical" separation (a term used more for convenience than exactitude to describe the ultimate limiting separation on delta wing) will be produced. Such a separation

clearly requires the existence of fully laminar flow, which only can provide the extensive scale of separation involved. In the present investigation, this condition is believed to have existed on the force models at the lowest Reynold's numbers with $\delta_F = 30^\circ$.

Consider now the effect of increased local Reynold's no. (either caused by incidence or by free-stream Reynold's no. increase) on the "conical" separation. Transition will appear, first on the centre-ray of the conical bubble and spread laterally. From the known effect of onset of transition, this will lead to a progressive collapse of the conical bubble from the centre outwards, producing the two-lobe shaped separation boundary which has repeatedly appeared in the present experimental results. This type of flow develops into the "mixed" (laminar-turbulent) separation when, at a higher Reynold's no., transition precedes separation on the centre-chord. When the turbulent (or transitional) flow in the middle remains attached, a divided bubble results. (fig. 42 ).

Another type of separation is produced when (e.g. at higher incidence) the combination of local M and R is scuh that the given flap angle exceeds the incipient separation angle for turbulent (or transitional) flow. This causes separation across the whole span of the hinge-line, the divided bubble configuration giving way to one more akin to separation observed on low aspect ratio two-dimensional models. This separation pattern is also found rather similar to that obtained at subsonic speeds (fig. 45 ). This oil-flow visualisation has indicated details within the separated flow which may be relevant to the high speed case, and will lead to complicated heat transfer distribution in the separation region.

A notable aspect of the three-dimensional separations observed is the presence of pressure gradients in the separation bubbles. These

imply rather complex flows within the separated regions, and the simple model of two-dimensional separations (with sharp pressure rise at separation and the bubble as a "dead air" region) can be misleading when attempting to locate boundaries of separated flow from surface pressure measurements. The complicated subsonic flow within the bubbles is of particular concern to the prediction of heat transfer rates and may pose a serious problem in vehicle design when large areas of the wing are under separated flow.

8.2 Wave Phenomena

Most of the schlieren photographs of the flapped delta wings show a plane shock originating from the flap corner (or "flap shock"), irrespective of the presence and extent of separated flow (see figs. 25 and 31 ). The measured flap shock angle has been plotted versus the flap incidence with respect to the free-stream in fig. 46 . These data cover all three flap angles. The flap shock angle is seen to correlate well with the two-dimensional shock angle in the whole range of measurement. The inference is that the flap shock as seen in the photographs is associated with the deflection of the free-stream by the portions of the flap surface which lie outside the flow field processed by the wing shock, and over which the flow is always attached. It then follows that the pressure over such regions of the flap will be well below the pressure generated by successive compression through the wing and flap shocks. Some measurements obtained in the tip region of the flap in a typical configuration (fig. 47 ) indicate that the pressures here are even below the single (two-dimensional) shock prediction, evidently the result of tip relief (specially at the upstream-most location which is closest to the flap tip).

The phenomenon of wing-shock/flap-shock interaction has also been optically visualised on the flapped delta models. A typical shadowgraph

is presented in the upper part of fig. 48 which clearly shows the reflected expansion emanating from the intersection of the shocks.

As explained in sec. 2.1, the position of the impingement of the reflected expansion on the flap surface may be calculated using shock-expansion theory. In applying this procedure to the delta wing, the wing shock angle in the centre-plane may be obtained from theories of Squire or Kennet when the leading-edge shock is detached (while two-dimensional shock angle is assumed with attached shocks). The local Mach no. on the wing is calculated from two-dimensional shock or tangent-cone theories, and a plane flap shock is assumed. Then, using eq. 1, the impingement position on the flap centre- line is obtained.

A comparison of the calculated and measured reflected-wave impingement postions on the centre-line is shown in fig. 49 . (The experimental data in this figure are for the force models). While a reasonably good agreement is obtained for the 76° delta, the calculations are found to greatly underestimate the forward movement of the reflected expansion on the flap of the 70° delta wing.

The poor agreement with calculation in case of the 70° delta is believed to be mainly the effect of separation, which, as illustrated in the lower part of fig. 48 modifies the inviscid shock interaction (by introducing additional waves and reducing local Mach no.) in such a way as to cause an earlier intersection of the shocks. Thus, the greater length of separation occuring on the 70° delta leads to a much more upstream shift of the reflected expansion impingement relative to the inviscid prediction than in case of the 76° delta wing.

The three-dimensional geometry of the delta wing shock envelope and its interaction with the (assumed) plane flap shock may now be considered, fig. 50 . It is evident that since the wing shock stand-off angle decreases when going from the centre-chord towards the leading

edges, the reflected-expansion impingement will occur progressively earlier on the flap with increasing spanwise distance. With an attached leading-edge shock, the impingement distance from the hinge-line will decrease to zero at the extremities. Even with a detached shock, in the range of conditions of interest in the present study, the expansion impingement will approach the hinge-line extremities closely. It follows that the outboard portions of the flap, except at small deflection angles, will in general lie in the reflected wave influence (see sketch on the right of fig. 50 ) even when no impingement occurs on the centre-line.

With the above model of three-dimensional wave interaction on a flapped delta, an attempt was made to calculate the reflected-expansion impingement boundary for the case of the 76° delta with 30° of flap. Eq. 1 was evaluated in planes normal to the wing surface lying along different rays from the vertex, using the charts presented by Squire (ref. 25) to calculate the wing shock angle in these planes. The calculated points for four incidence angles are compared with flap pressure contour measurements and oil-dot visualisation results in fig. While the oil flow pictures directly show the reflected expansion boundaries, it is not difficult to deduce the boundaries from the isobars bearing in mind that a fairly sharp drop in pressure occurs across the reflected-expansion impingement. Considering the simplified procedure adopted in these calculations, the agreement with experiment is quite good.

8.3 Balance Measurements

The normal force, axial force and pitching-moment coefficients ¤ are plotted versus incidence in fig.52 & 53. These tests were carried out at $R_L' = 0.85 \times 10^6$. It was considered preferable to present the data in the balance-axis form as this allowed the two aerodynamic force components to be studied as separate balance outputs. Thus, any anomalies

¤ Tabulated in Appendix

arising from balance errors in the individual components could be readily identified.

Both the force coefficients are in general smoothly varying and show systematic increments with incidence and flap angle. An exception is noted in the case of 76° delta with $\delta_F = 30^\circ$ where a change of slope of the $C_N, \alpha_o$ curve occurs at about $\alpha_o = 10^\circ$, which is close to the shock detachment condition over the tip portions of the flap (which "see" the free-stream flow). A corresponding break is also evident in the $C_A$ and $C_M$ curves. Due to the larger flap aspect ratio on the 70° delta, the reduced loading after shock detachment on the tip regions will be relatively less significant, and it is the effects of flap-induced separation that are evidently more important in determining the aerodynamic characteristics of this wing.

The effect of more extensive separation on the 70° delta is clearly demonstrated through reductions in the normal force and, even more dramatically, in the pitching moment characteristics of the 70° delta in comparison with the 76° wing. The differences are less evident in the axial force characteristics mainly because a smaller component of the flap load is measured in the axial direction, and also due to the contributions from base drag as well as the side area of the flap blocks. The $C_A$ data for $\delta_F = 30^\circ$ however show the influence of flap shock detachment at the higher incidence angles leading to falling off in the rate of increase of the flap load, as was found in the measurements of ref. 35.

Centre of pressure

The position of the centre of pressure (i.e. the inter-section of the aerodynamic force vector with the balance axis) derived from the normal force and pitching moment measurements is plotted in fig. 54

versus incidence for each of the three flap angles.

The general trend of these data, showing a forward movement of the c.p. with incidence, is in conformity with the increasing contribution of the wing panel pressure relative to the flap load with increasing incidence. The greater movement of the c.p. on the $70^{\circ}$ delta is also consistent with the greater loss in flap effectiveness due to more extensive separation in this case.

Lift/drag ratio

The L/D ratio, a parameter of particular importance to cruise vehicles, calculated from the balance measurements are presented in fig. 55 . Before discussing the experiemntal data, the theoretical shape of the L/D vs. incidence curve may be considered. For a flat plate wing at incidence $\alpha_w$ in inviscid supersonic flow, where the aerodynamic force is exclusively pressure generated (i.e. axial force being zero), we have $L/D = \text{Cot}\alpha_w$, irrespective of the magnitude and distribution of pressure. This is merely a consequence of the force vector remaining normal to the wing plane with varying incidence. At hypersonic speeds, for a flat-bottomed configuration at incidence angles when the upper surfaces are lee-ward and therefore aerodynamically insignificant, this simple expression for L/D is still valid.

Introduction of viscosity and therefore of an axial force generated by friction will cause L/D to be only slightly less than $\text{Cot}\alpha_w$ so long as the pressure force is dominant. With reducing incidence (and therefore increasing relative magnitude of the axial force due to friction) L/D progressively falls below $\text{Cot}\alpha_w$ and finally drops sharply towards zero as the upper surfaces become windward.

These features are evident in the theoretical curve shown for $\delta_F = 0^{\circ}$ (fig.55 ) which fairly well predicts the present test results as well as those of Opatowski becoming practically coincident with $\text{Cot}\alpha_w$ for $\alpha_o > 15^{\circ}$ (or $\alpha_w > 18^{\circ}$).

The flapped wing on the other hand experiences a relatively large axial force due to the flap pressure load, and in this case the L/D will obviously be much below $\text{Cot}\alpha_w$. However, when the flap load is relatively so large as to dominate the aerodynamic characteristics of the configuration (as with increasing flap area and/or deflection), we may expect L/D to approximate to $\text{Cot}\alpha_F$ (where $\alpha_F = \alpha_w + \delta_F$). The measurements follow this trend increasingly with incidence and flap angle. At $\delta_F = 30^\circ$, the data are reasonably well predicted by this simple law throughout the incidence range. The two-dimensional shock theory also tends closer to the $\text{Cot}\alpha_F$ curves with increasing incidence and flap deflection. These comparisons clearly show that the aerodynamic characteristics of the configurations under study are essentially flap-dominated when $\alpha_F > 20^\circ$.

Comparison with free-flight tunnel results

The $76^\circ$ delta with $10^\circ$ and $20^\circ$ flap angles was tested by the free-flight method in the N.P.L. Shock Tunnel at Mach 8.6 and Reynold's number (based on centre-chord length) of $0.56 \times 10^6$ (see ref. 43 for details). The force coefficients are compared in fig. 56 , and the centre of pressure results in fig. 55 . The lift/drag ratio comparisons are given in fig. 54 .

The N.P.L. model was somewhat thinner (the angle between upper ridge line and the bottom surface being $5^\circ$). Due to the method of construction (from expanded polysterene beads to achieve light weight necessary for the free-flight technique), the leading edges and the apex were visibly blunter in comparison with the present metal model.

Considering these small differences in the model geometry as well as in the test conditions between the balance and free-flight tests, the agreement between the two sets of results is regarded as excellent. No systematic discrepancies are noticeable in these comparisons to

suggest a measurable aerodynamic interference effects of the balance sting on the present measurements.

Comparison with estimates

The inviscid aerodynamic coefficients of the 76° flapped delta were calculated using the following methods:

1. Two-dimensional shock theory - The pressures over the windward surfaces of the wing and flap were assumed to be uniform and given by two-dimensional shock compression of the free-stream through the wing and flap shocks respectively.

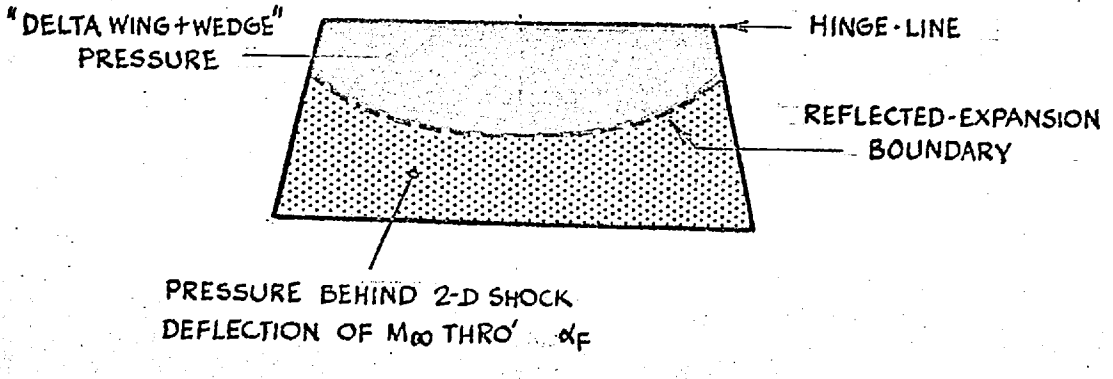
2. Delta wing + wedge - Here again uniform pressures over the wing and flap surfaces were assumed. When the leading-edge shocks were detached (i.e. $\alpha_o > 3^\circ$) the wing pressure was calculated from Kennet's theory using eqs. 4 and 5.* The flap pressure was then obtained via two-dimensional shock compression starting with the calculated delta wing pressure. Since the wing pressure according to Kennet's theory (for detached shocks) is below the two-dimensional value, the flap loads calculated by this method are significantly less (and more realistic) than the two-dimensional shock theory predictions specially at higher incidence and flap angles.

3. Reflected-expansion effect - For the case of $\delta_F = 30^\circ$, when the flap load was substantially influenced by the reflected expansion as already noted, a simplified flap pressure field was assumed to estimate this effect. The reflected-expansion impingement boundary was calculated as described in 8.2, and uniform but different pressure levels assigned to the portions of the flap on either side of the boundary. Between the hinge-line and the expansion impingement, the pressure was

---

* These equations are convenient as they directly give the average windward pressure coefficient. Virtually the same result would be obtained by integrating the delta wing pressure distributions calculated from Squire's theory, (see fig. 6).

calculated by the method 2 above. The pressure over the rest of the flap was obtained from two-dimensional shock compression resulting from a deflection of the free-stream through the flap incidence angle $\alpha_F = \alpha_w + \delta_F$. This scheme is illustrated in the following sketch:*




The contributions of the upper surfaces when leeward (i.e. $\alpha_o > 3^\circ$) and of the base were found to be negligible in the calculations of the overall aerodynamic coefficients.

The $76^\circ$ delta configuration was chosen for the purpose of comparing the measurements with estimates (figs. 57 to 59 ) since the effects of separation in this case were evidently smaller and therefore a better assessment of the inviscid predictions was possible.

At $\delta_F = 10^\circ$ when separation is absent or limited, the aerodynamic coefficients are quite well predicted by the two-dimensional shock theory.

With increasing separation at higher flap deflections, the two-dimensional shock predictions increasingly over-estimate the coefficients. The use of more realistic calculations for the delta wing

---

* The measured pressure field over the flap in typical cases (e.g. fig. 51 ) provide support for this simplified model.

pressure, however, significantly improves the comparison with experiment and indicates that the separation effects on flap loads are not as large as suggested by the disparity between the two-dimensional shock calculations and measurements (see comparisons for $\delta_F = 20^\circ$).

With $\delta_F = 30^\circ$, a substantial over-estimate of the force and moment coefficients is still evident relative to the delta wing + wedge prediction, particularly at the higher incidence (best seen in the $C_M$ comparisons, fig.58 ). When the estimated correction for the reflected-expansion effect is applied, however, a rather remarkable agreement with the measured data is obtained. Note that the agreement continues up to the incidence when a break in the aerodynamic coefficients (believed to mark the onset of the flap shock detachment) occurs, in all three components.

While the procedure adopted here for estimating the reflected expansion effect on the flap load is a highly simplified one, it is nevertheless successful in providing the magnitude of an evidently important phenomenon.

For the case of the $76^\circ$ delta wing, the simple inviscid calculations give a reasonably good prediction of the aerodynamic load components even in the presence of separation over a fairly wide range of incidence and flap deflection.

## 9. FLOW REGIMES ON FLAPPED DELTA WINGS

The various regimes of flow that appear over a delta wing with trailing-edge flaps at hypersonic speeds in the range of incidence and flap deflection can now be summarised in broad terms. This is conveniently done with reference to fig. 60 , which depicts the different viscous and inviscid influences that primarily determine flap effectiveness, and provides an indication of the regimes where the dominating

physical factors must be taken into consideration in any prediction procedure. This diagram has been prepared on the basis of present experimental results and analysis for the 76° delta, for purpose of illustration. For other delta wings, operating at different free-stream conditions, the boundaries will shift but qualitatively the presentation in fig. 60 will remain valid. The parameters which affect these boundaries are discussed below.

The first boundary is that corresponding to laminar incipient separation (estimated from the data shown in fig. 36 ). The favourable shift relative to the two-dimensional prediction is noted. Increasing Mach no. and reducing Reynold's no. raise the incipient separation boundary to higher flap angles. It should be noted that crossing this boundary (which is based on the centre-chord Reynold's no.) does not necessarily lead to separation over the entire span. Within the regime of unseparated flow, and with limited separation, simple inviscid theory using appropriate average pressure on the delta wing (according to attached or detached leading-edge shock), followed by two-dimensional shock compression over the flap gives a good estimate of the overall aerodynamic characteristics.

Above the incipient separation boundary, increasing separation with flap deflection at $\alpha_o = 0°$ culminates in a laminar "conical" separation covering most of the wing surface and causing substantial loss in flap effectiveness. With increasing incidence (or local $R_L$) however, the onset of transition causes separation to diminish rapidly.

At higher incidence and flap anles the pressures over the flap surface are increasingly influenced by the reflected expansion (arising from the interaction of the wing and flap shocks) resulting in a progressive loss of flap effectiveness. This is primarily an inviscid boundary, and increasing Mach no. and flap chord will accelerate its

appearance. In this regime, the effects of separation are found to be relatively less important. An inviscid approach, using available theories to calculate the wing shock envelope and its interaction with an assumed two-dimensional flap shock, permits a reasonable prediction of the flap loads.

Finally, at large incidence and flap deflection, when the local Mach no. on the wing reduces to low values, detachment of the flap shock occurs. Across this boundary (which is reasonably well predicted from two-dimensional shock theory) a strong shock appears over the flap causing large and discontinuous adverse changes in the aerodynamic characteristics. Previous investigations have covered this regime, which is of particular relevance to re-entry type vehicles.

## 10. SUMMARY OF RESULTS

The delta wing force coefficients without flap were in agreement with previous measurements and reasonably well estimated by available inviscid theories upto $\alpha_w = 23^\circ$, the maximum tested. The centre of pressure movement with incidence followed the predicted behaviour with respect to the viscous interaction effect. The wing shock stand-off angle in the centre-plane was also in good agreement with theory, outside the viscous interaction regime. Some data on centre-line transition on the two delta wings (from schlieren photographs) were obtained which confirmed the known trends of $R_T$ with unit Reynold's no. and leading-edge sweep. Pressure measurements on the windward surface of the delta wings up to $18^\circ$ incidence were in general agreement with available hypersonic data and with Squire's theory.

Flow visualisation studies and pressure measurements over the flapped delta surfaces provided a consistent physical description of the varying three-dimensional separation patterns. At low values of local

Reynold's no., the greatly thickened boundary layer on the wing centre-line (resulting from a viscous interaction effect peculiar to the delta) allowed considerable upstream propagation along the centre-chord of the interaction due to separation. At increased Reynold's no. the first appearance of transition on the centre-chord caused a local collapse of separation while outboard the flow was still separated These changing separation patterns together with reflected wave impingement produced complex pressure fields on the flap. The separated flows were qualitatively similar on the two delta wings.

At the Reynold's no. of the balance tests ($R_L' = 0.85 \times 10^6$) flap induced separation was largely transitional. The earlier onset of transition produced consistently smaller separation length on the $76^\circ$ delta, which resulted in better flap effectiveness on this wing at all incidences and flap angles.

The force and moment coefficients varied smoothly in the range of incidence and flap deflection. The balance measurements were in good agreement with the results of free-flight tests provided by NPL (for $76^\circ$ delta, $\delta_F = 10^\circ$ and $20^\circ$). Comparison with results of simple inviscid calculations showed that while the two-dimensional shock theory predicted the aerodynamic coefficients for $\delta_F = 10^\circ$ (i.e. when separation was absent or limited), it increasingly over-estimated the loads at greater flap deflection. The assumption of a two-dimensional compression across the flap shock applied to a more rational theory (such as Kennet's) for the delta wing pressure at incidence (corresponding to detached leading-edge shock) allowed a good estimate for the $76^\circ$ delta upto $\delta_F = 20^\circ$ even with separation present.

With $30^\circ$ flap deflection, the dominating influence was the impingement of reflected expansion wave from the wing shock/flap shock interaction. A simplified calculation of the impingement boundary over

the flap using a model of three-dimensional interaction of the theoretical wing shock envelope with a plane flap shock, (which agreed with experimentally observed boundary on the 76° delta) provided a good prediction of the aerodynamic coefficients. These results indicated that a proper description of the inviscid hypersonic flow field over the 76° flapped delta, which is possible by the application of available theories, could lead to useful engineering estimate of the flap effectiveness even in the presence of separation. With the 70° delta, however, on which the effects of separation were more severe in the range of the present tests, an inviscid approach would be less successful for $\delta_F > 10°$.

Limited data for the 76° delta suggested that the flap angle for laminar incipient separation was higher on the delta wing than for the two-dimensional case. Also, the transitional incipient separation boundary shifted to a smaller Reynold's no. corresponding to earlier onset of transition. However, the incipient separation for turbulent flow on the delta appeared to be the same as for two-dimensional.

## REFERENCES


1. Mueller, G.E., "The new future for manned spacecraft developments" Astronautics and Aeronautics. Mar. 69. Vol. 7, No.3, p.24.
2. Bertram, M.H. et al, "The aerodynamics of hypersonic curising and boost vehicles" NASA SP-23. 1962.
3. Kaufman, L.G. et al, "A review of hypersonic flow separation and control characteristics". ASD TDR 62-168, 1962.
4. Sterret, J.R. and Emery, J.C., "Experimental separation studies for two-dimensional wedges and curved surfaces". NASA TN-1014. 1962.
5. Miller, D.S. et al, "Mach 8 to 22 studies of flow separation due to deflected control surfaces". AIAA Journal. Feb. 1964. Vol. 2, no.2 p.312.
6. Needham, D.A. and Stollery, J.L., "Boundary layer separation in hypersonic flow". AIAA Paper 66-455. 1966.
7. Johnson, C.B., "Pressure and flow-field study at Mach number 8 of flow separation on a flat plate with deflected trailing-edge flap". NASA D-4308. 1968.
8. Fiore, A.W., "An investigation of aerodynamic controls at hypersonic Mach numbers" . Ph.D. Thesis. The Ohio State Univ., 1966.
9. Hill, W.G.Jr., "Analysis of experiments on hypersonic flow separation ahead of flaps using simple flow model". Grumman Aircraft Eng. Corp. RM-383. 1967.
10. Needham, D.A., "Laminar separation in hypersonic flow". Ph.D. Thesis, London University, 1965.
11. Bird, G.A., "Effect of wave interactions on pressure distributions in supersonic and hypersonic flow". AIAA Journal. Vol. 1, pp.634-639. 1963.
12. Fitzgerald, P.E., "The effect of bow-shock - flare-shock interaction on the static longitudinal stability of flare-stabilized bodies at hypersonic speeds." NASA TM X-664. 1962.

13. Popinski, Z. and Ehrlich, C.F., "Development design methods for predicting hypersonic aerodynamic control characteristics". AFFDL-TR-66-85. 1966.

14. Chapman, D.R. et al, "Investigation of separated flows in supersonic and subsonic streams with emphasis on the effect of transition." NASA Report 1356. 1958.

15. Sterrett, J.R. and Emery, J.C., "Extension of boundary layer separation criteria to a Mach no. of 6.5 by utilizing flat plates with forward facing steps." NASA TN D-618. 1960

16. Putnam, L.E., "Investigation of effects of ramp span and deflection angle on laminar boundary layer separation at Mach 10.03". NASA TN D-2833, 1965.

17. Chernyi, G.G., "The planar wing in hypersonic flow". Doklady Akad. Nauk. S.S.S.R., Vol. 161, no.4, 1965. (R.A.E. Lib. Trans. no.1112).

18. Dunavant, J.C., "Investigation of heat transfer and pressures on highly swept flat and dihedralled delta wings at Mach numbers of 6.8 and 9.6 and angles of attack to 90°". NASA TM X-688, 1962.

19. Collis, D.C., "A hypersonic wind tunnel study of a thick delta wing". A.R.L. (Austr.) Aero. Note 232, 1964.

20. Babaev, D.A., "Numerical solution of the problem of supersonic flow past the lower surface of a delta wing". AIAA Journal, Vo. 1, no. 9, Sept. 1963.

21. Opatowski, T., "An experimental study of the flow around and the forces developed by hypersonic lifting vehicles". Ph.D. Thesis, London Univ. 1967.

22. Messiter, A.F., "Lift of slender delta wings according to Newtonian theory". AIAA Journal, Vo. 1, pp.794-802, 1963.

23. Hida, K., "Thickness effect on the force of slender delta wings in hypersonic flow". AIAA Journal, Vol. 3, pp.427, 1965.

24. Squire, L.C., "Calculated pressure distributions and shock shapes on thick conical wings at high supersonic speeds". Aero. Quart. Vol. XVIII, pp.185-206. 1967.

25. Squire, L.C., "Calculations of the pressure distribution on lifting conical wings with applications to the off-desig. behaviour of wave-riders". AGARD C.P.30, 1968.

26. Bertram, M.H. and McCauley, W.D., "Investigation of the aerodynamic characteristics at high supersonic Mach numbers of a family of delta wings having double-wedge sections with the maximum thickness at 0.18 chord". NACA RM L54G28, 1954.

27. Post J., "Lift and drag-due-to-lift of thin delta wings at hypersonic speeds and high angles of attack". SR-126-TM-A-6, Convair.

28. Close, W.H., "Hypersonic longitudinal trim, stability, and control characteristics of a delta-wing configuration at high angles of attack". NASA TM X-240, 1960.

29. Kennet, H.M., "The inviscid hypersonic flow on the windward side of a delta wing". AIAA Paper no. 63-55, 1963.

30. Nagel, A.L. et al, "Analysis of hypersonic pressure and heat transfer tests on delta wings with laminar and turbulent boundary layers". NASA CR-535, 1966.

31. Ginoux, J.J., "On some properties of re-attaching laminar and transitional high speed flows". VKI TN 53, 1969.

32. Cheng, H.K. et al, "Boundary layer displacement and leading-edge bluntness effects in high temperature hypersonic flow". J. Aero. Sci., vol. 128, no.5, p.353, 1961.

33. ASD-TDR-63-772 (Classified report prepared by Cornell Aeronautical Laboratory for U.S. Air Force).

34. Davies, L., "On the effects of viscous interaction for a flat delta wing at incidence". NPL Aero. Rep. 1315, 1970.

35. Meckler, L., "Effects of separation on the characteristics of aerodynamic controls on a representative hypersonic configuration at Mach 8". Grumman Res. Dept. Report RE-312, 1967.

36. Creager, M.O., "The effect of leading-edge sweep and surface inclination on the hypersonic flow field over a blunt flat plate". NASA Memo 12-26-58A, 1959.

37. Fetterman, D.E. and Luther, N.Jr., "An analysis of the delta-wing hypersonic stability and control behaviour at angles of attack between 30° and 90°". NASA TN D-1602, 1963.

38. Fetterman, D.E., "A method for predicting the normal-force characteristics on delta wings at angles of attack from 0° to 90°." NASA TM X-757, 1963.

39. Keyes, J.W. and Ashby, G.C., "Calculated and experimental hinge moments on a trailing-edge flap of a 75° swept delta wing at Mach 6". NASA TN D-4268, 1967.

40. Whitehead, A.H. and Keyes, J.W., "Flow phenomena and separation over highly swept delta wings with trailing-edge flaps at Mach 6". AIAA Paper no. 68-97, 1968.

41. Keyes, J.W., "Pressures and heat transfer on a 75° swept delta wing with trailing-edge flap at Mach 6 and angles of attck to 90°". NASA TN D-5418, 1969.

42. Mukherejee, D., "Flow visualisation and control effectiveness studies of a delta wing with full and part span trailing-edge flaps at hypersonic speeds". M.Sc. Thesis, London.Univ., 1969.

43. Davies, L. et al, "A comparison between free flight and balance measurements for a 76° swept delta with a full span trailing-edge flap at hypersonic speed". NPL Report (to be published), 1970.

44. Pate, S.R. and Schueler, C.J., "An investigation of radiated aerodynamic noise effects on boundary layer transition in supersonic and hypersonic tunnels." AIAA Paper no. 68-375, 1968.

45. Moeckel, W.E., "Some effects of bluntness on boundary layer transition and heat transfer at supersonic speeds". NACA Rep. 1312, 1957.

46. Owen, P.R. and Randall, D.G., "Boundary layer transition on a swept back wing". R.A.E. TM Aero 277, 1952.

47. Chapman, G.T., "Some effects of leading-edge sweep on boundary layer transition at supersonic speeds". NASA TN D-1075, 1961.

48. Jillie, D.W. and Hopkins, E.J., "Effects of Mach number, leading-edge bluntness and sweep on boundary layer transition on a flat plate". NASA TN D-1071.

49. Deem, R.E. and Murphy, J.S., "Flat plate boundary layer transition at hypersonic speeds". AIAA Paper no. 65-128, 1965.

50. Dunning, R.W. and Ulmann, E.F., "Effects of sweep and angle of attack on boundary layer transition on wings at Mach number 4.04". NACA TN 3473, 1955.

51. Chapman, G.T., "Transition of the laminar boundary layer on a delta wing with $74^{\circ}$ sweep in free flight at Mach numbers from 2.8 to 5.3". NASA TN D-1066, 1961.

52. Wilson, J.L. et al, "Heat transfer and transition measurements at M = 8.5 on a delta model and a flat plate at incidence". R and M No. 3574, 1969.

53. Brown, C.S. and Goldsmith, E.L., "An experimental and theoretical comparison at M = 4 of the lift-to-drag ratio of some possible aircraft shapes". R.M. no. 3600, 1969.

54. Richards, B.E., "Transitional and turbulent boundary layers on a cold flat plate in hypersonic flow". Aero. Quarterly, 18, August 1967.

55. Libby, P.A. et al, "Laminar boundary layer near the plane of symmetry of a hypersonic inlet". AIAA Journal, Vol.1, p.2732, 1963.

56. Cooke, J.C., "Leading-edge effects on caret wings". R.A.E. T.N. Aero 2943, 1964.

57. Hamilton, H.H. and Dearing, J.D., "Effects of hinge-line bleed on heat transfer and pressure distribution over a wedge-flap combination at Mach 10.4". NASA TN D-4686, 1968.

58. Opatowski, T., "Gun Tunnel measurements of lift, drag and pitching moment on a 20° cone, a flat delta and a caret wing at a Mach number of 8.3", A.R.C. C.P. 908, 1966.

59. Fancett, R.K., "Boundary layer re-attachment in hypersonic flow". Ph.D. Thesis, London University, 1968.

60. Erdos, J. and Palone, A., "Shock-boundary layer interaction and flow separation". Avco. Tech. Rep. RAD-TR-61-23, 1961.

61. Needham, D.A., "Progress report on the Imperial College hypersonic gun tunnel". Aero. Dept. Report No. 118, 1963.

62. Mayer, J.P., "A limit pressure coefficient and an estimation of limit forces on airfoils at supersonic speeds". NACA RM L8F23. 1948.

63. Rogers, E.W.E., "A note on the aerodynamic problems of hypersonic controls". N.P.L. Aero. Memo. 58. 1968.

## APPENDIX

### Balance Data

$\delta_F = 0^\circ$

$\Lambda = 70^\circ$

| $\alpha_o$ (deg) | $C_N$ | $C_A$ | $\frac{X_{C.P}}{L'}$ |
|---|---|---|---|
| 5 | .076 | .0086 | .660 |
| 10 | .158 | .0215 | .661 |
| 15 | .266 | .0302 | .663 |
| 20 | .391 | .0345 | .663 |

$\Lambda = 76^\circ$

| | | | |
|---|---|---|---|
| 5 | .071 | .0097 | .660 |
| 10 | .158 | .0195 | .664 |
| 15 | .257 | .0260 | .667 |
| 20 | .365 | .0325 | .667 |

## APPENDIX (Contd.)

### Balance Data, $\Lambda = 70^\circ$

| $\alpha_o$ (deg) | $C_N$ | $C_A$ | $-C_M$ | |
|---|---|---|---|---|
| 0 | .033 | .0234 | .0096 | |
| 5 | .128 | .0324 | .0140 | $\delta_F = 10^\circ$ |
| 10 | .239 | .0485 | .0192 | |
| 15 | .371 | .0795 | .0247 | |
| 0 | .106 | .0648 | .0265 | |
| 2.5 | .166 | .0780 | .0338 | |
| 5 | .236 | .103 | .0405 | $\delta_F = 20^\circ$ |
| 10 | .358 | .172 | .0470 | |
| 15 | .510 | .215 | .0421 | |
| 0 | .194 | .154 | .0575 | |
| 2.5 | .280 | .196 | .0645 | |
| 5 | .355 | .236 | .0651 | |
| 10 | .520 | .345 | .0630 | |
| 12.5 | .586 | .378 | .0610 | $\delta_F = 30^\circ$ |
| 15 | .678 | .400 | .0565 | |
| 17.5 | .750 | .410 | .0510 | |
| 20 | .827 | .431 | .0510 | |

## APPENDIX (Contd.)

### Balance Data, $\Lambda = 76^\circ$

| $\alpha_o$ (deg) | $C_N$ | $C_A$ | $-C_M$ | |
|---|---|---|---|---|
| 0 | .046 | .0192 | .0110 | |
| 5 | .148 | .0320 | .0182 | |
| 10 | .270 | .0511 | .0244 | $\delta_F = 10^\circ$ |
| 15 | .386 | .0735 | .0298 | |
| 0 | .129 | .086 | .0314 | |
| 2.5 | .193 | .--- | .0392 | |
| 5 | .271 | .114 | .0495 | $\delta_F = 20^\circ$ |
| 7.5 | .357 | .145 | .0575 | |
| 10 | .426 | .145 | .0636 | |
| 15 | .600 | .192 | .0764 | |
| 0 | .224 | .150 | .0577 | |
| 1.5 | .286 | .192 | .0660 | |
| 2 | .294 | .202 | .0700 | |
| 2.5 | .320 | .209 | .0700 | |
| 5 | .395 | .243 | .0773 | $\delta_F = 30^\circ$ |
| 10 | .576 | .313 | .0907 | |
| 12 | .613 | .342 | .0950 | |
| 15 | .960 | .351 | .0826 | |
| 20 | .820 | .414 | .1020 | |

## List of Figures


1. Idealised windward pressure distributions over flapped wing at hypersonic speeds.
2. Idealised windward pressure distributions over flapped wing with separated flow.
3. Flap effectiveness in two-dimensional flow.
4. Examples of three-dimensional effects in two-dimensional flap-induced separation.
5. Predicted inviscid flow over windward surface of flat delta wings at hypersonic speed (after Chernyi).
6. Comparison of inviscid theories for windward normal force on a flat delta wing.
7. Viscous hypersonic flow over windward surface of delta wing.
8. Two-dimensional force model.
9. Flapped-delta force model (typical).
10. 76° delta wing and flap pressure model.
11. 70° delta wing and flap pressure model.
12. 70° flapped-delta pressure model mounted on variable incidence support.
13. Powder flow visualisation on two-dimensional model.
14. Local conditions on windward surface.
15. Two-dimensional separation data.
16. Incremental normal force and pitching moment on two-dimensional model.
17. 76° delta without flap - balance data.
18. 70° delta without flap - balance data.
19. Delta wing shock angle data.
20. 76° delta without flap - centre-chord pressure distribution.
21. 76° delta without flap - centre-chord pressure vs. incidence.
22. 76° delta centre-chord pressures ($M_\infty$ = 6.8 to 9.6).

23. Pressure distribution normal to leading-edge on delta wings ($\delta_F = 0^\circ$).

24. Delta wing transition data.

25. Schlieren photographs - increasing $\delta_F$ .

26. Flap-induced separation length on delta wings at $\alpha_o = 0^\circ$.

27. Centre-chord pressure distribution on flapped delta. $\alpha_w = 3^\circ$. $\delta_F = 30^\circ$.

28. Powder patterns of separated flow - effect of flap angle at $\alpha_o = 0^\circ$.

29. Constant $C_p$ contours. $\Lambda = 70^\circ$. $\alpha_w = 3^\circ$. $\delta_F = 30^\circ$.

30. Reynold's no. effect on flap pressures. $\Lambda = 76^\circ$. $\delta_F = 30^\circ$. $\alpha_w = 0^\circ$.

31. Typical sequence of schlieren photographs. $\Lambda = 76^\circ$. $\delta_F = 0^\circ$ to $15^\circ$.

32. Flap-induced separation length with flap angle and incidence.

33. Reynold's effect on separation length.

34. Centre-chord pressure distribution on $76^\circ$ flapped delta. $\alpha_w = 8^\circ$. $\delta_F = 30^\circ$.

35. Ditto. $\alpha_w = 13^\circ$. $\delta_F = 30^\circ$.

36. Incipient separation.

37. Powder patterns of separated flow- effect of incidence for $20^\circ$ flap.

38. Surface flow pattern with "mixed" separation (after Whitehead and Keyes).

39. Flap-induced separation at incidence.

40. Constant $C_p$ contours on $76^\circ$ delta wing with and withoutflap.

41. Constant $C_p$ contours on delta wings. $\delta_F = 30^\circ$. $\alpha_w = 3^\circ$.

42. Oil dot visualisation of "mixed" separation.

43. Effect of flap deflection angle on hinge-line pressure distribution.

44. Effect of incidence on hinge-line pressure distribution. $76^\circ$ delta. $\delta_F \doteq 20^\circ$.

45. Flap-induced separation at subsonic speed.

46. Flap shock angle.

47. Pressures over flaptip region.

48. Wing-shock/flap-shock interaction.

49. Calculated and experimental impingement of reflected-expansion on flap centre-line.

50. Three-dimensional shock interaction on flapped delta wing.

51. Comparison of calculated and experimental reflected-expansion impingement boundary.

52. Flapped delta wings - normal force measurements.

53. Flapped delta wings - axial force and pitching-moment measurements.

54. Centre-of-pressure position.

55. Lift/drag ratio of delta wings with and without flaps.

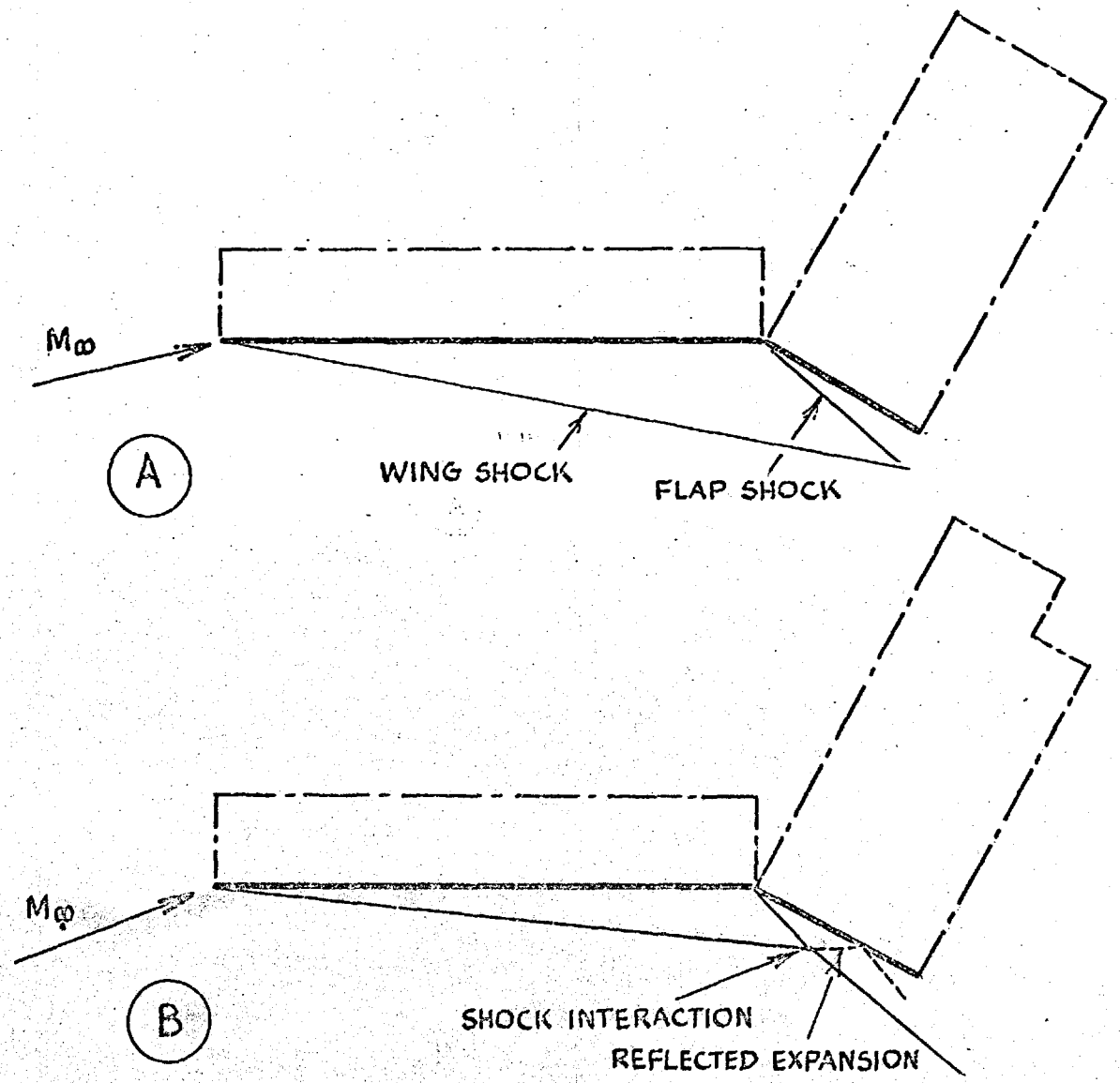
56. Comparison of balance and free-flight (N.P.L.) data for 76° flapped-delta.

57. Normal force comparison with estimates.

58. Pitching-moment comparison with estimates.

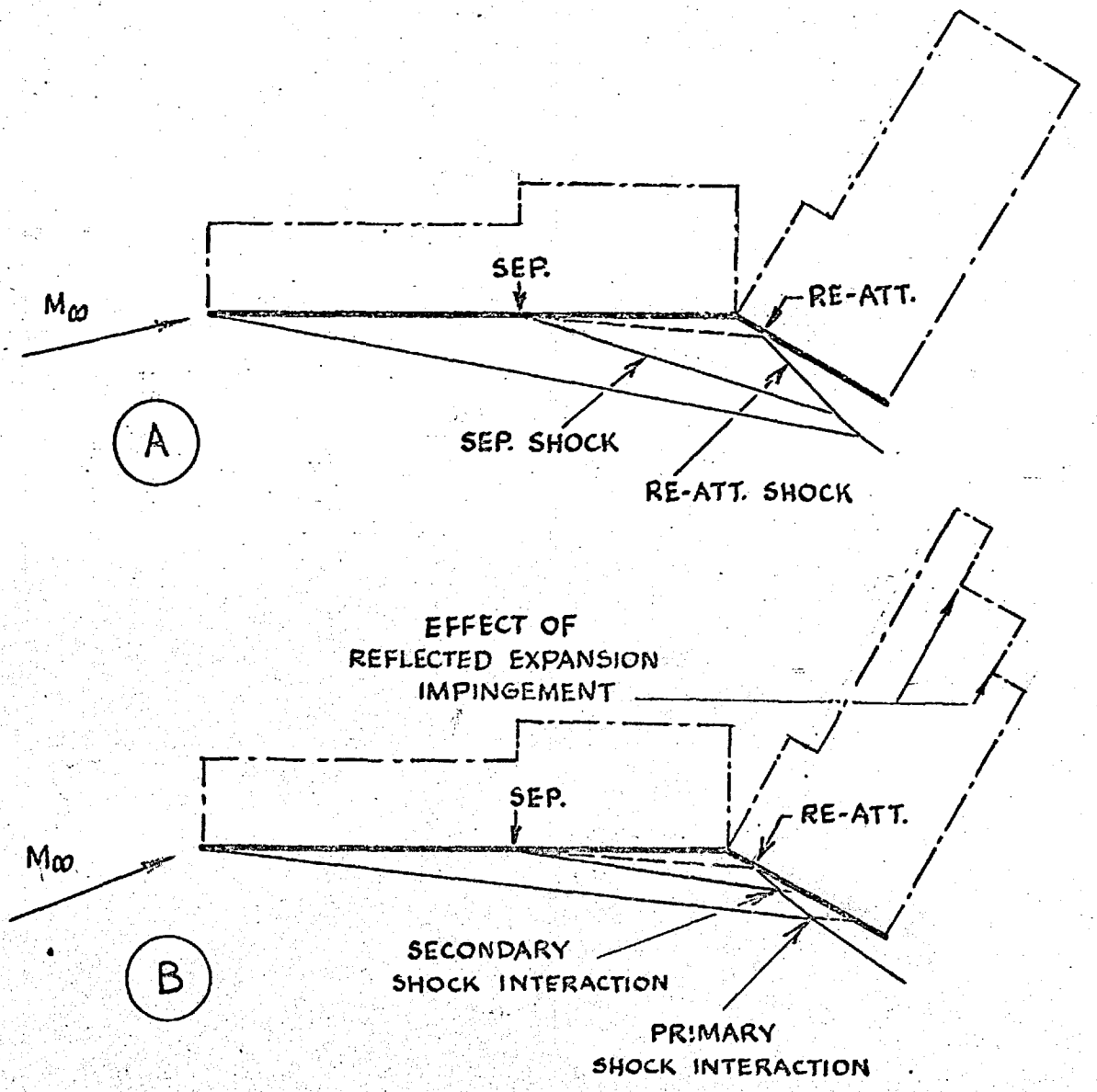
59. Axial force comparison with estimates.

60. Flow regions on 76° flapped delta.




IDEALISED WINDWARD PRESSURE DISTRIBUTIONS OVER FLAPPED WING AT HYPERSONIC SPEED.

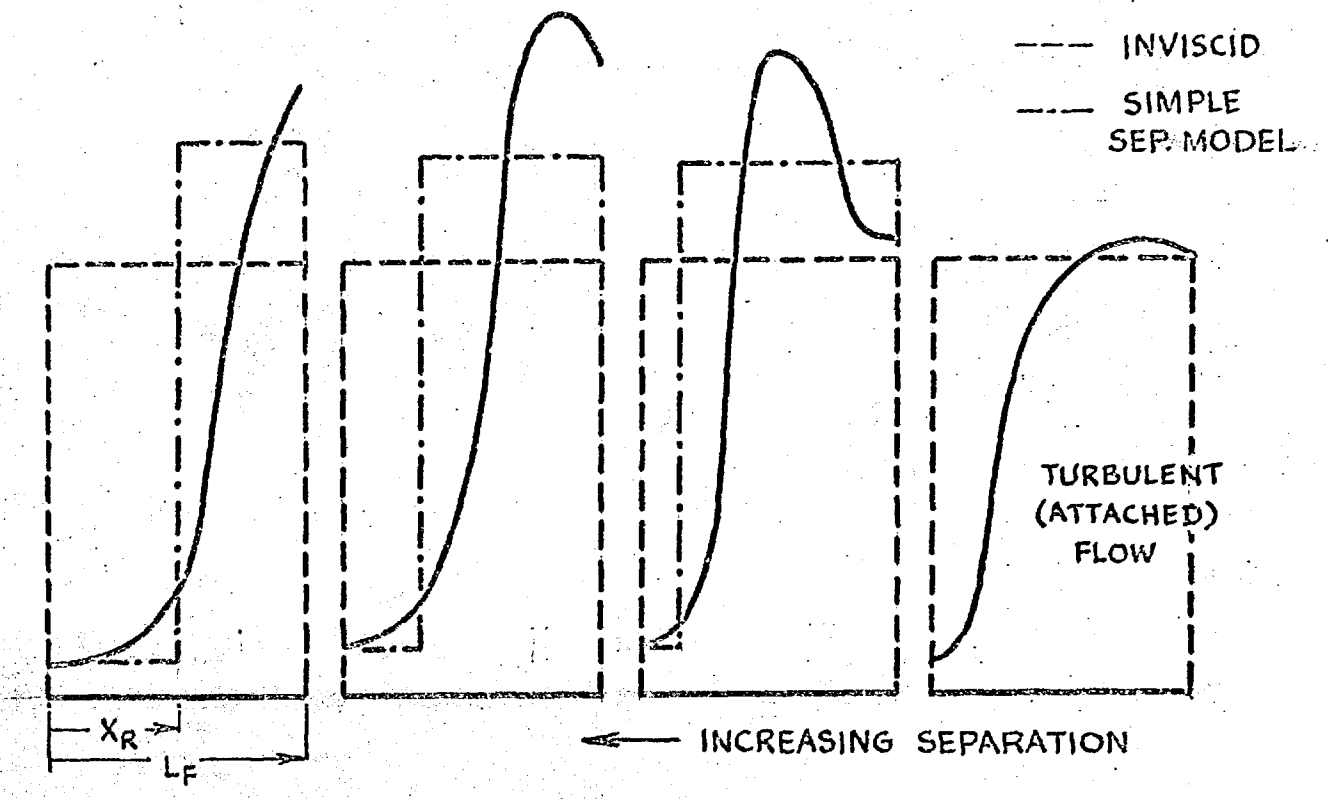
FIG. 1



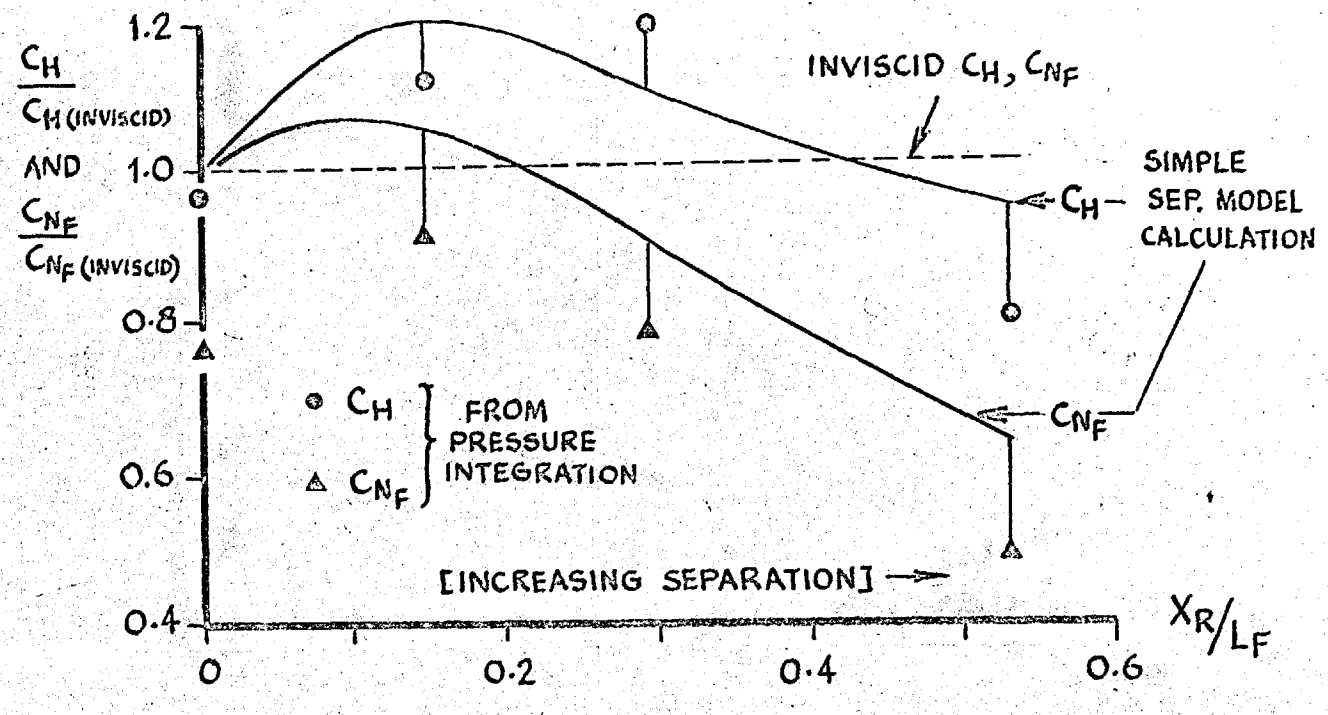

IDEALISED WINDWARD PRESSURE DISTRIBUTIONS OVER FLAPPED WING WITH SEPARATED FLOW

FIG. 2

(A) TYPICAL FLAP PRESSURE DISTRIBUTIONS (JOHNSON, REF. 7)

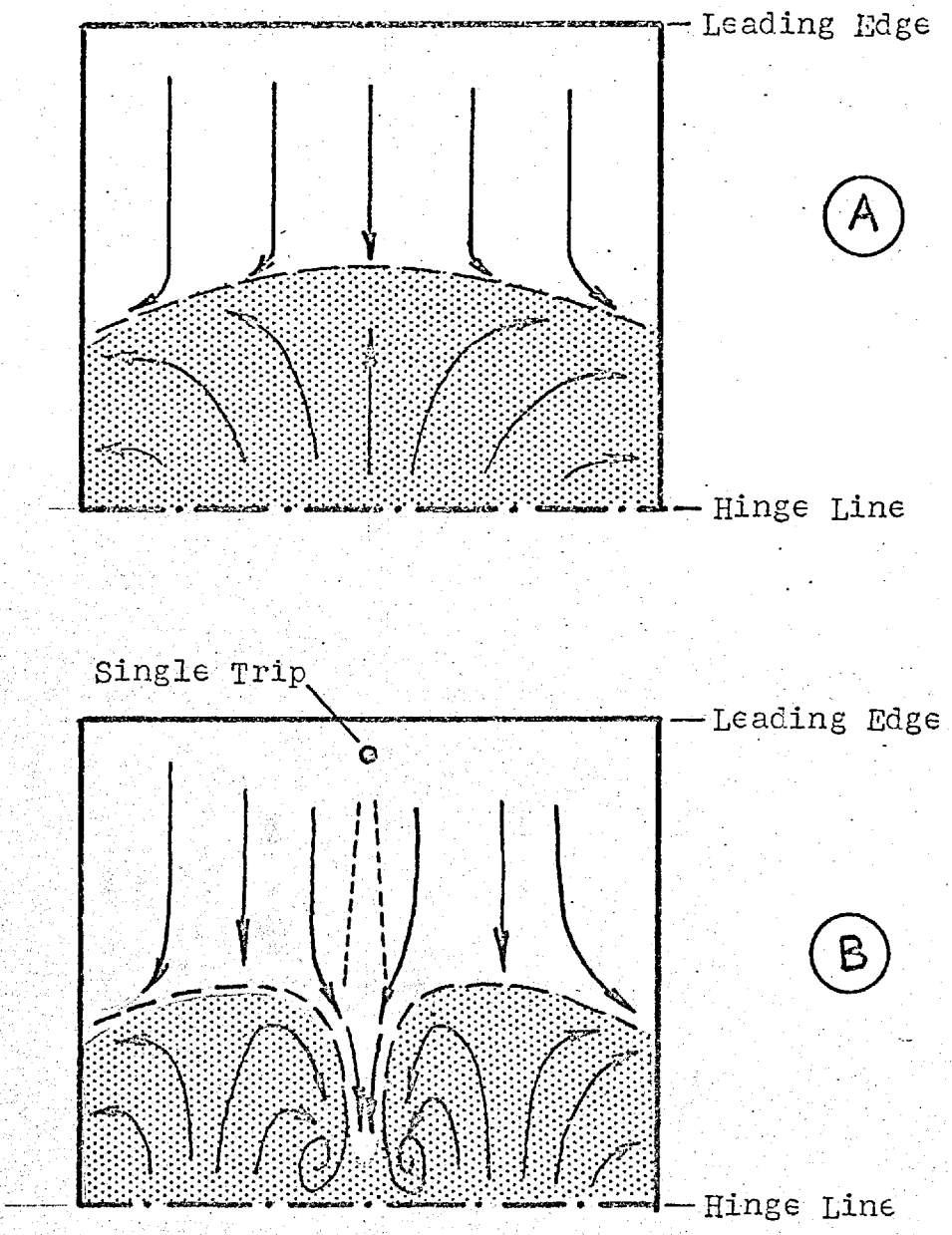



(B) FLAP LOAD CHARACTERISTICS FROM INTEGRATED PRESSURES



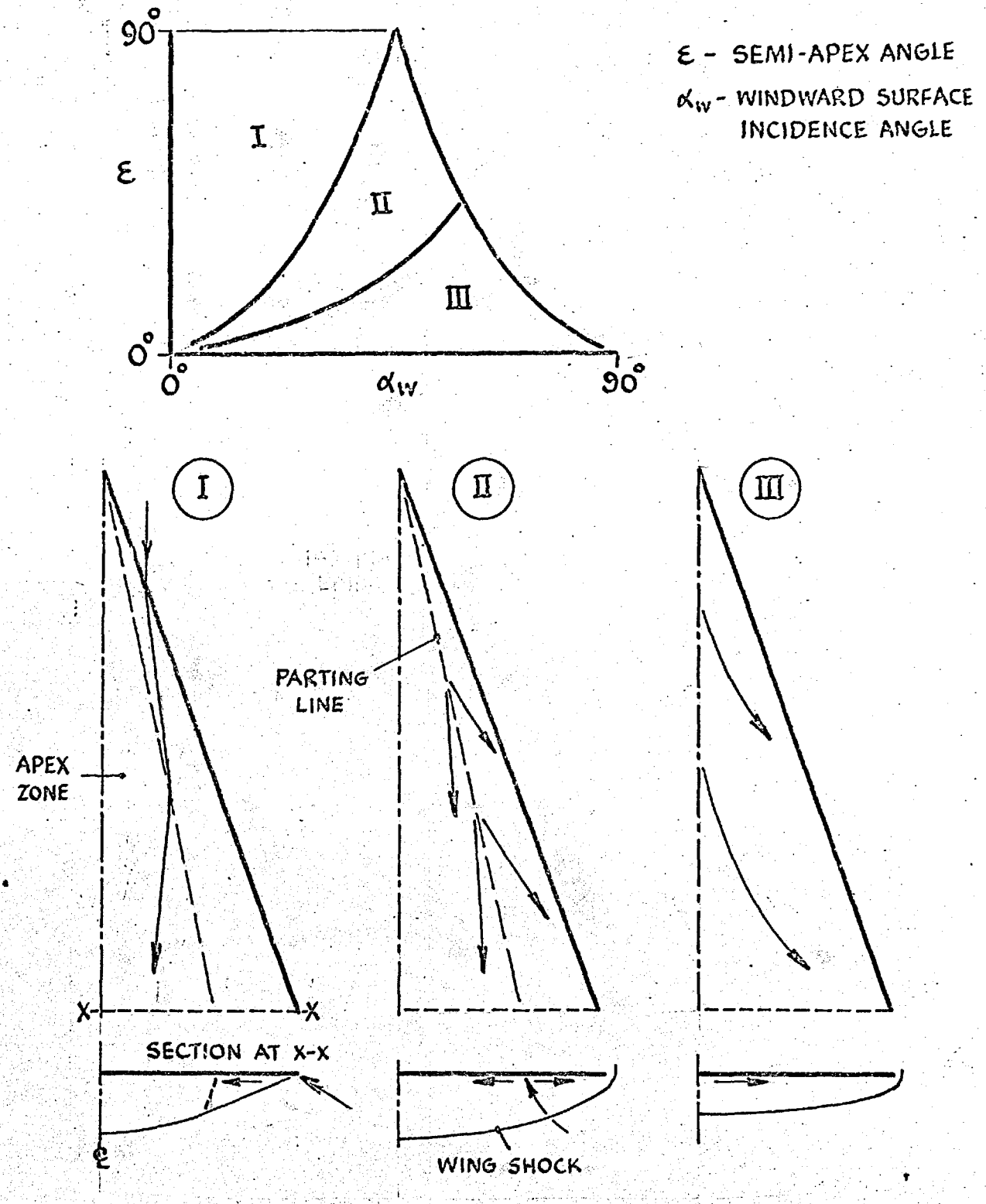

FLAP EFFECTIVENESS IN TWO-DIMENSIONAL FLOW

FIG. 3



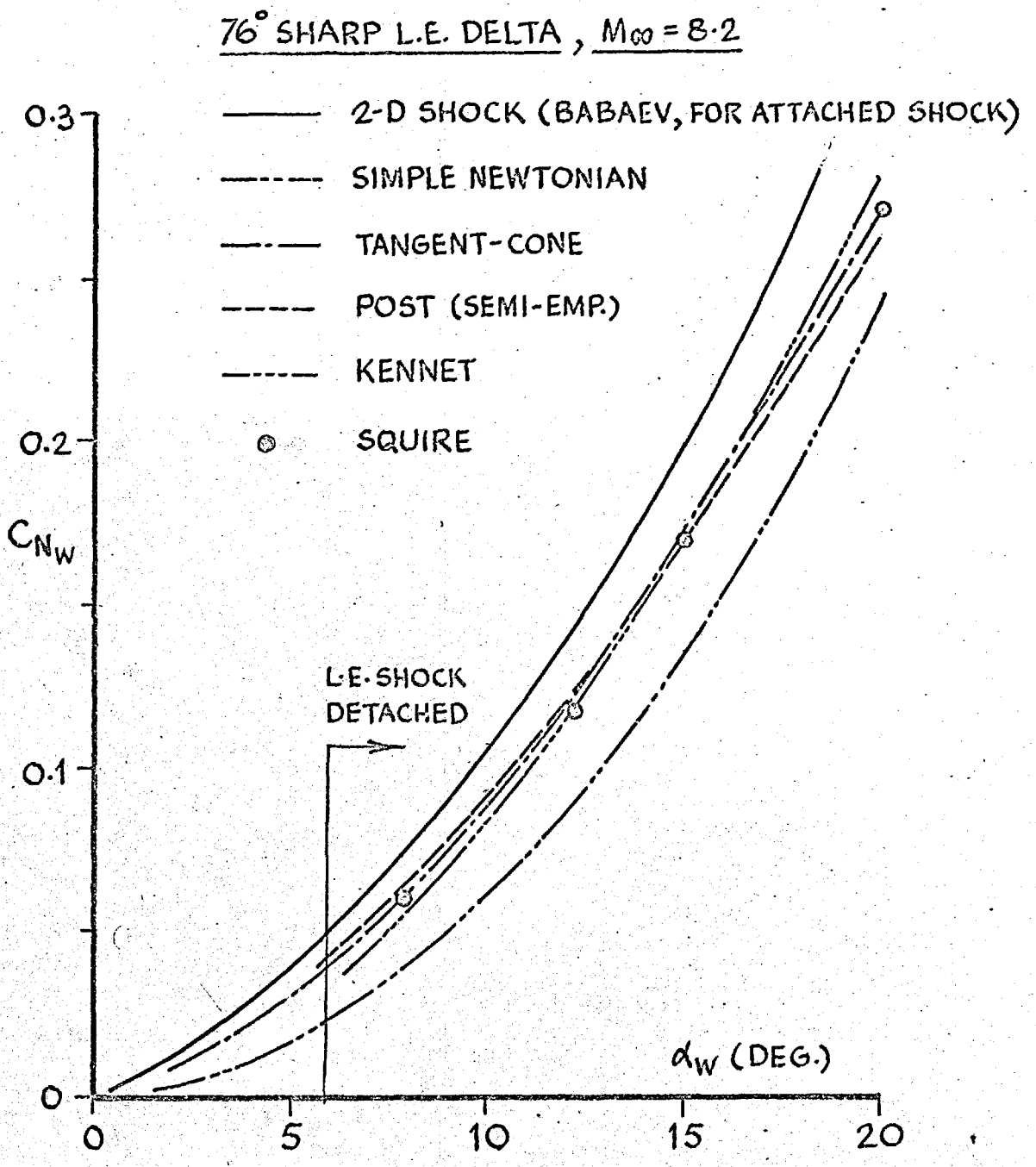

EXAMPLES OF THREE-DIMENSIONAL EFFECTS
IN TWO-DIMENSIONAL FLAP-INDUCED SEPARATION

FIG. 4



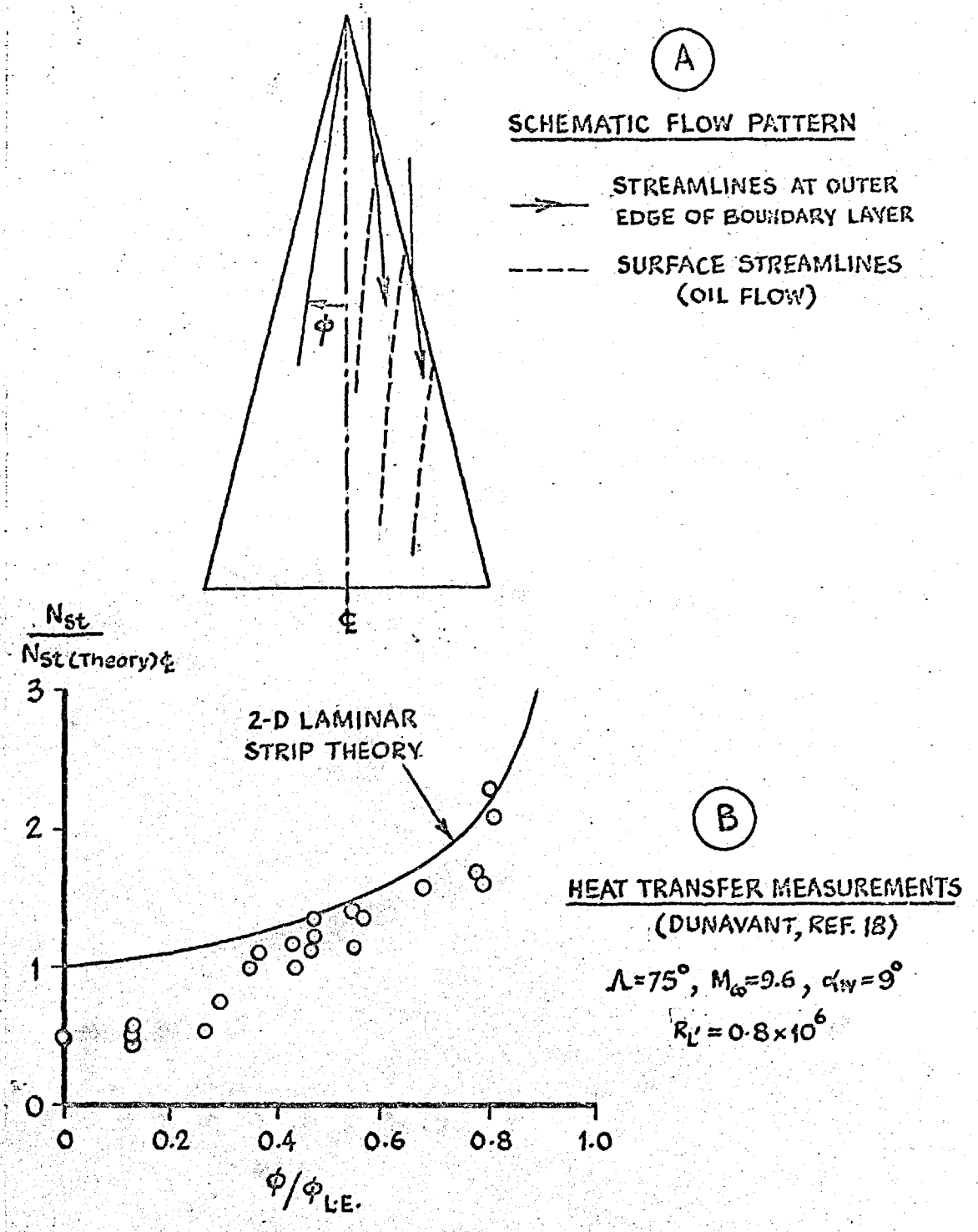

PREDICTED INVISCID FLOW OVER WINDWARD SURFACE OF FLAT DELTA WINGS AT HYPERSONIC SPEED (AFTER CHERNYI)

FIG. 5



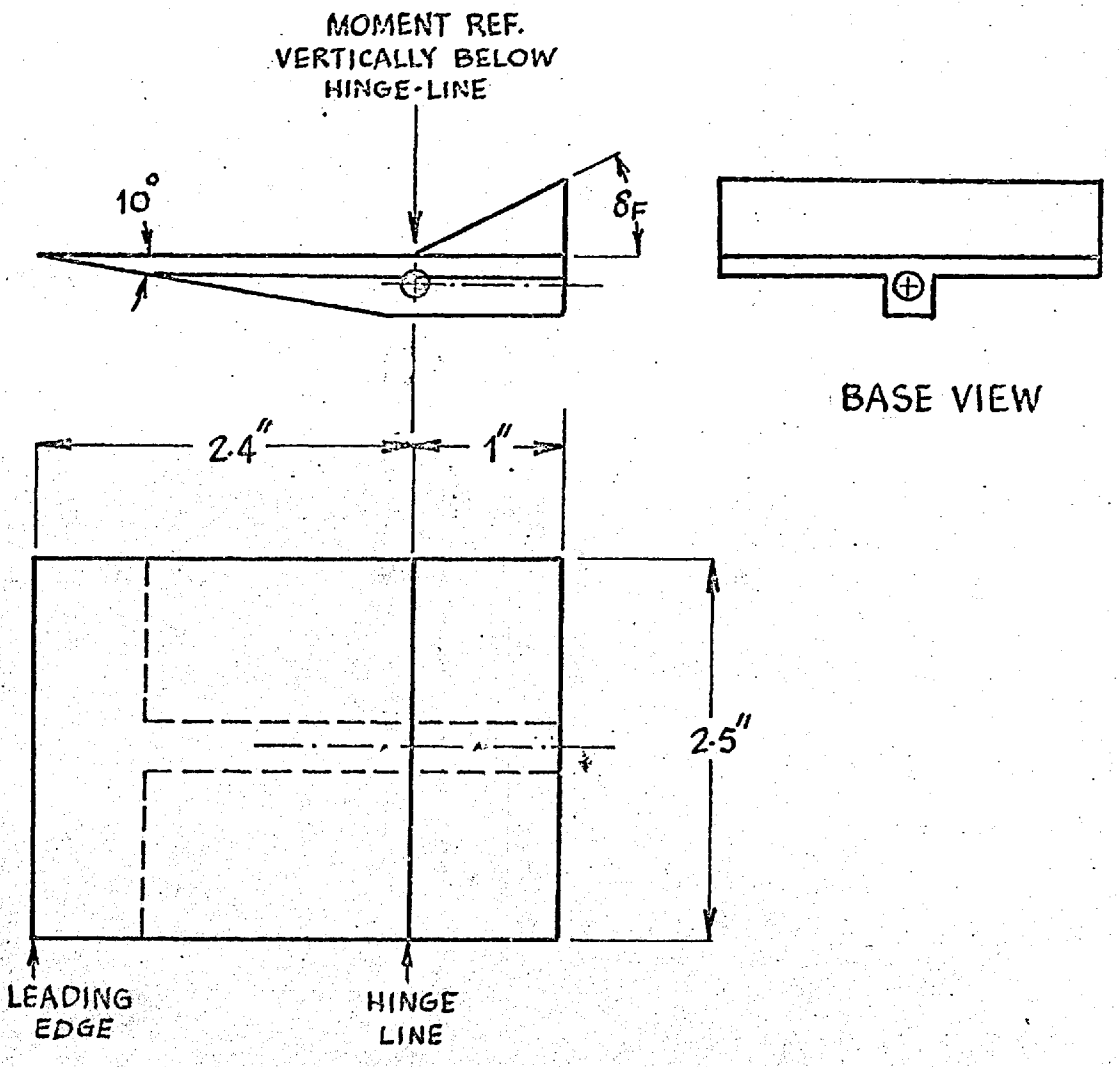

COMPARISON OF INVISCID THEORIES FOR WINDWARD NORMAL FORCE ON A FLAT DELTA WING

FIG. 6



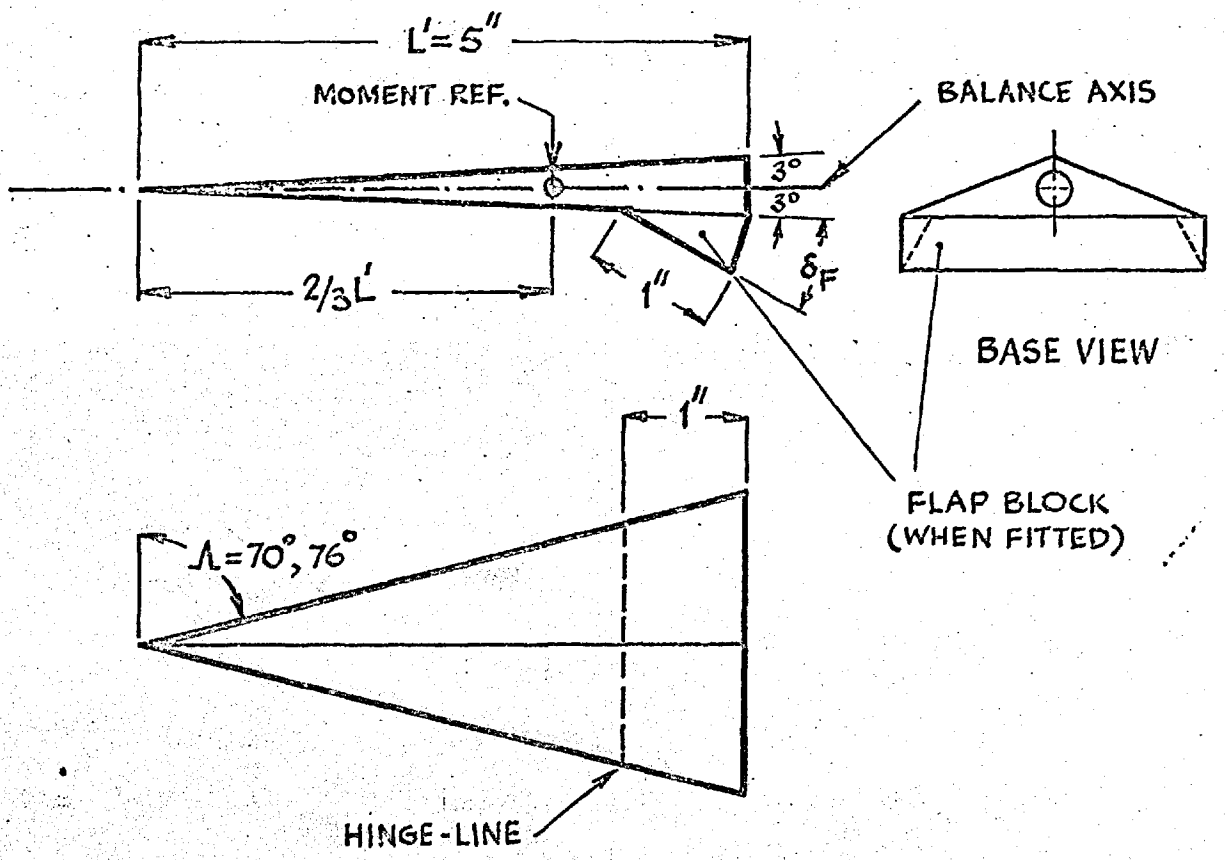

VISCOUS HYPERSONIC FLOW OVER WINDWARD SURFACE OF DELTA WING

FIG.7



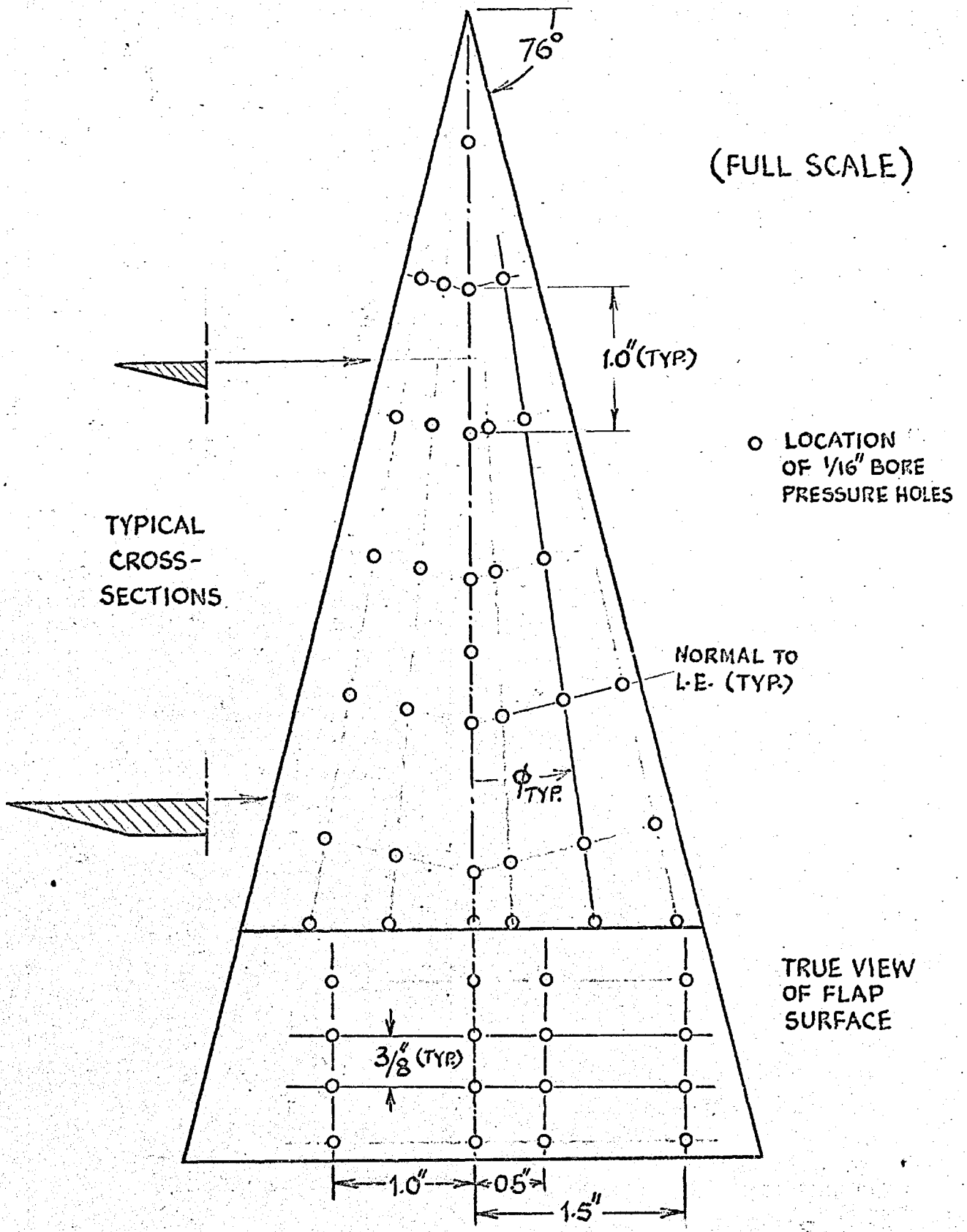

TWO-DIMENSIONAL FORCE MODEL

FIG. 8



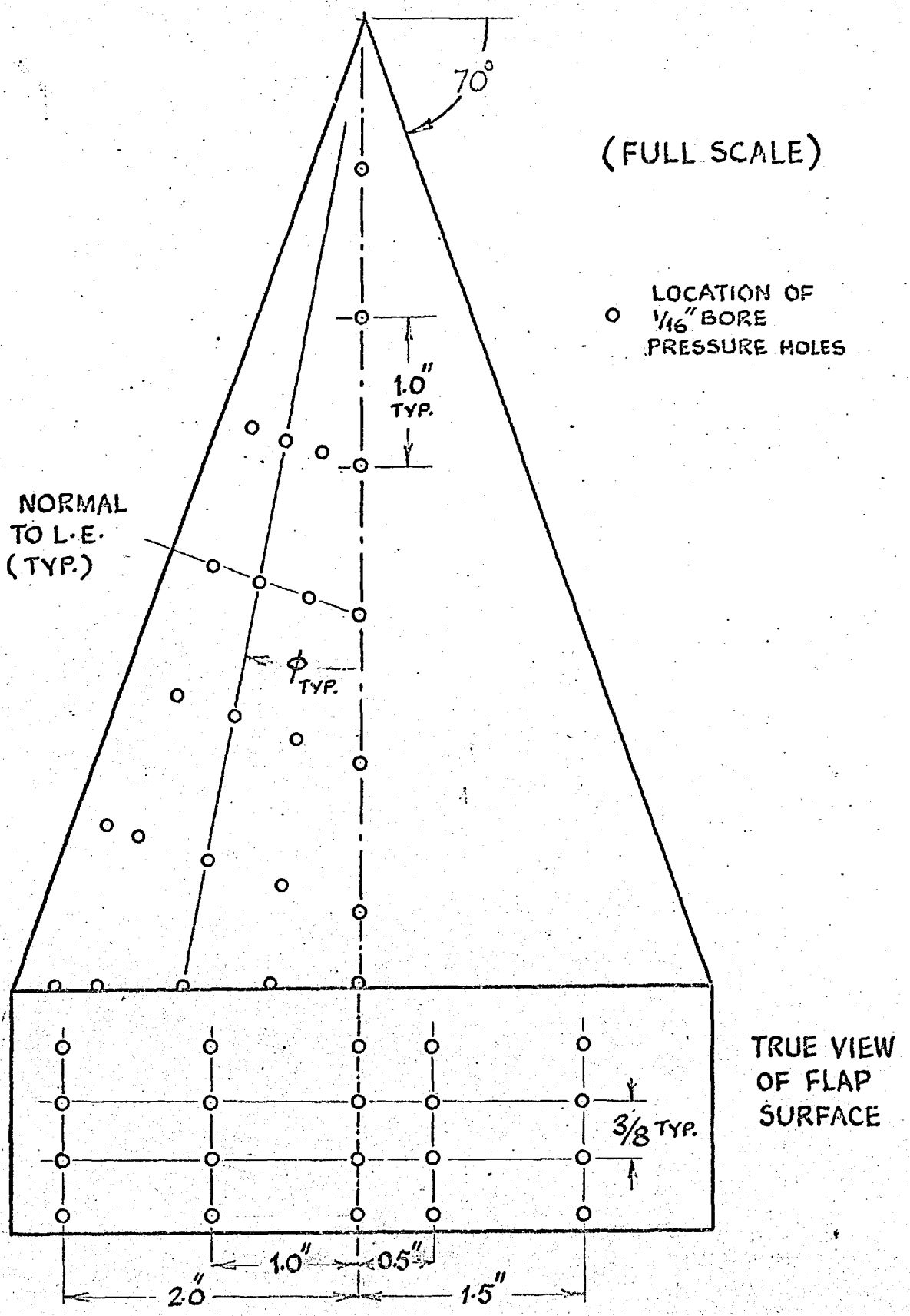

FLAPPED-DELTA FORCE MODEL (TYPICAL)

FIG. 9



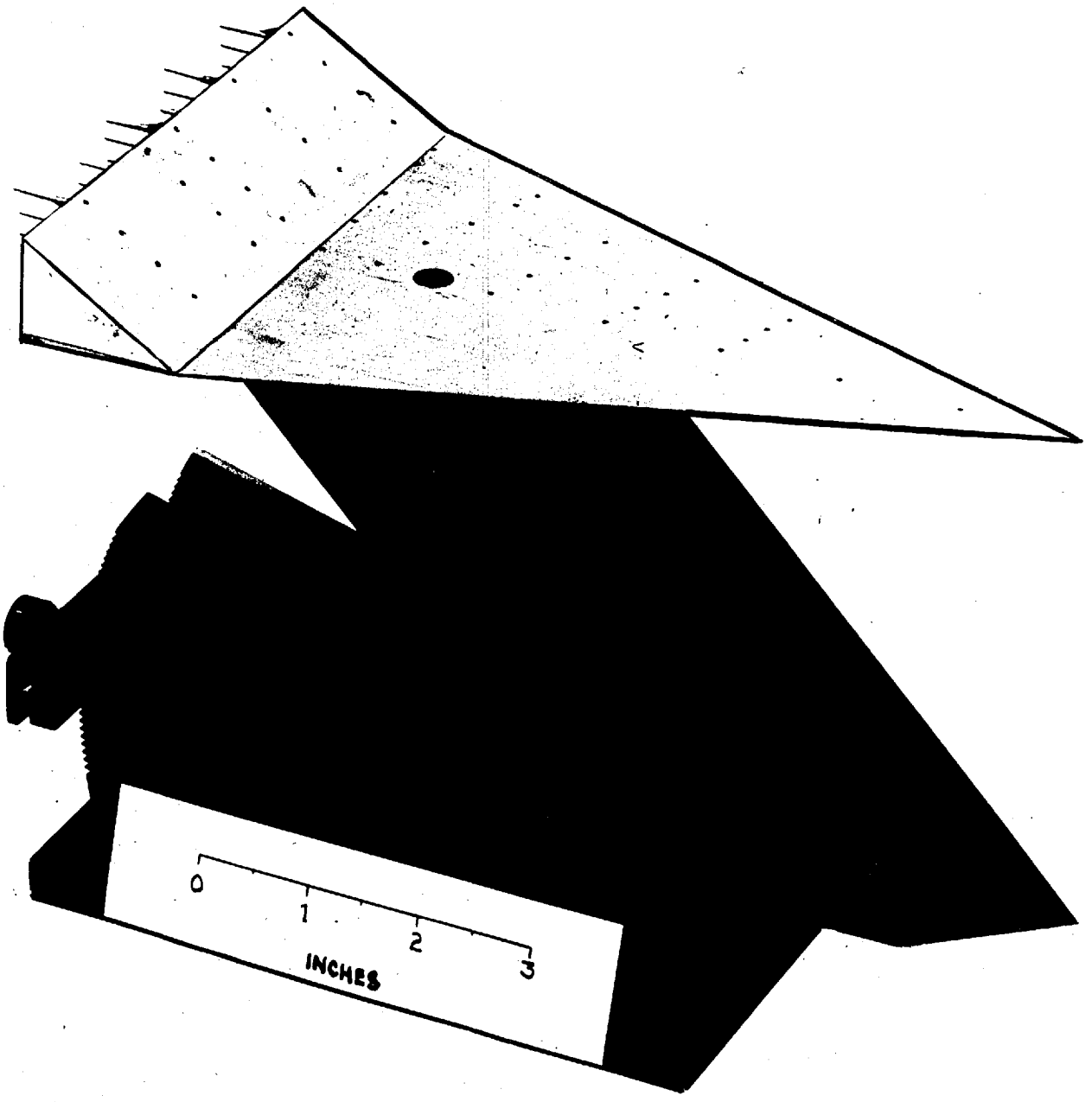

76° DELTA WING AND FLAP PRESSURE MODEL

FIG. 10




70° DELTA WING AND FLAP PRESSURE MODEL

FIG. 11




70° FLAPPED-DELTA PRESSURE MODEL
MOUNTED ON VARIABLE INCIDENCE SUPPORT

FIG. 12

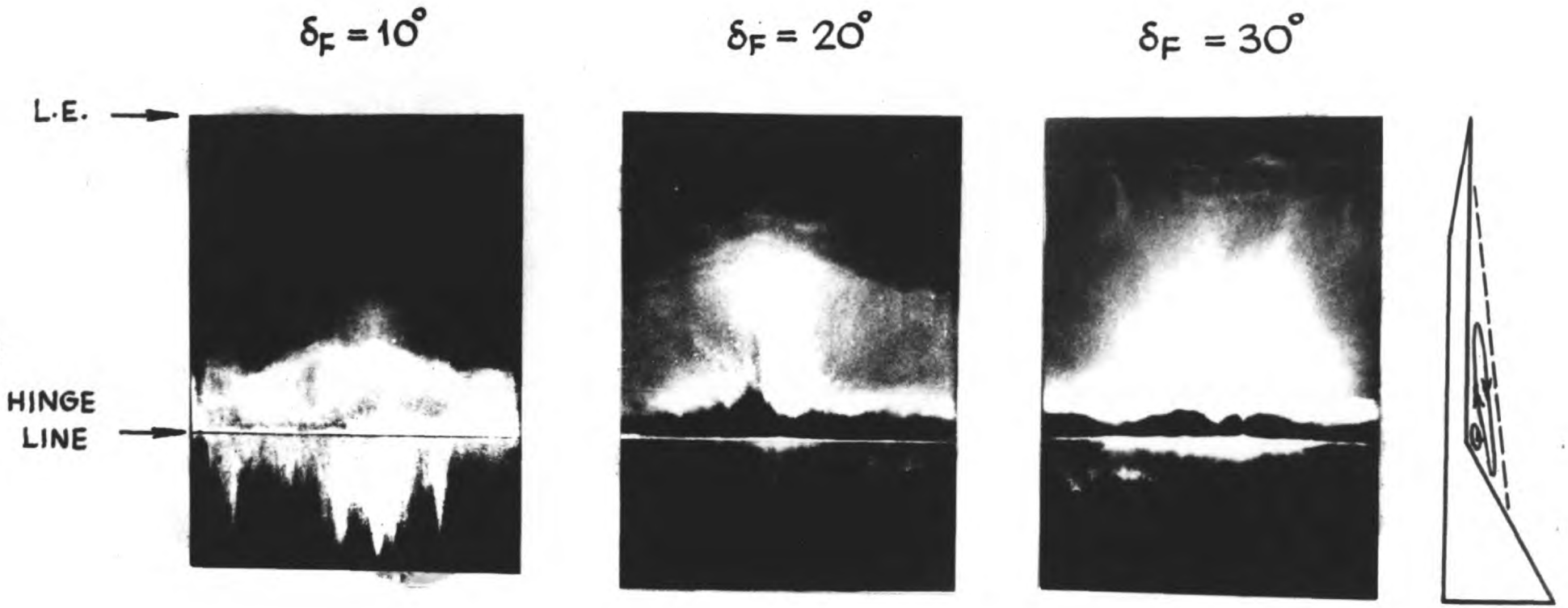
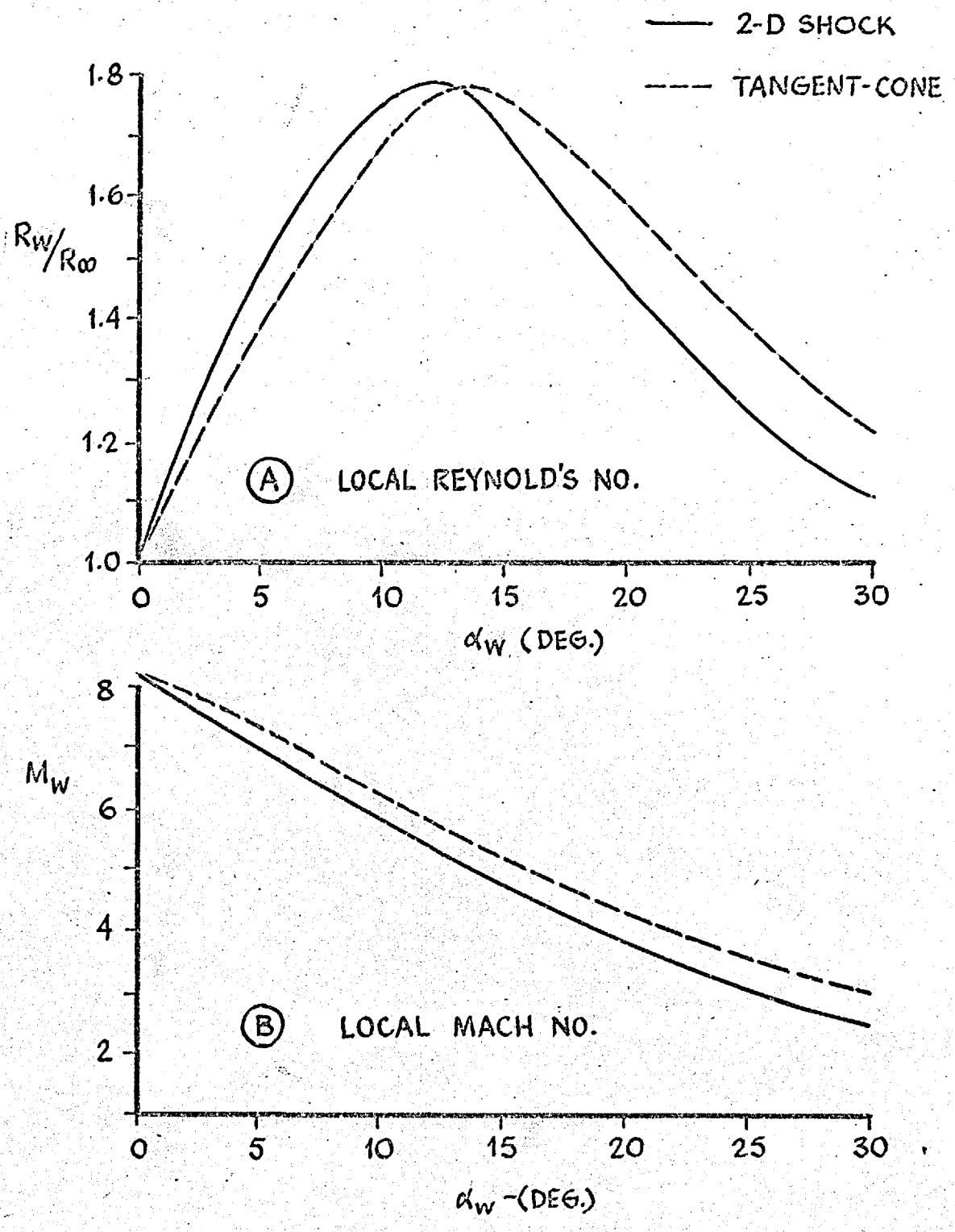
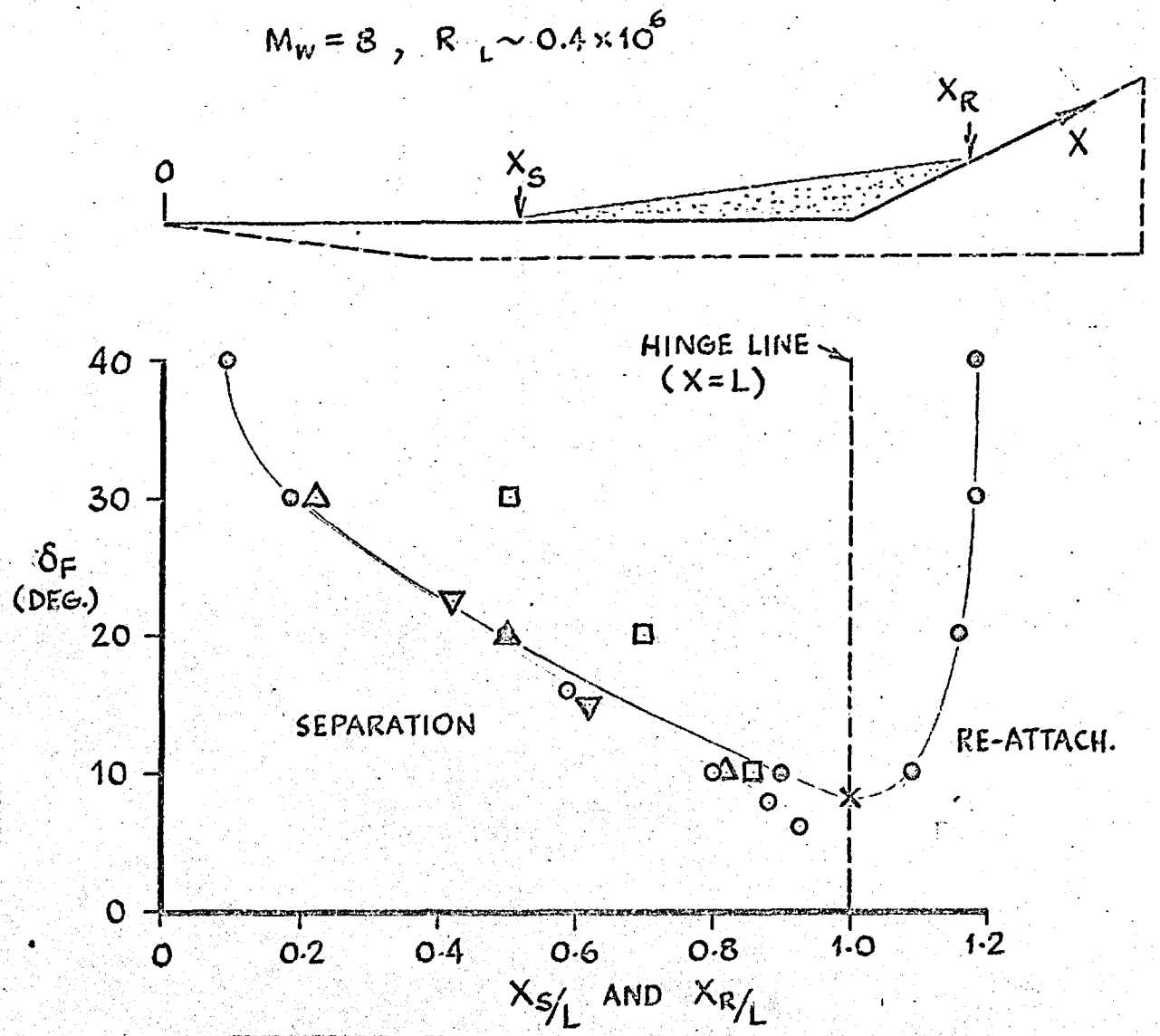



FIG. 13 POWDER FLOW VISUALISATION ON TWO-DIMENSIONAL MODEL



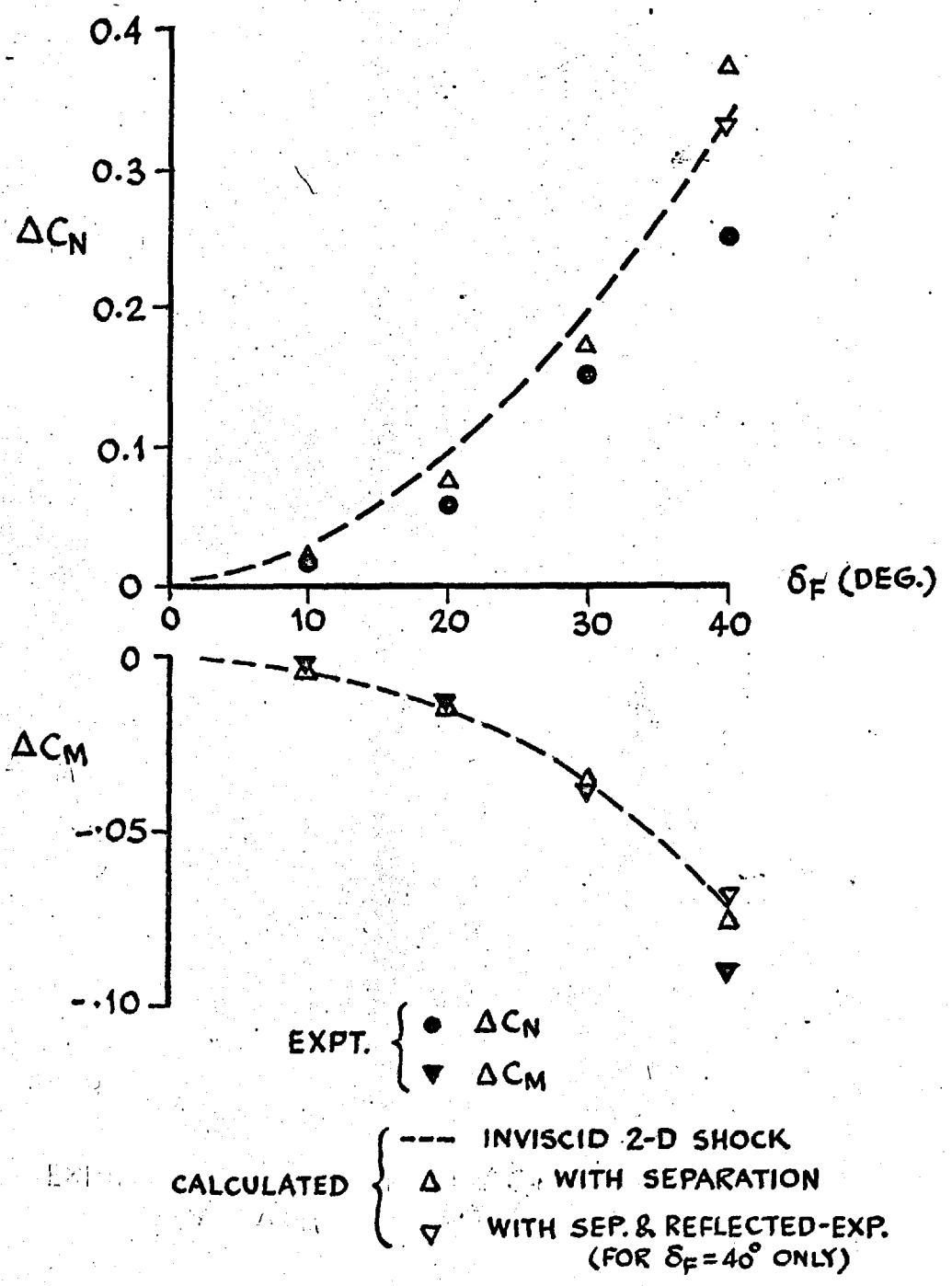

LOCAL CONDITIONS ON WINDWARD SURFACE

FIG. 14



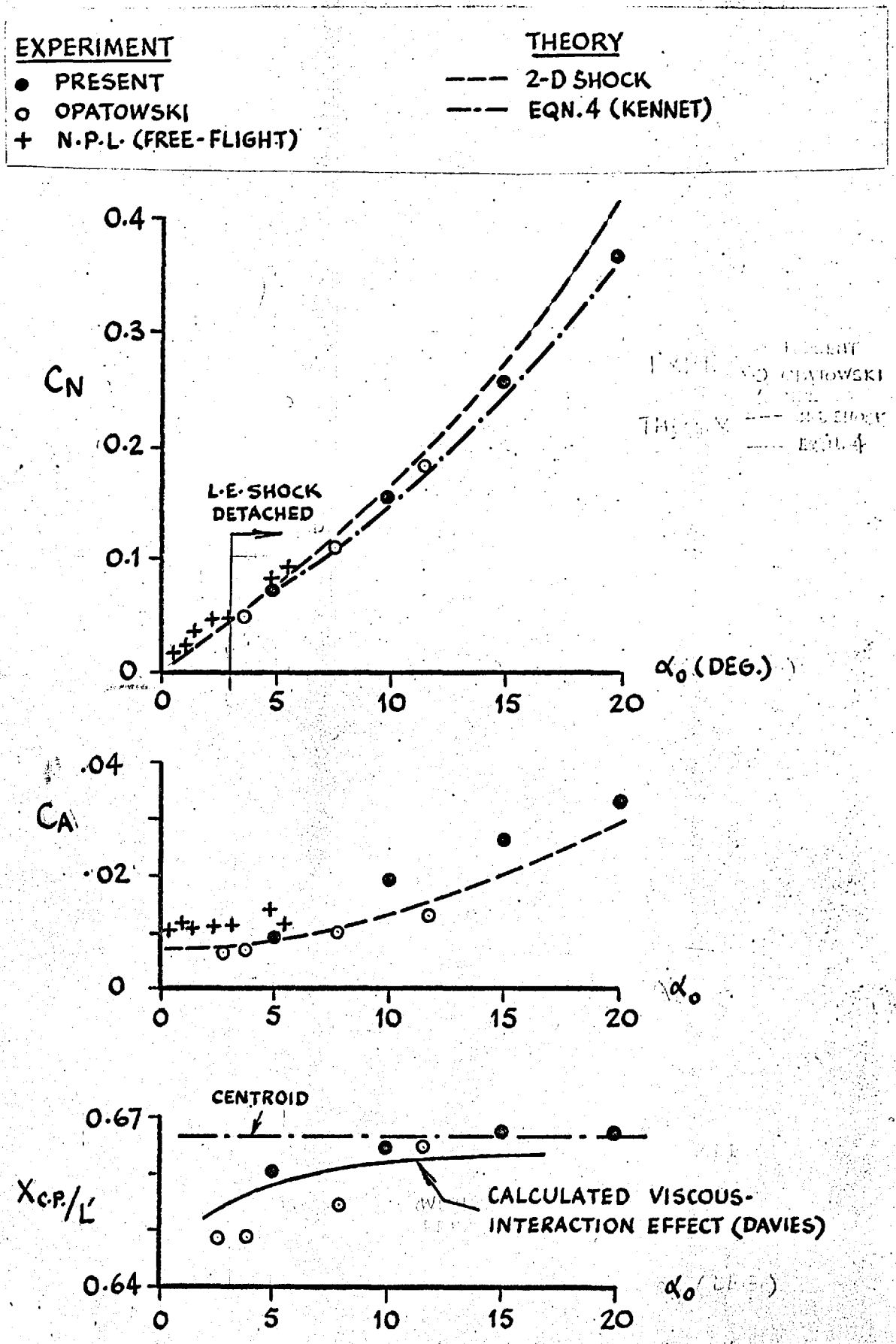

TWO-DIMENSIONAL SEPARATION DATA

FIG. 15




INCREMENTAL NORMAL FORCE & PITCHING-MOMENT ON TWO-DIMENSIONAL MODEL

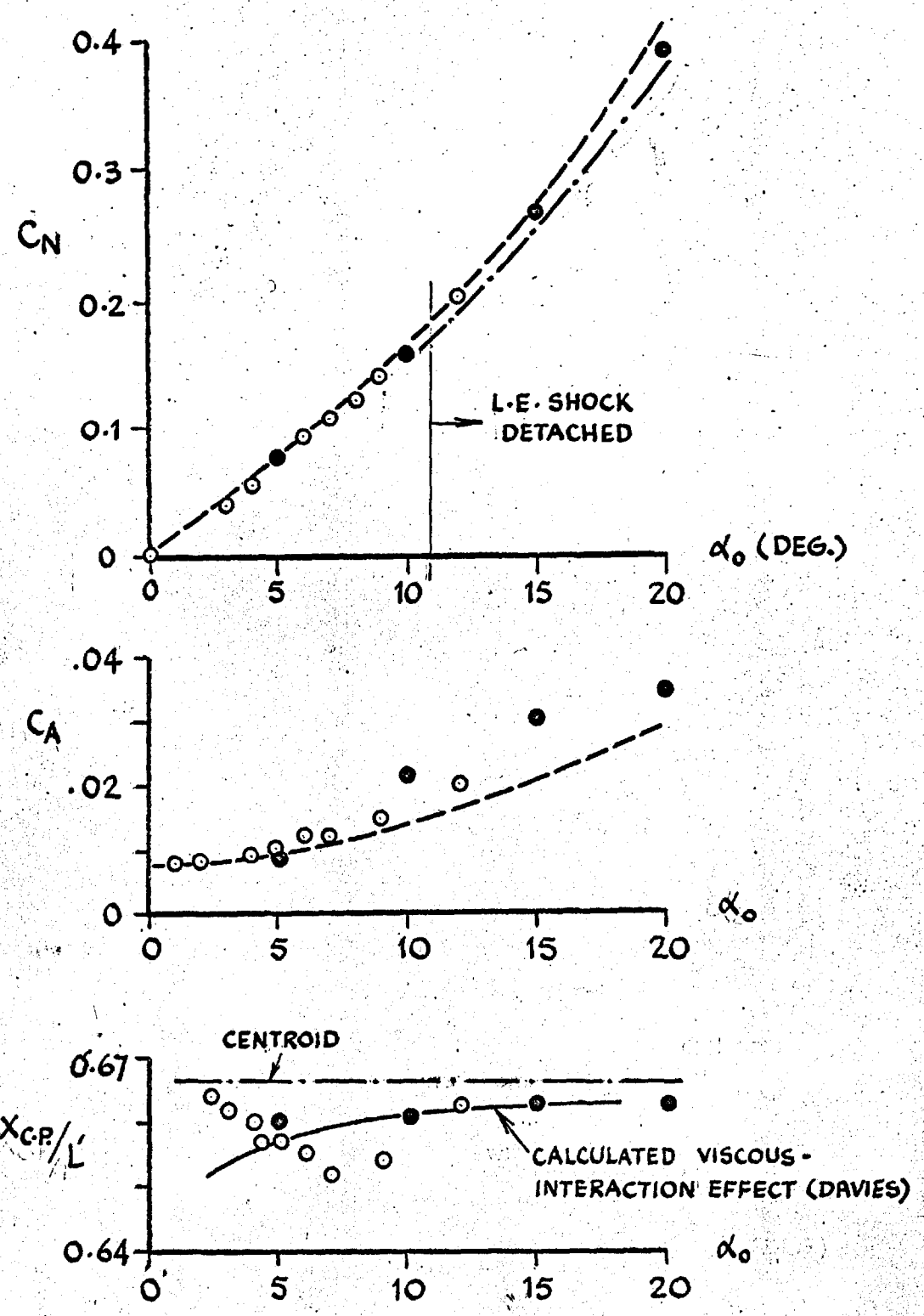
FIG. 16




76° DELTA WITHOUT FLAP - BALANCE DATA

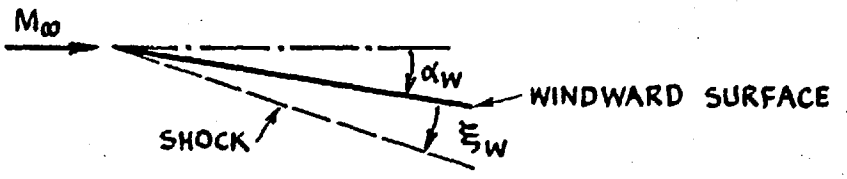
FIG. 17

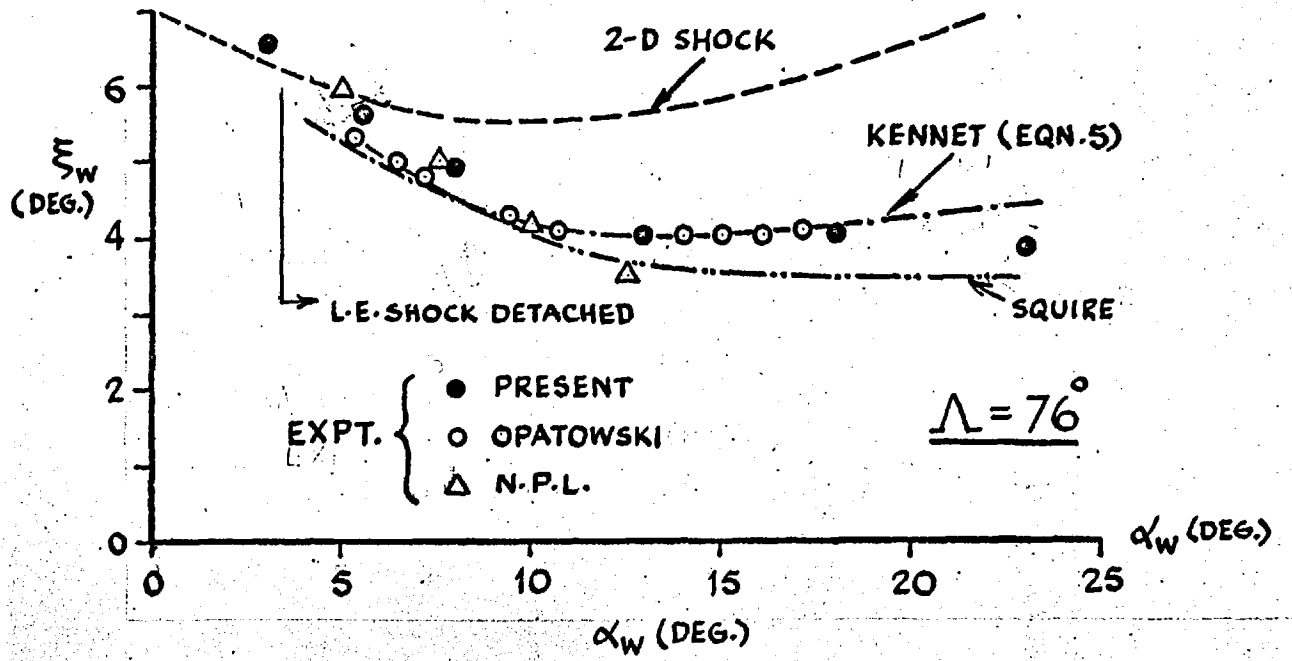
[FOR LEGEND, SEE FIG. 17]

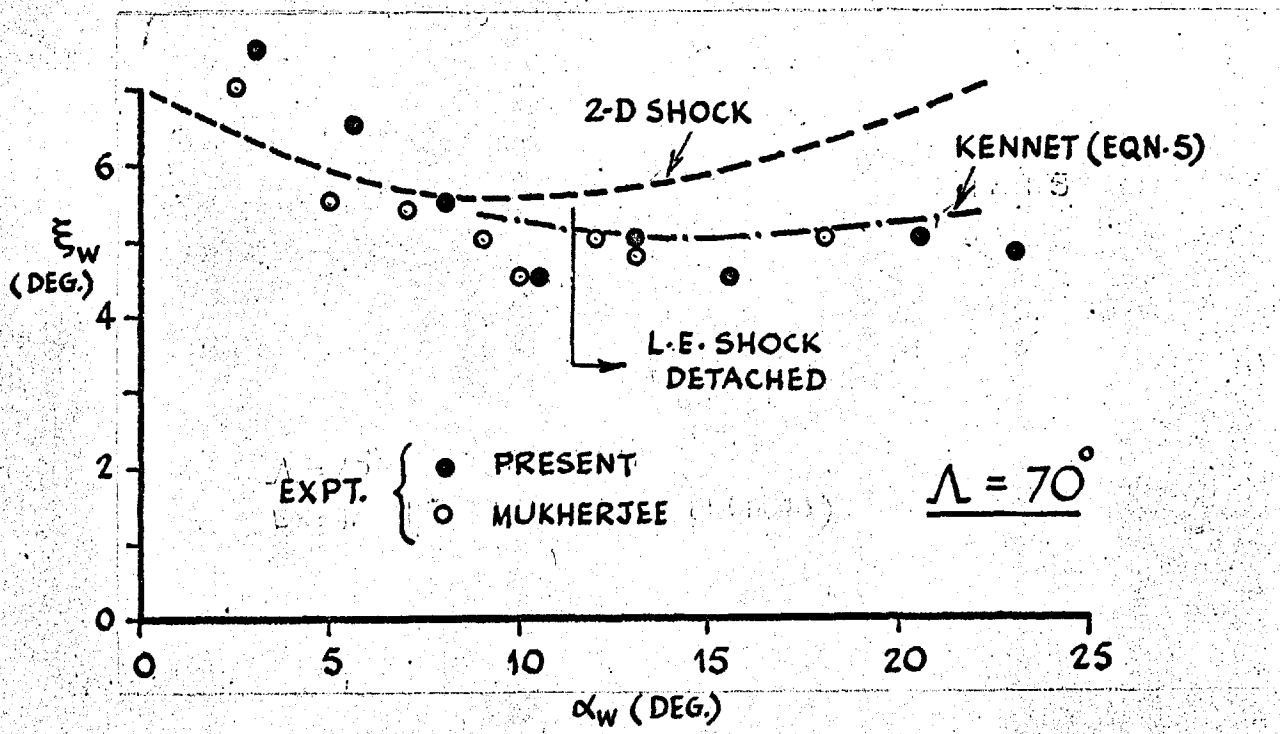



70° DELTA WITHOUT FLAP - BALANCE DATA

FIG. 18

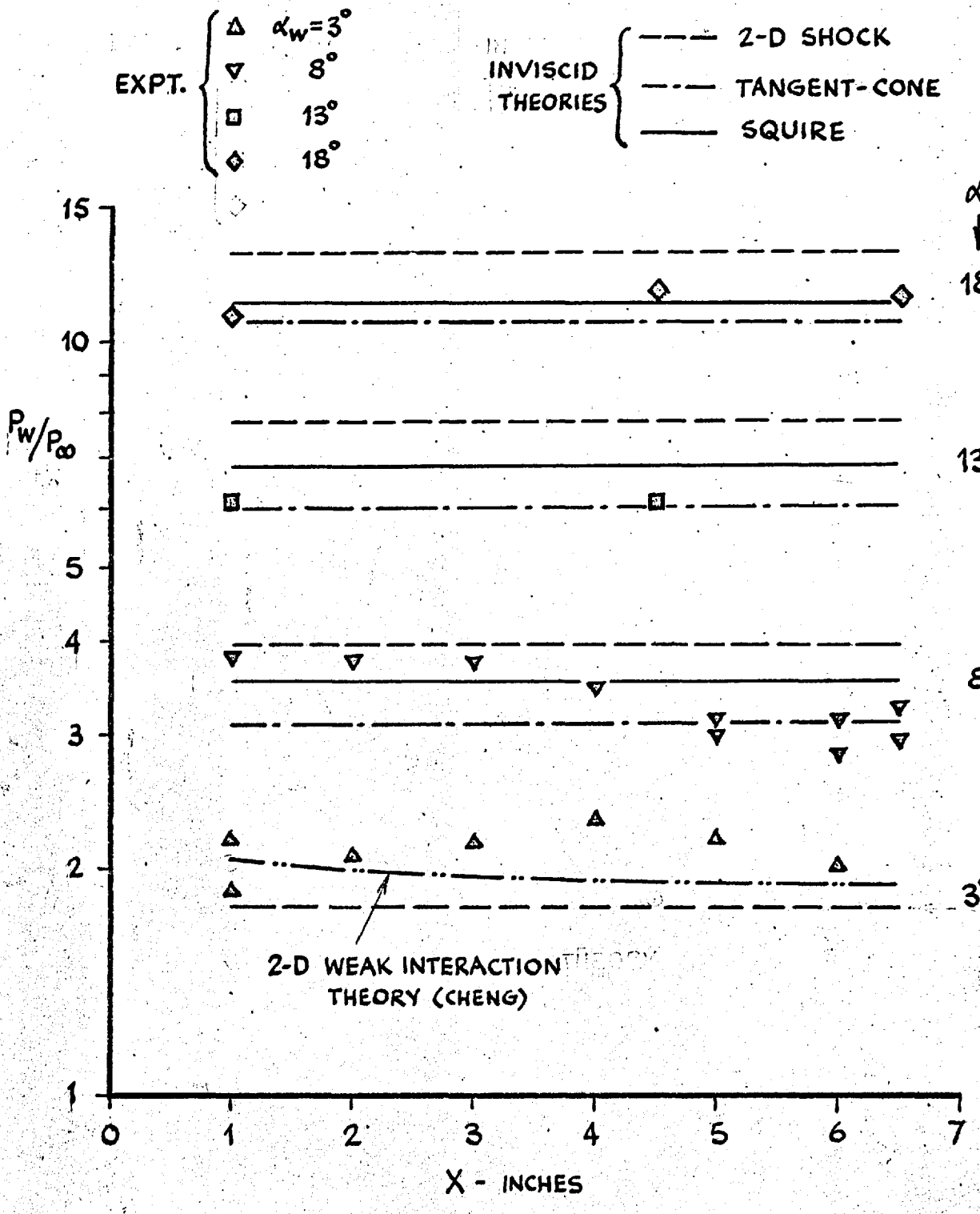


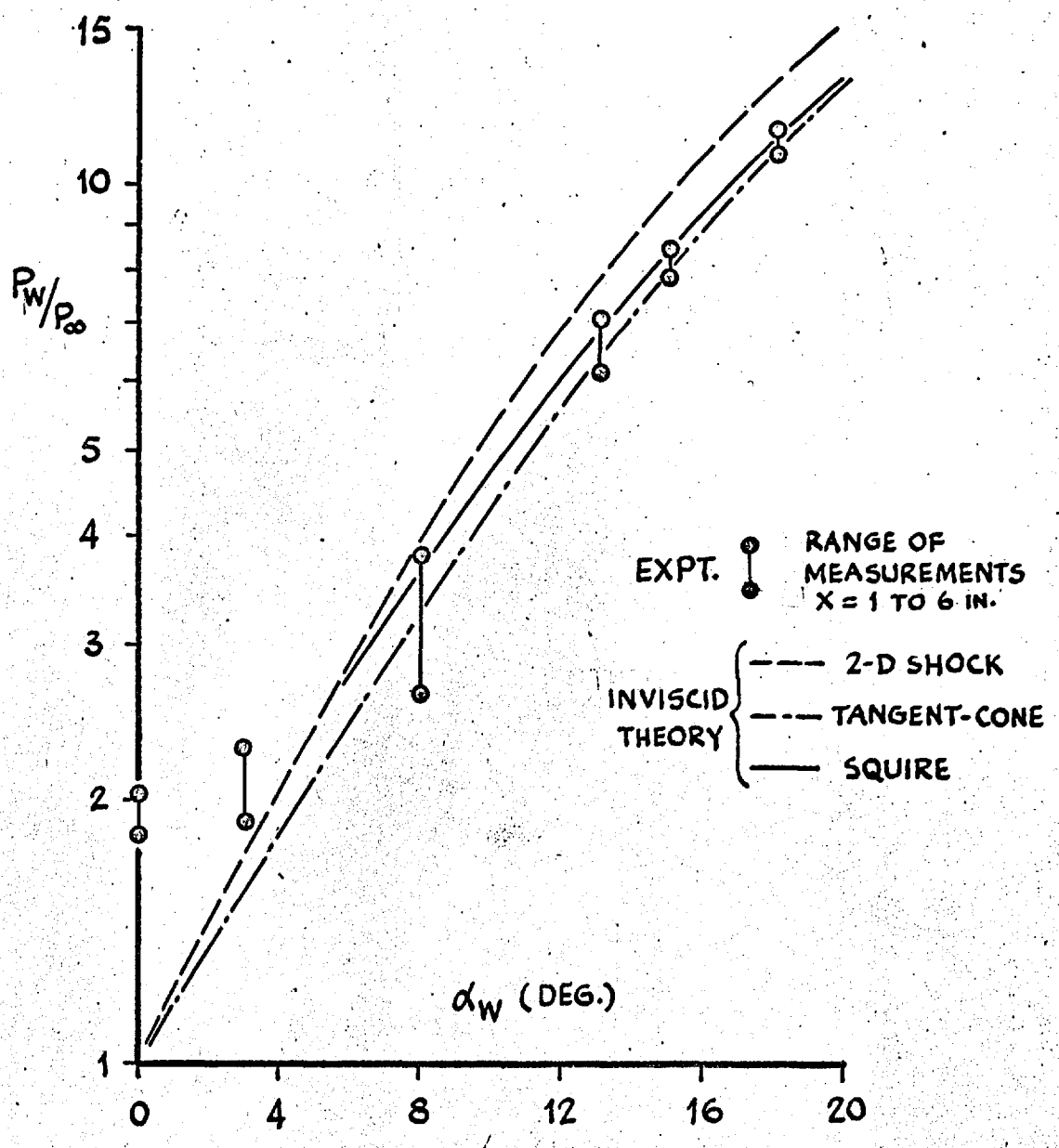

DELTA WING SHOCK ANGLE DATA

FIG. 19



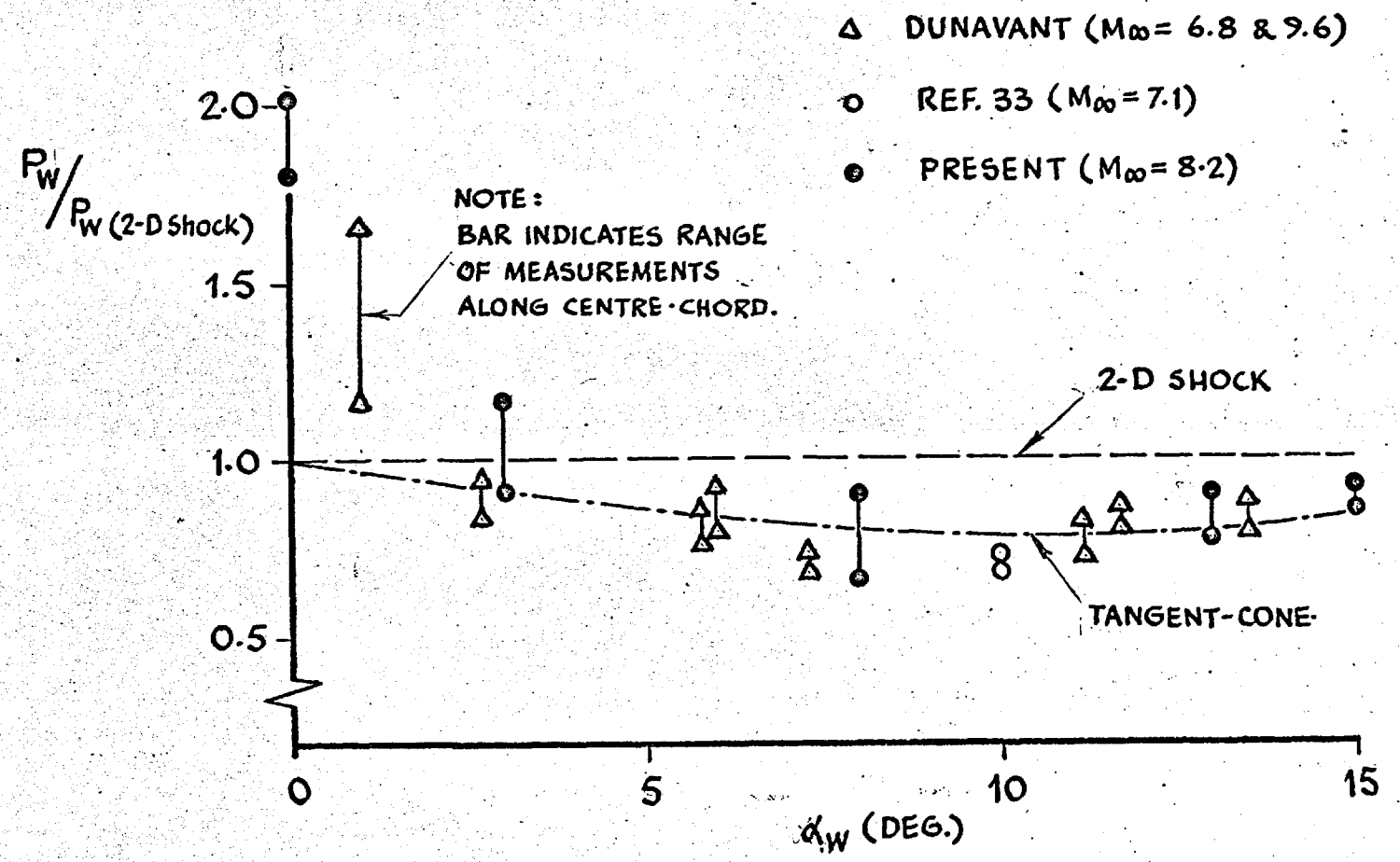

76° DELTA WITHOUT FLAP - CENTRE-CHORD PRESSURE DISTRIBUTIONS

FIG. 20



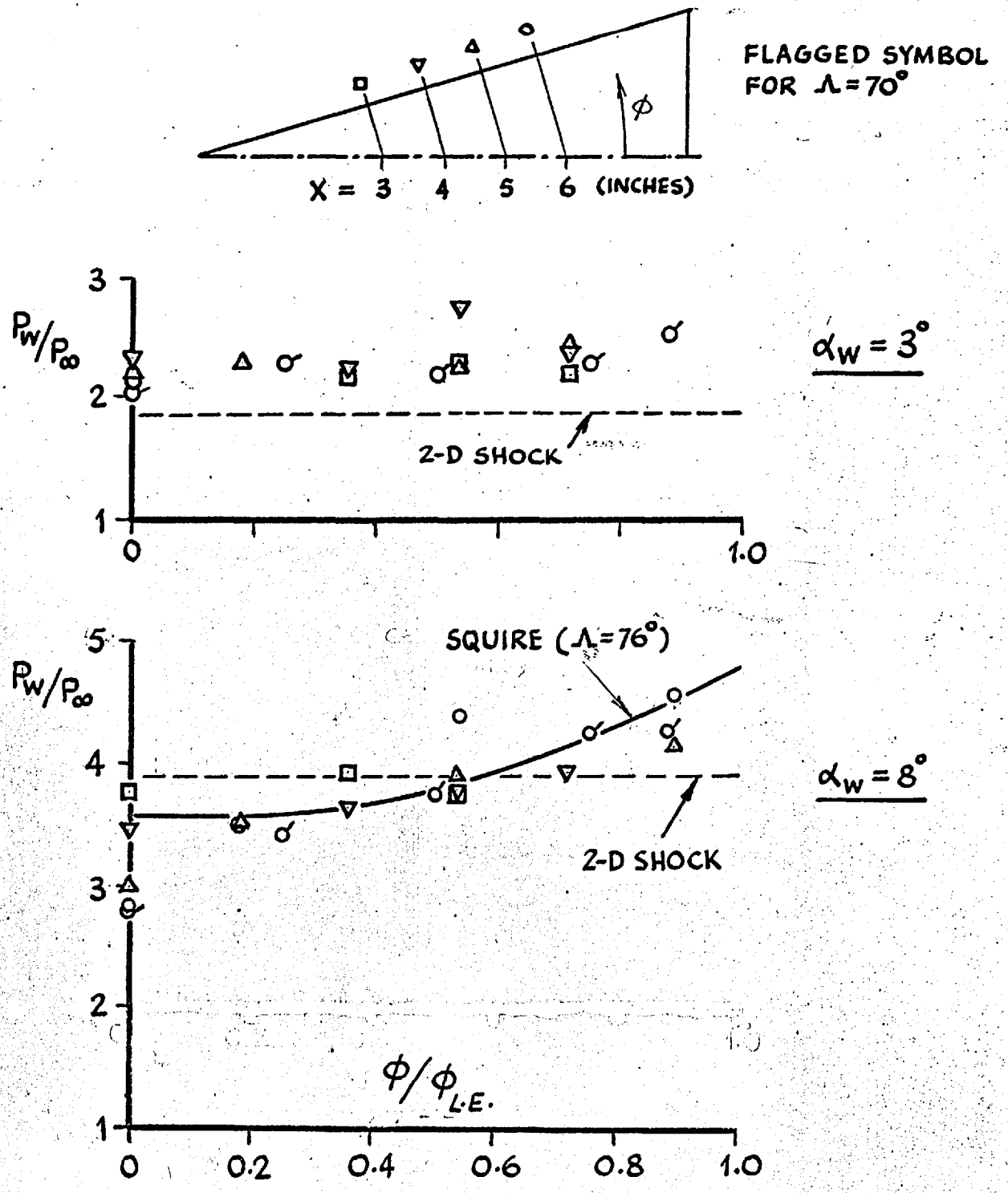

76° DELTA WITHOUT FLAP - CENTRE-CHORD PRESSURE vs. INCIDENCE

FIG. 21



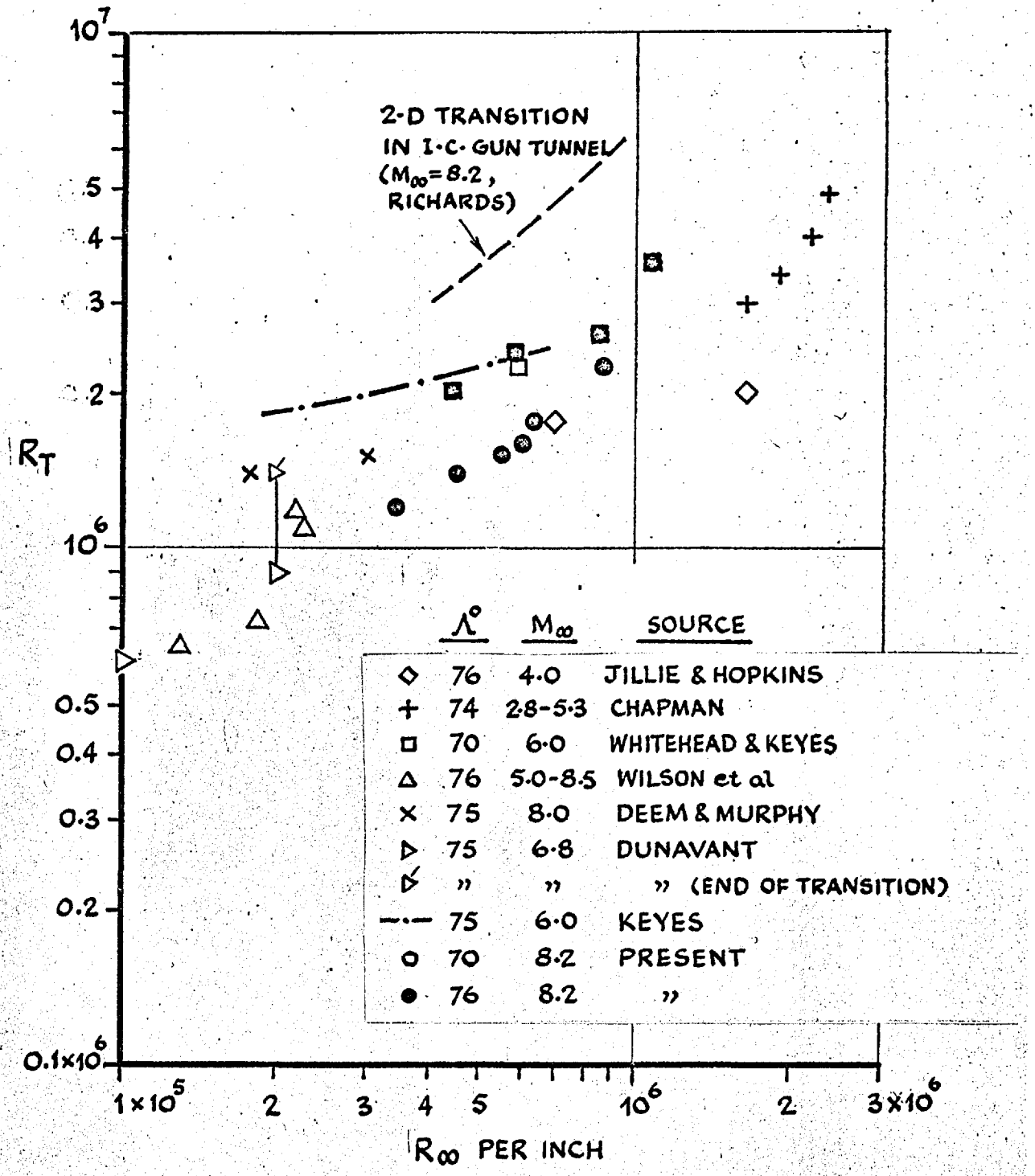

76° DELTA CENTRE-CHORD PRESSURES, $M_\infty$ = 6·8 TO 9·6.

FIG. 22




PRESSURE DISTRIBUTION NORMAL TO LEADING-EDGE ON DELTA WINGS ($\delta_F = 0°$)

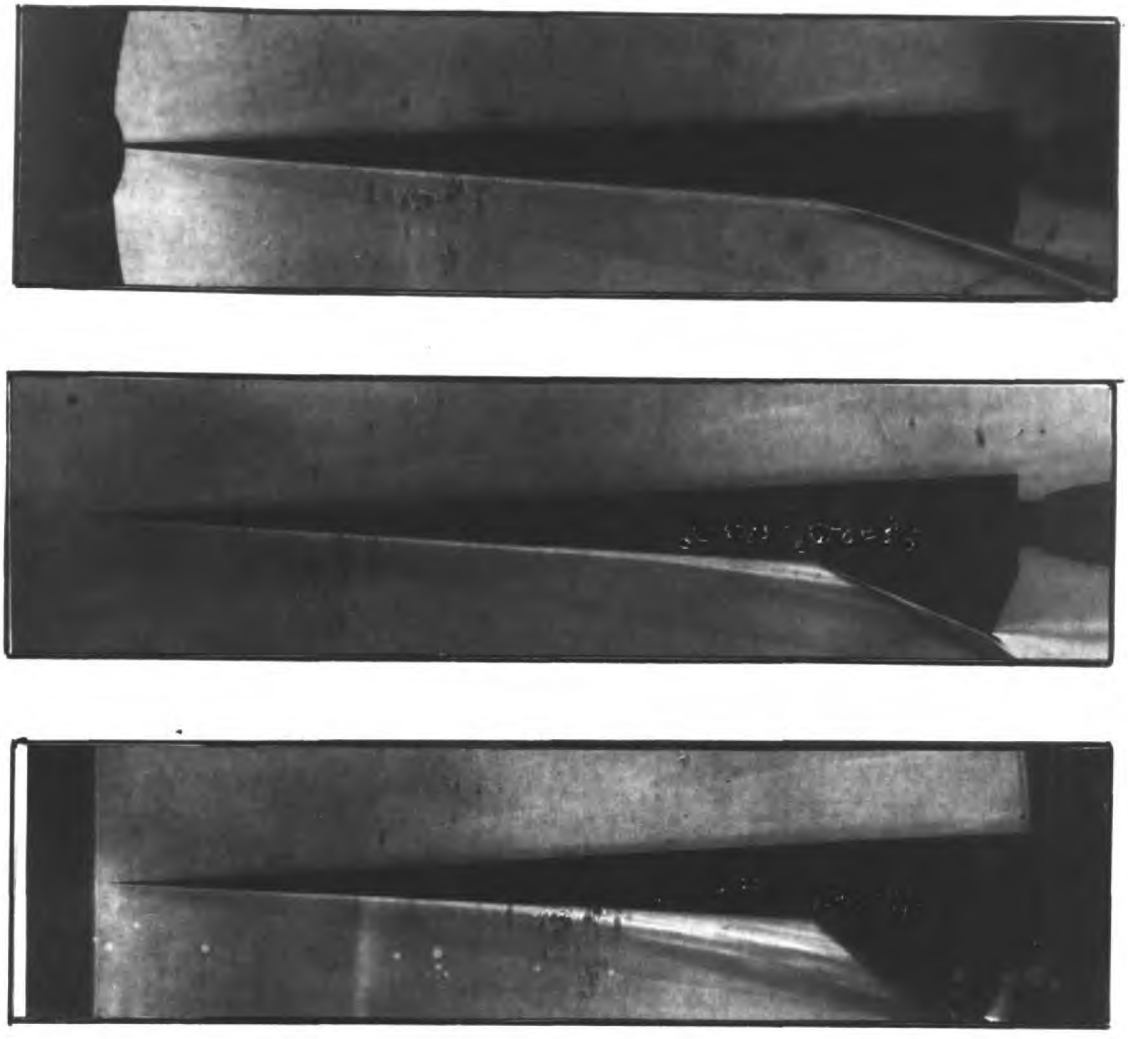
FIG. 23




DELTA WING TRANSITION DATA

FIG. 24

$\Lambda = 76^\circ$, $\alpha_o = 0^\circ$ ($\alpha_w = 3^\circ$)



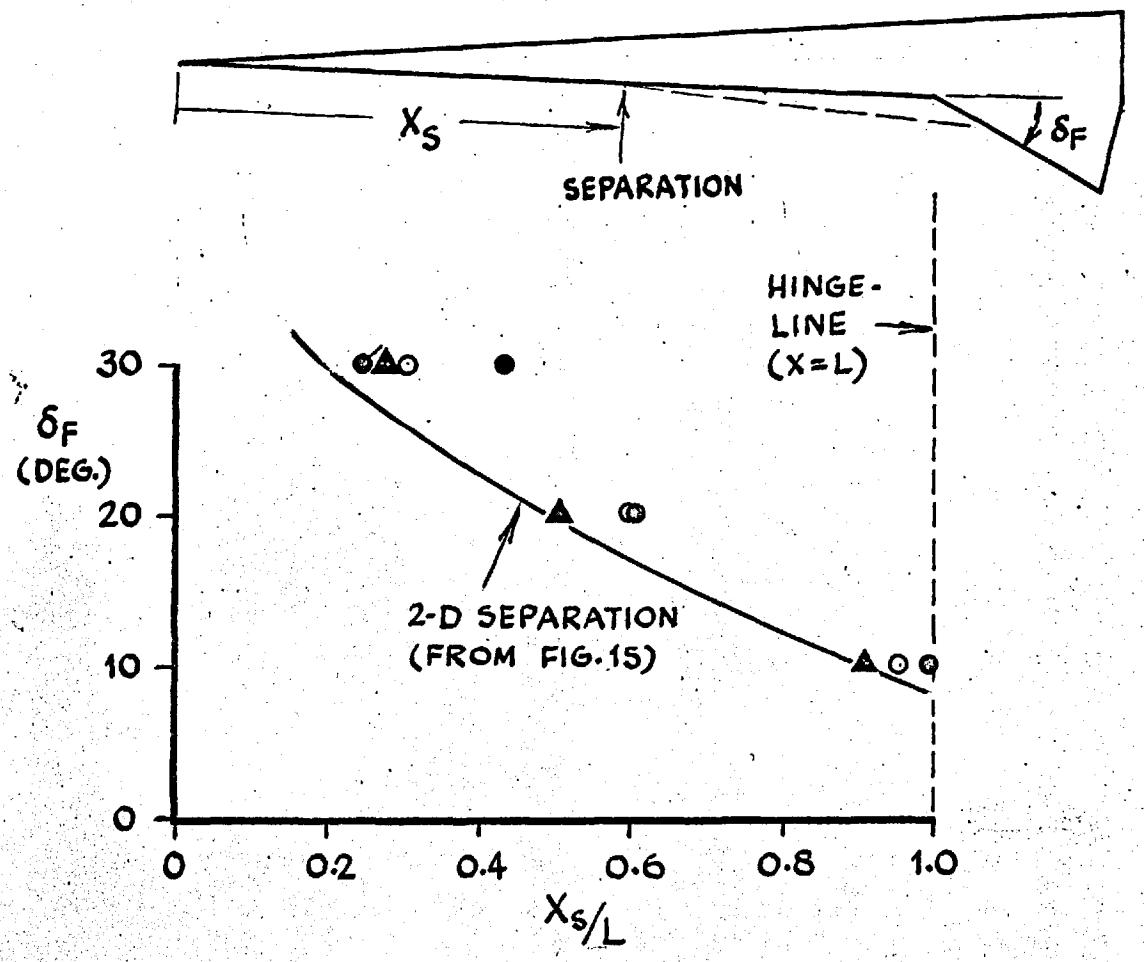
$\delta_F = 10^\circ$

$\delta_F = 20^\circ$

$\delta_F = 30^\circ$

SCHLIEREN PHOTOGRAPHS - INCREASING $\delta_F$ .

FIG. 25

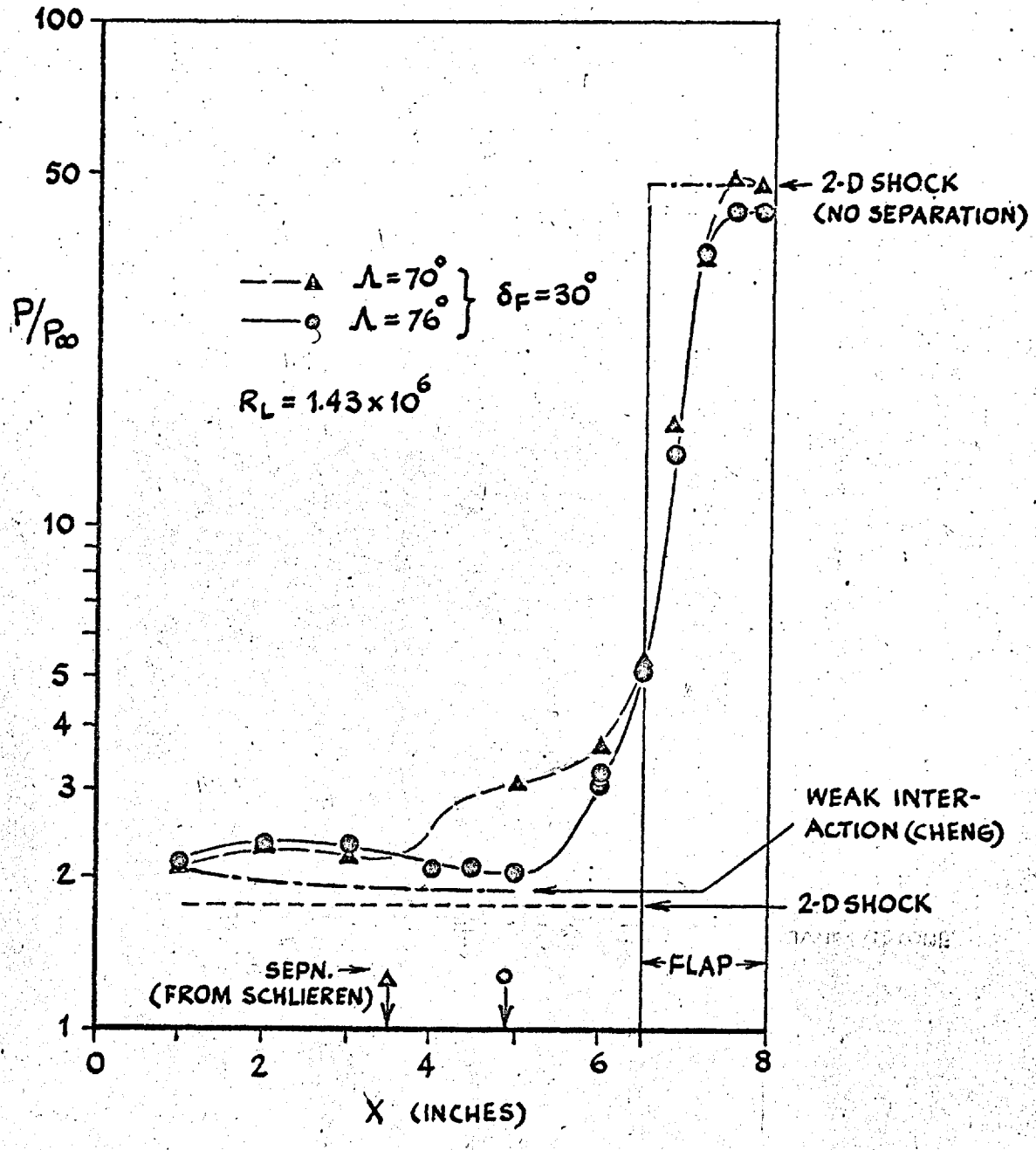



▲ $\Lambda = 70°$, PRESENT
● $\Lambda = 76°$, do.
○ $\Lambda = 76°$, N.P.L.
} $R_L \sim 0.85 \times 10^6$

✓ $\Lambda = 76°$, PRESENT. $R_L = 0.7 \times 10^6$

# LENGTH OF FLAP-INDUCED SEPARATION ON DELTA WINGS AT SMALL INCIDENCE

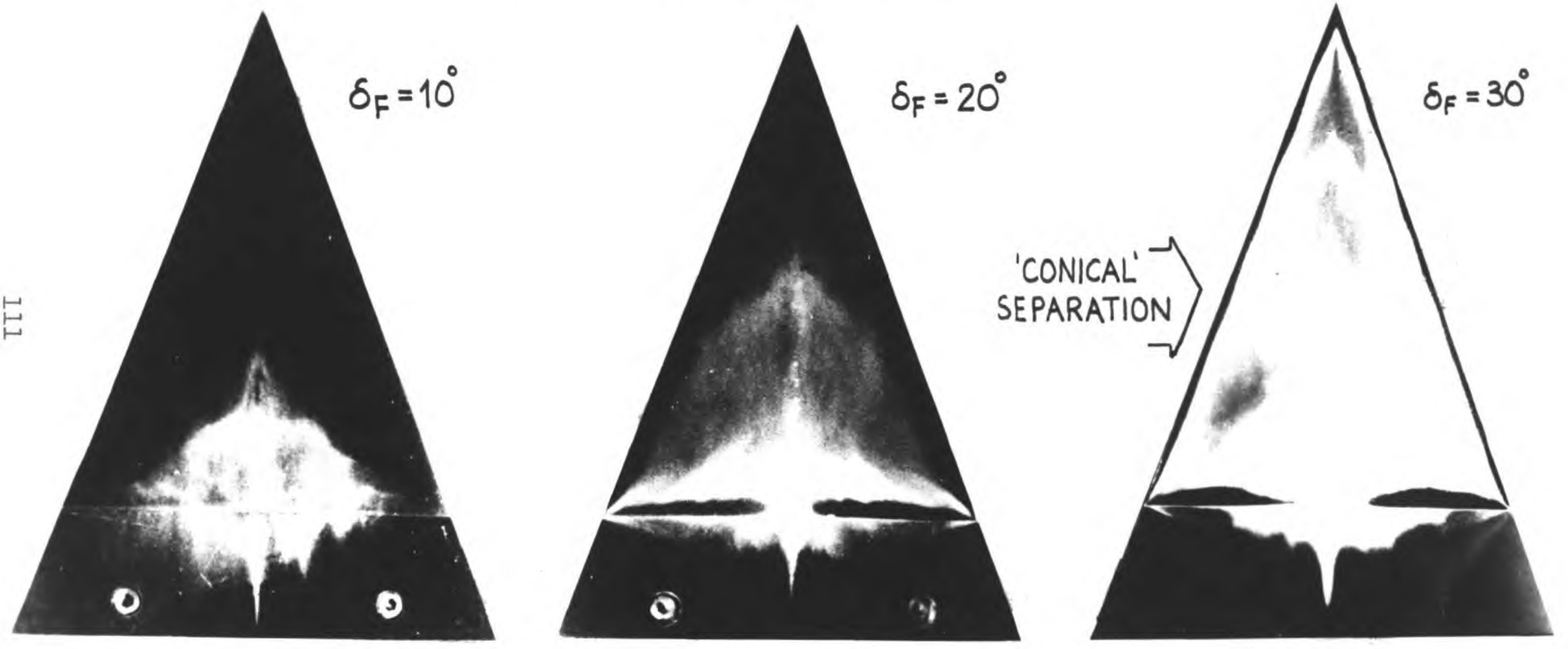
FIG. 26




CENTRE-CHORD PRESSURE DISTRIBUTION ON FLAPPED DELTAS. $\alpha_W = 3°$

FIG. 27

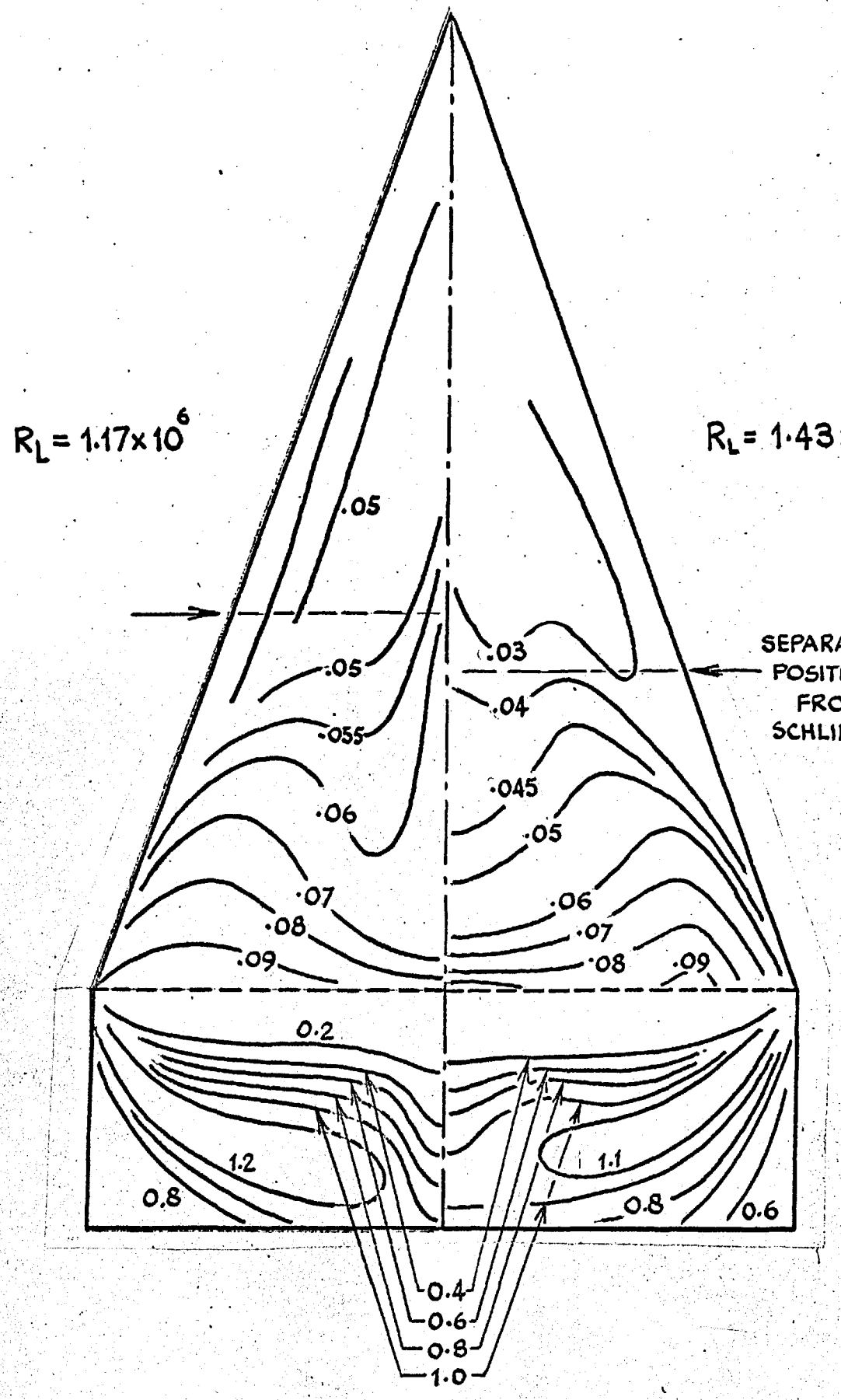
(WING L·E· SHOCK ATTACHED)




$\Lambda = 70^\circ$

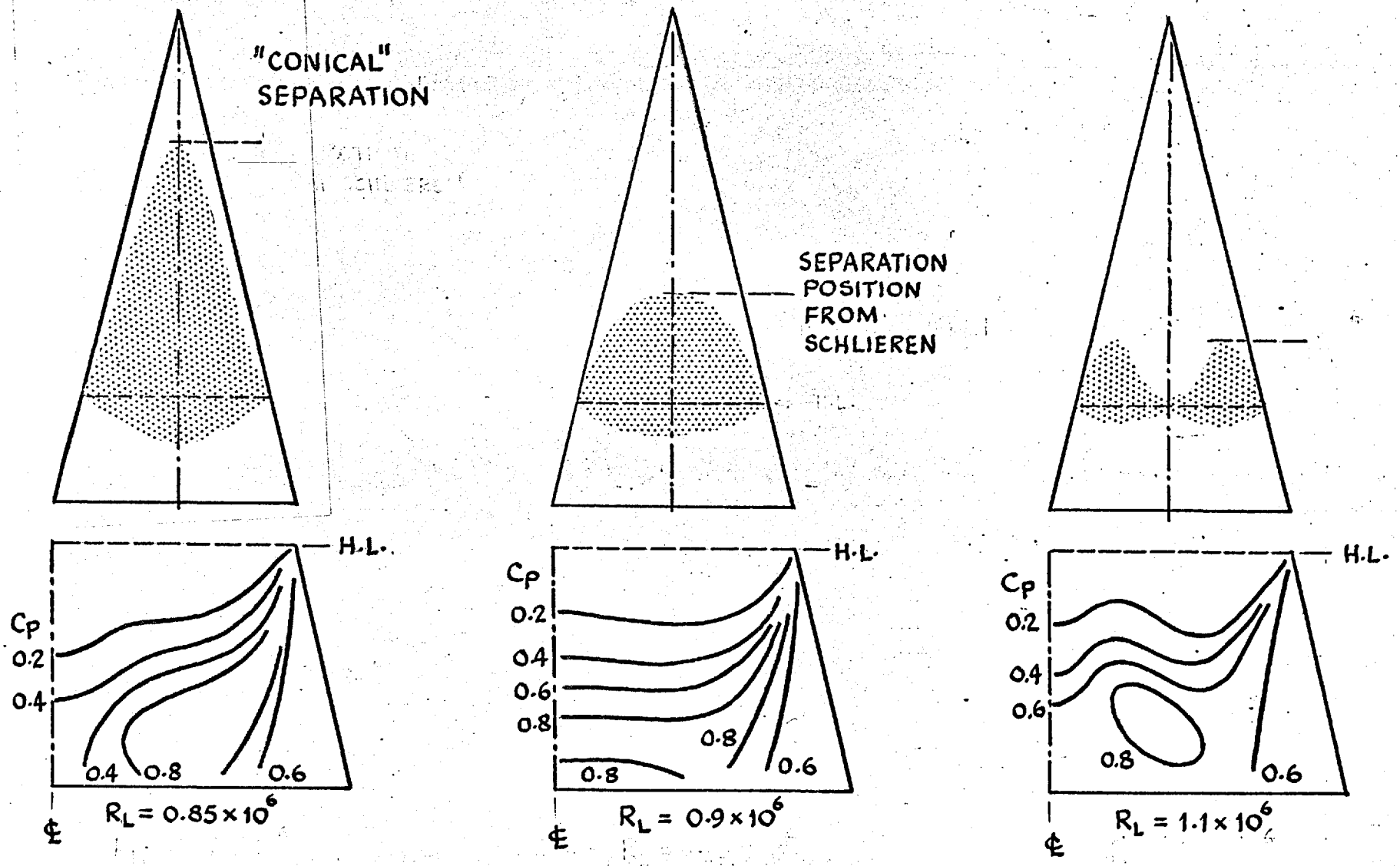
POWDER PATTERNS OF SEPARATED FLOW - EFFECT OF FLAP ANGLE AT $\alpha_o = 0^\circ$

FIG. 28




CONSTANT $C_p$ CONTOURS. $\Lambda = 70^\circ$. $\alpha_w = 3^\circ$. $\delta_F = 30^\circ$

FIG. 29




REYNOLD'S NO. EFFECT ON FLAP PRESSURES . $\Lambda = 76°$ . $\delta_F = 30°$ . $\alpha_W = 0°$

FIG. 30



$\alpha_o = 0°$



$\alpha_o = 2.5°$



$\alpha_o = 5°$



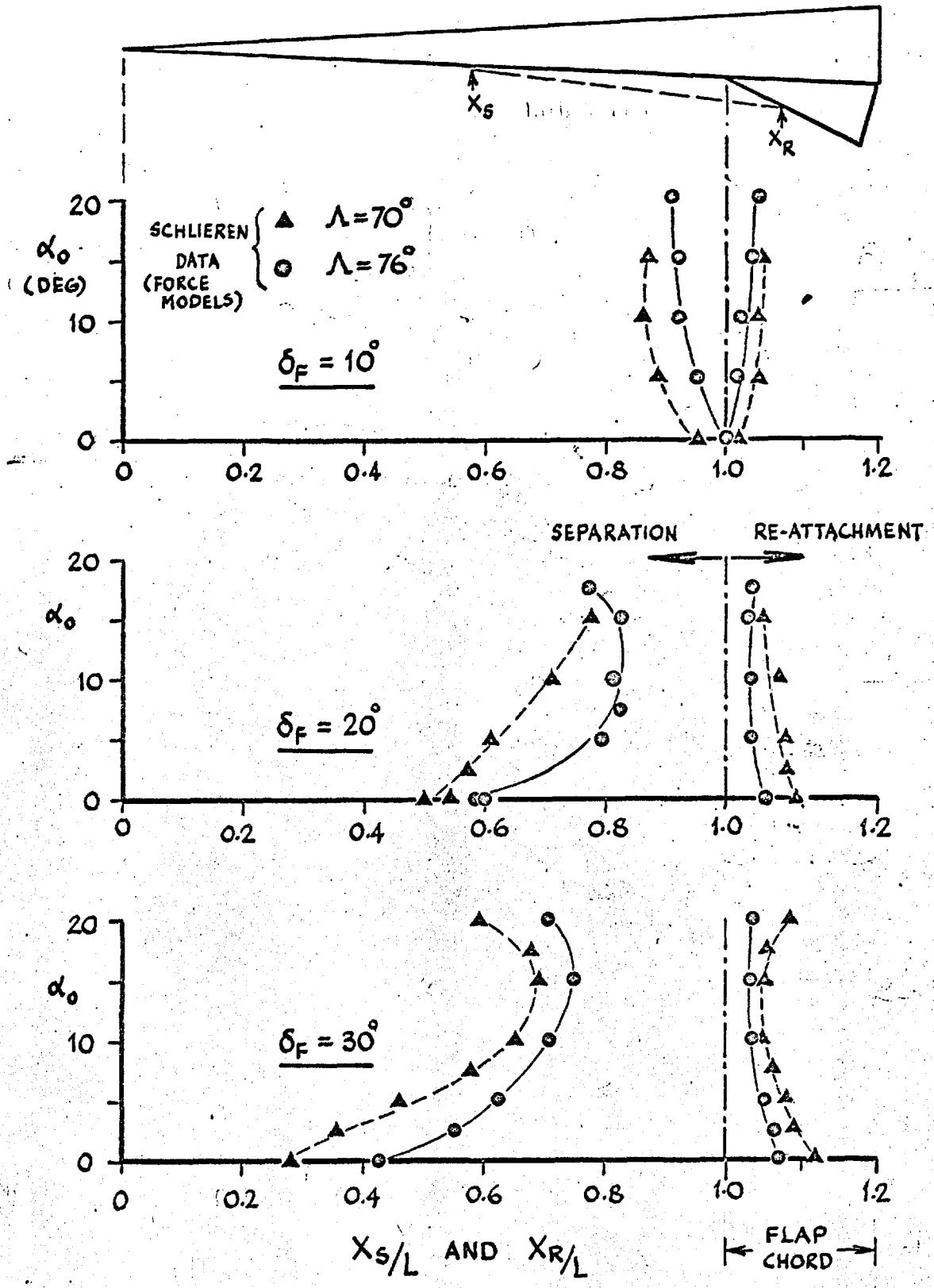
$\alpha_o = 10°$



$\alpha_o = 15°$

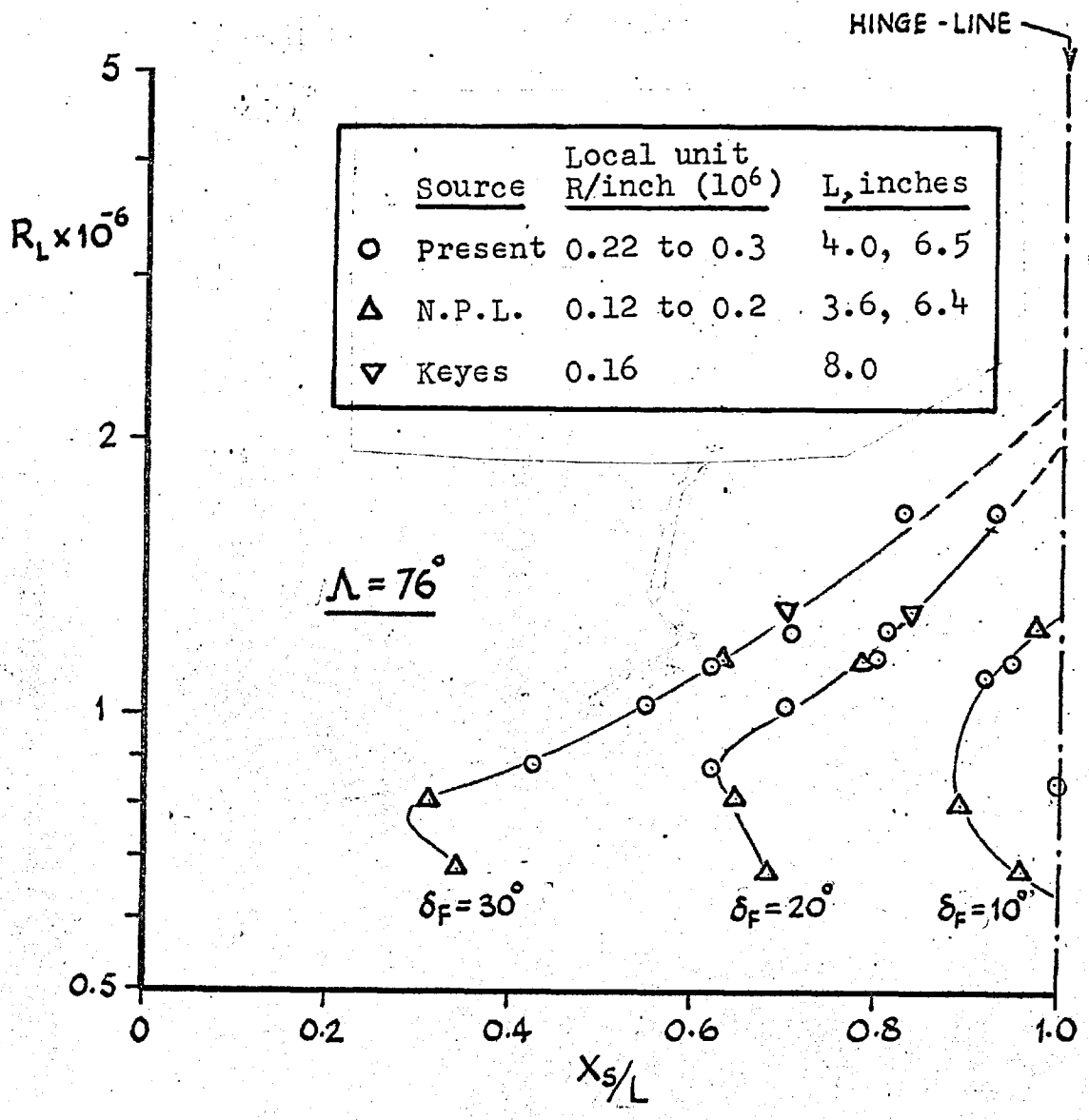
FIG.31 TYPICAL SEQUENCE OF SCHLIEREN PHOTOGRAPHS

76° DELTA. $\delta_F = 30°$



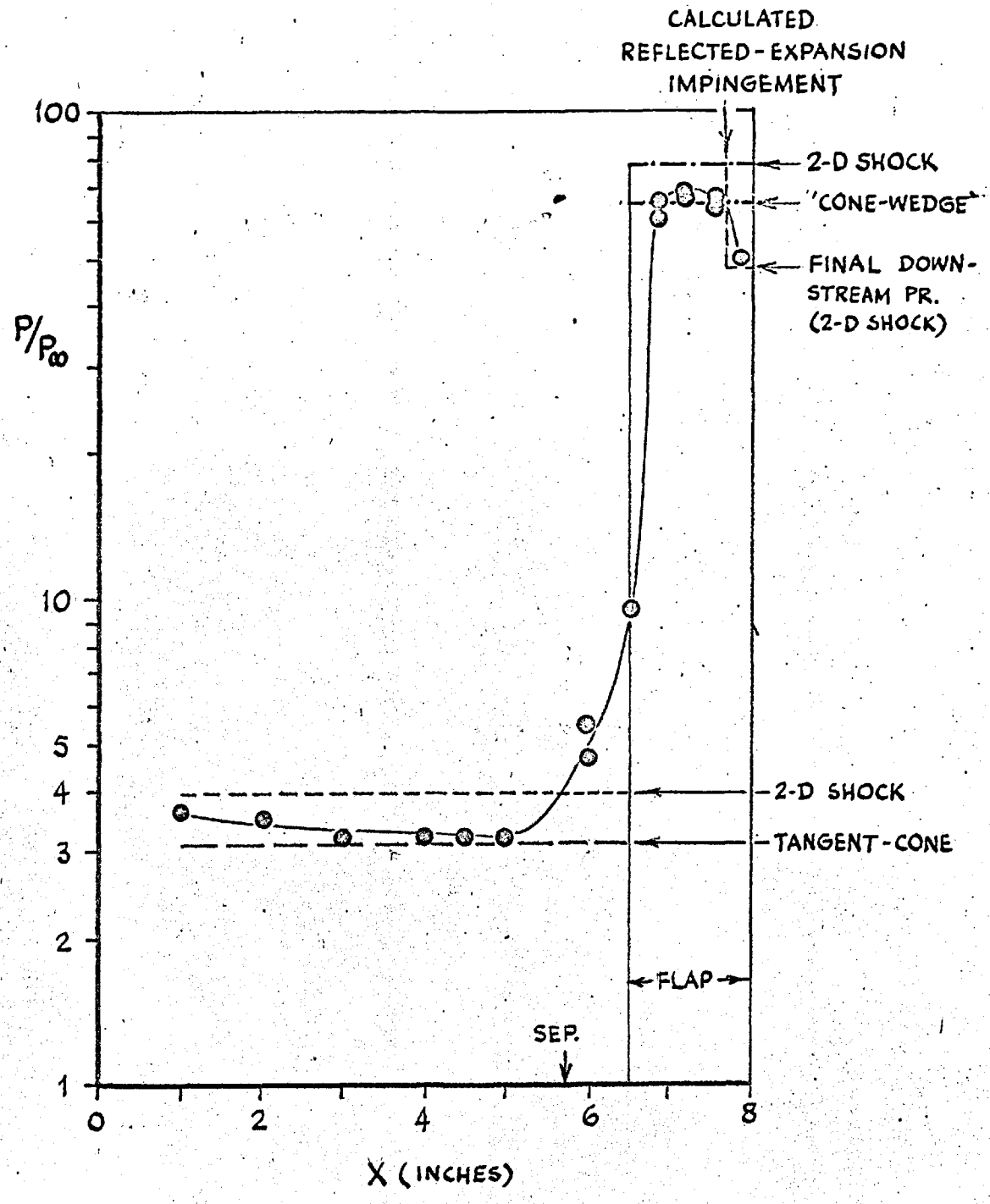

SEPARATION LENGTH WITH FLAP DEFLECTION AND INCIDENCE

FIG. 32




REYNOLD'S NO. EFFECT ON SEPARATION LENGTH

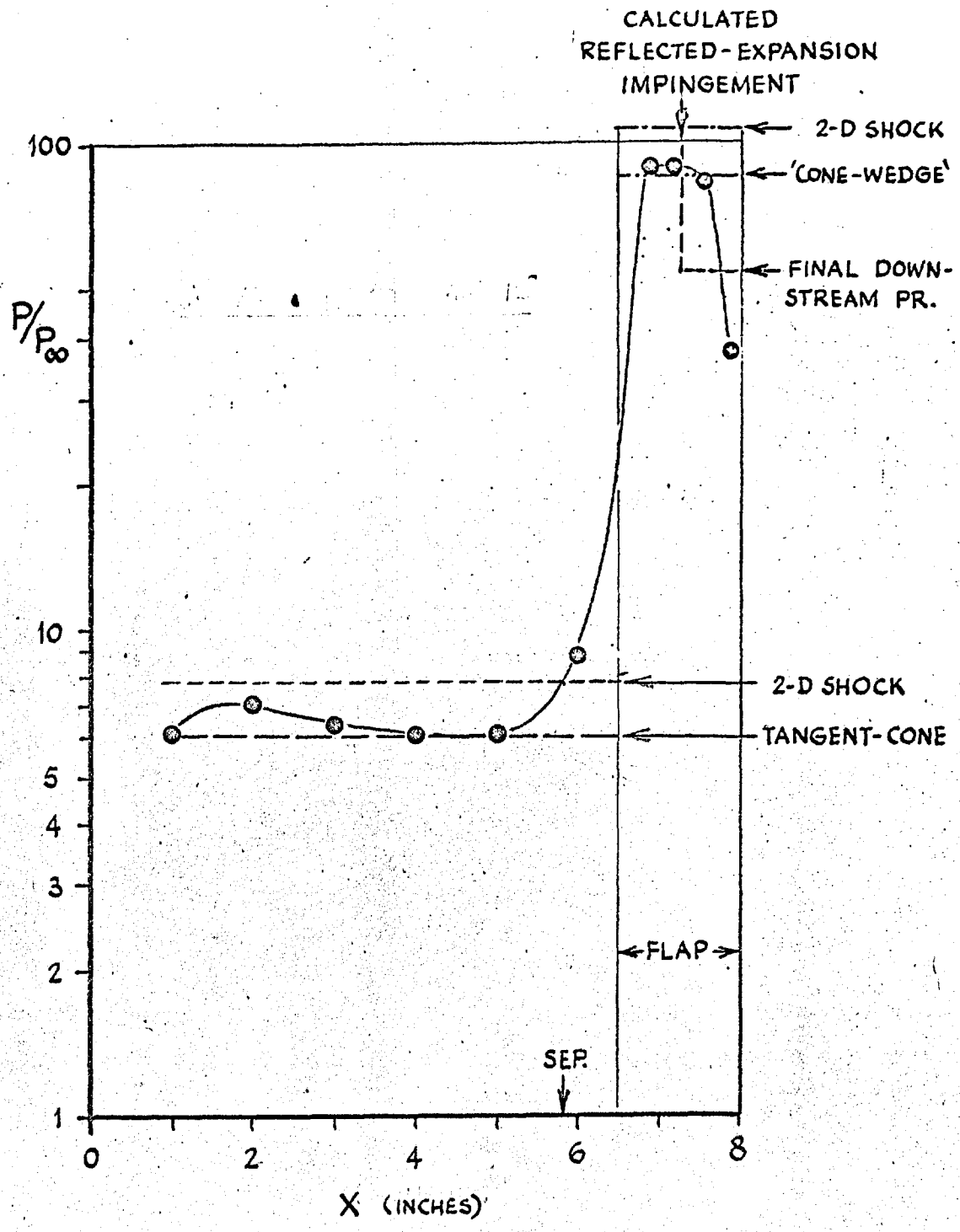
FIG. 33




CENTRE-CHORD PRESSURE DISTRIBUTION ON

76° FLAPPED-DELTA . $\alpha_W = 8°$ . $\delta_F = 30°$

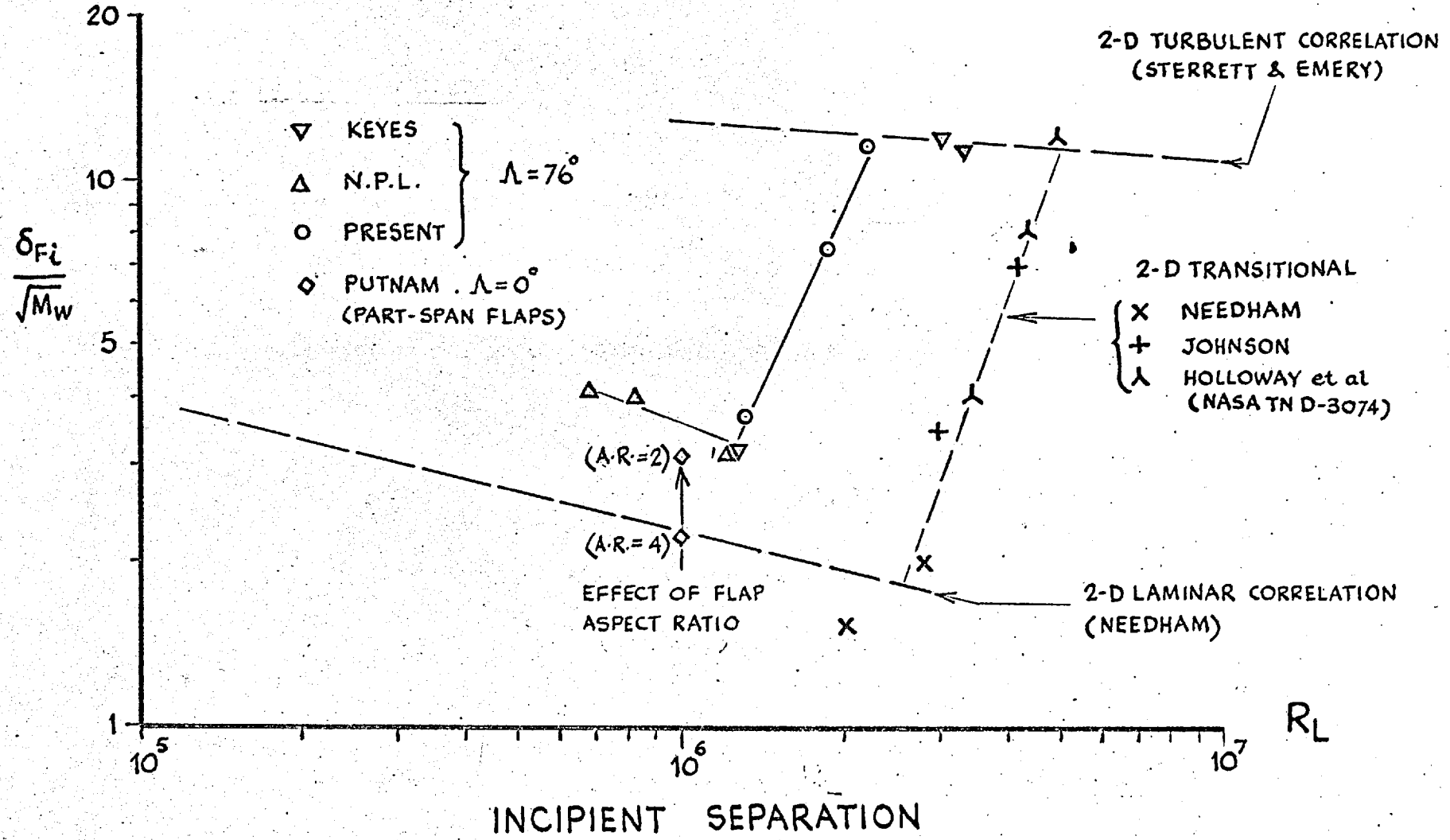
FIG. 34




CENTRE-CHORD PRESSURE DISTRIBUTION ON

76° FLAPPED DELTA. $\alpha_W = 13°$ · $\delta_F = 30°$.

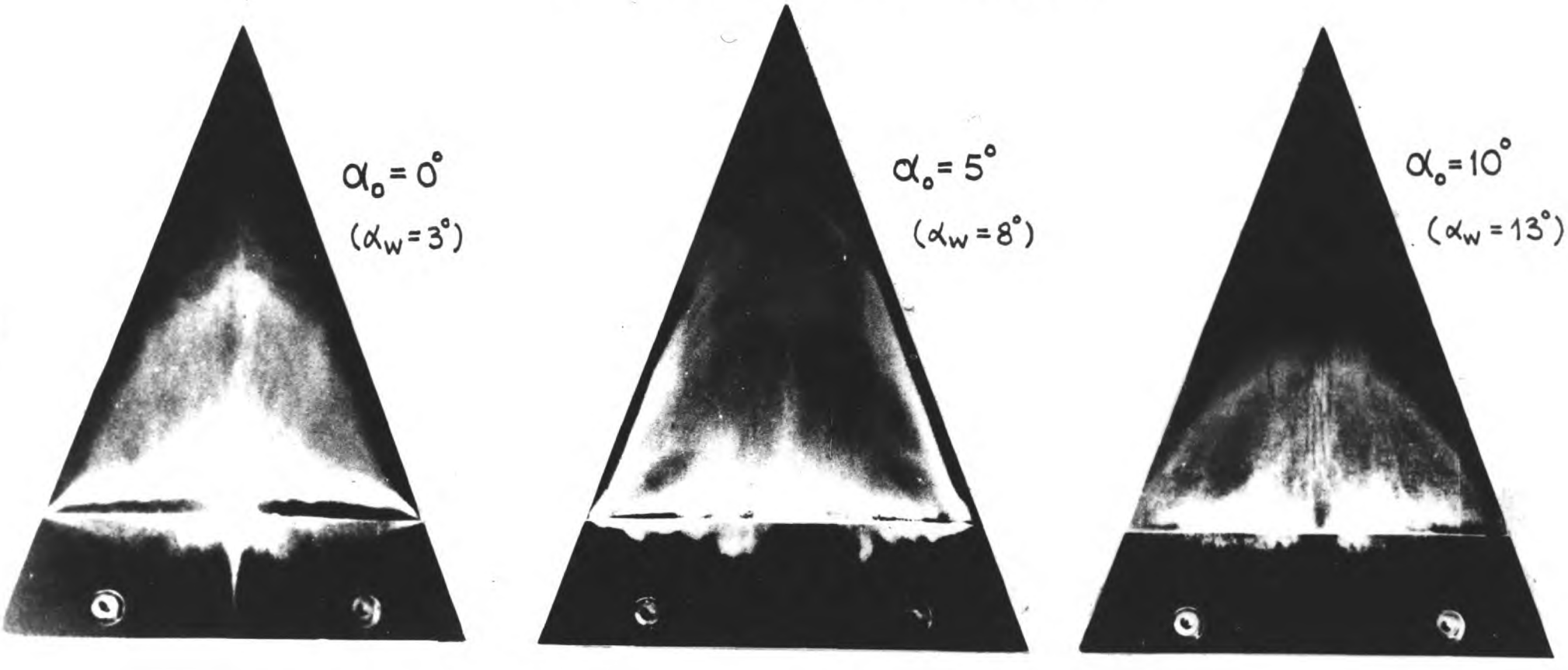
FIG. 35




INCIPIENT SEPARATION

FIG·36

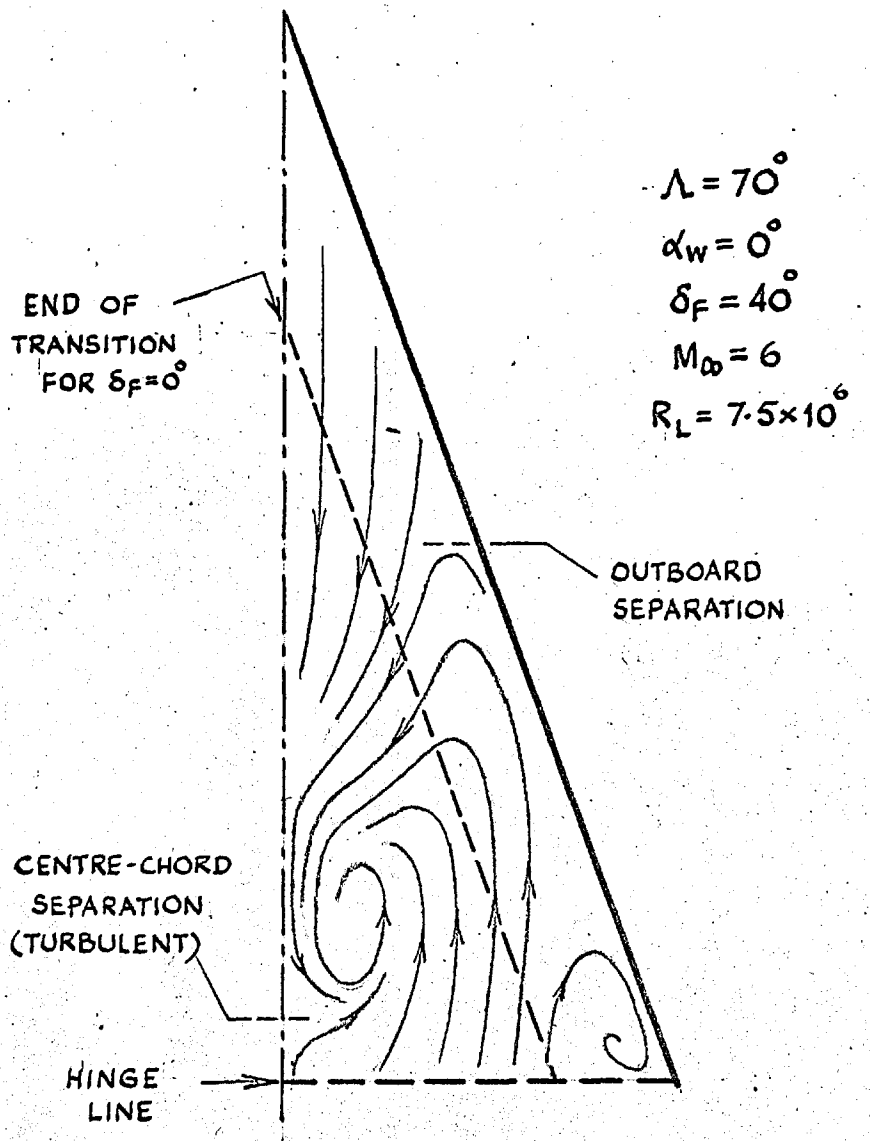
(WING L·E· SHOCK ATTACHED)




$\Lambda = 70°$

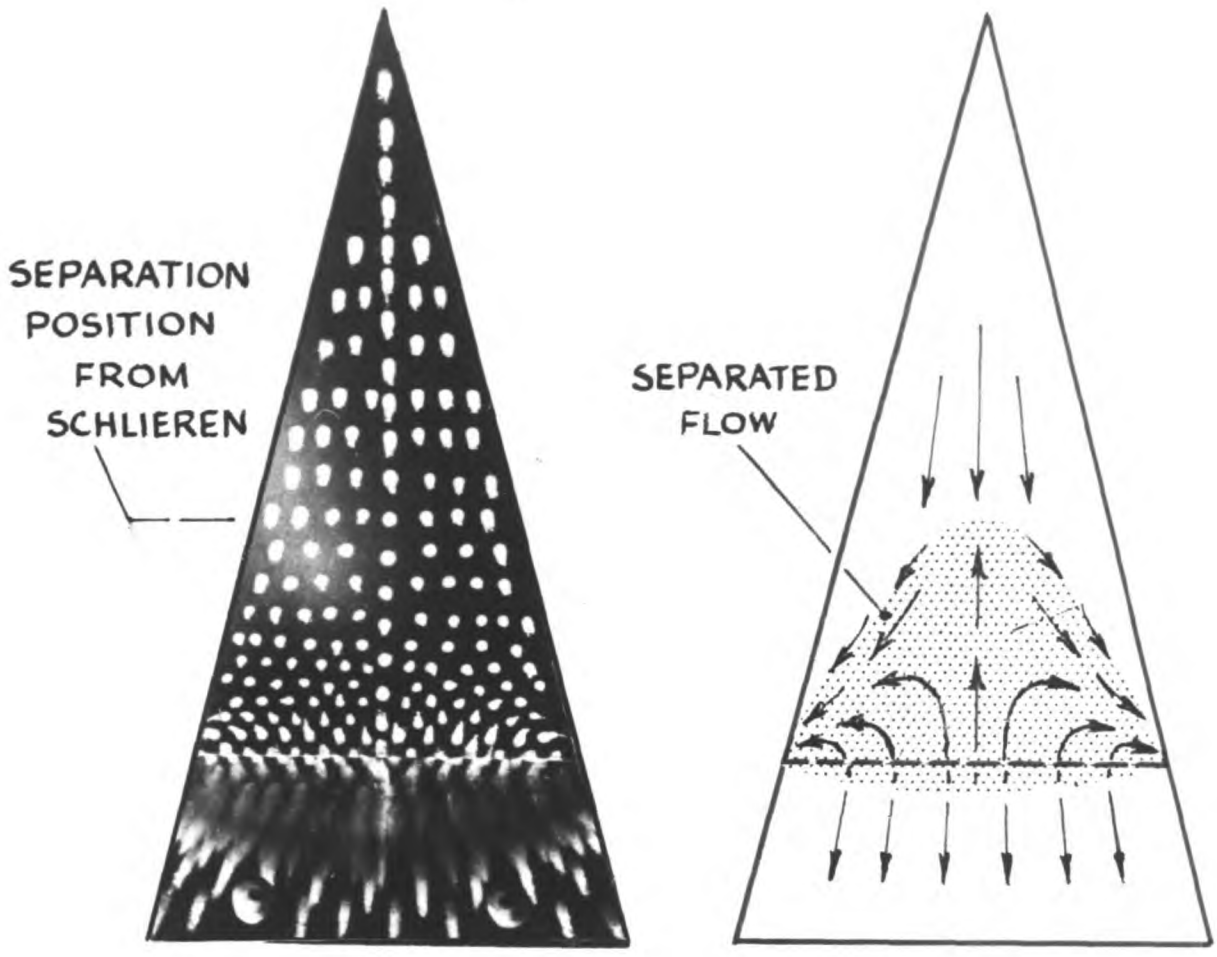
POWDER PATTERNS OF SEPARATED FLOW - EFFECT OF INCIDENCE FOR 20° FLAP

FIG. 37




SURFACE FLOW PATTERN WITH "MIXED" SEPARATION
(AFTER WHITEHEAD & KEYES)

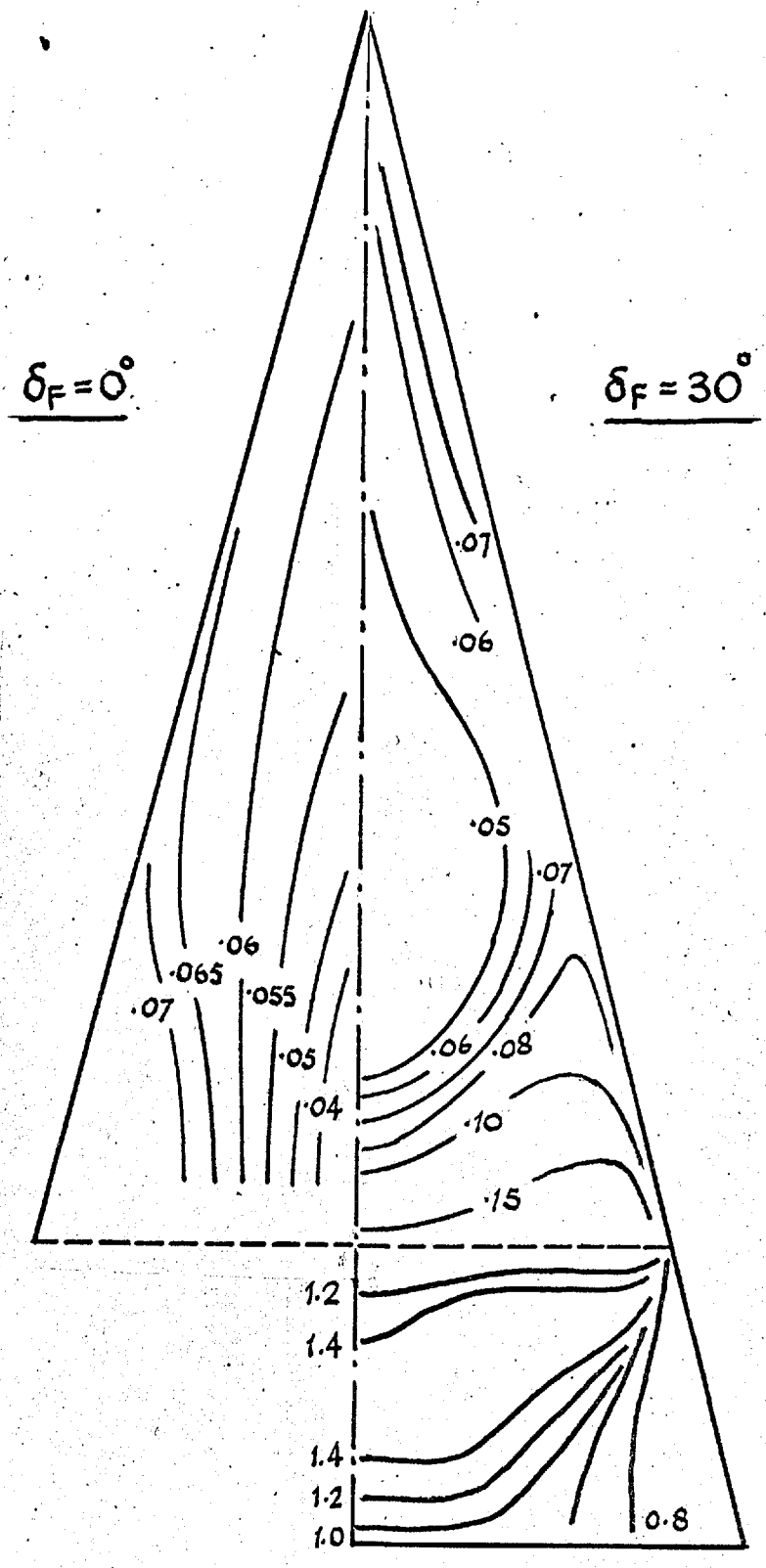
FIG. 38




$\Lambda = 76^\circ$, $\alpha_W = 23^\circ$, $\delta_F = 30^\circ$

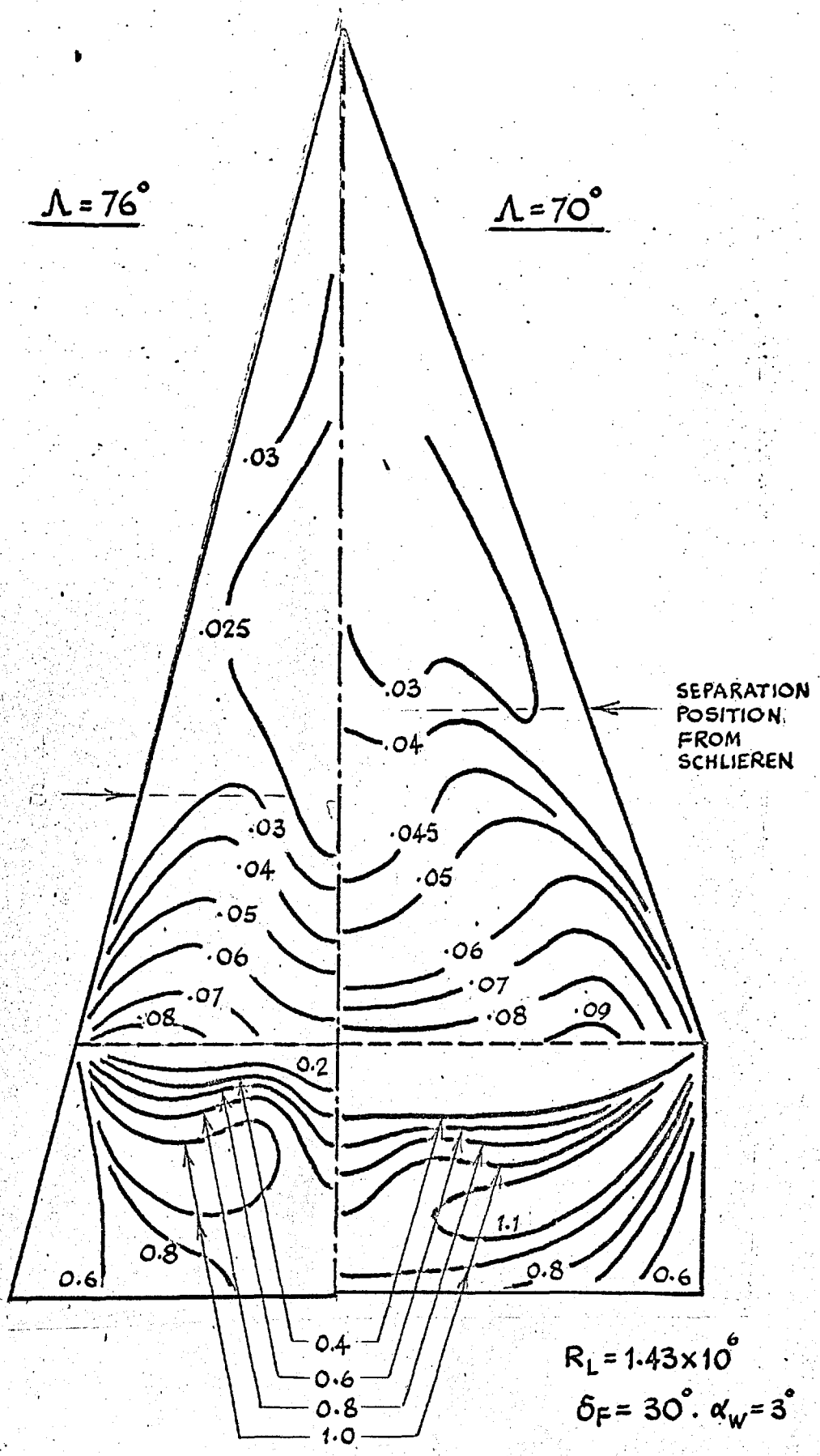
SEPARATION AT INCIDENCE

FIG. 39



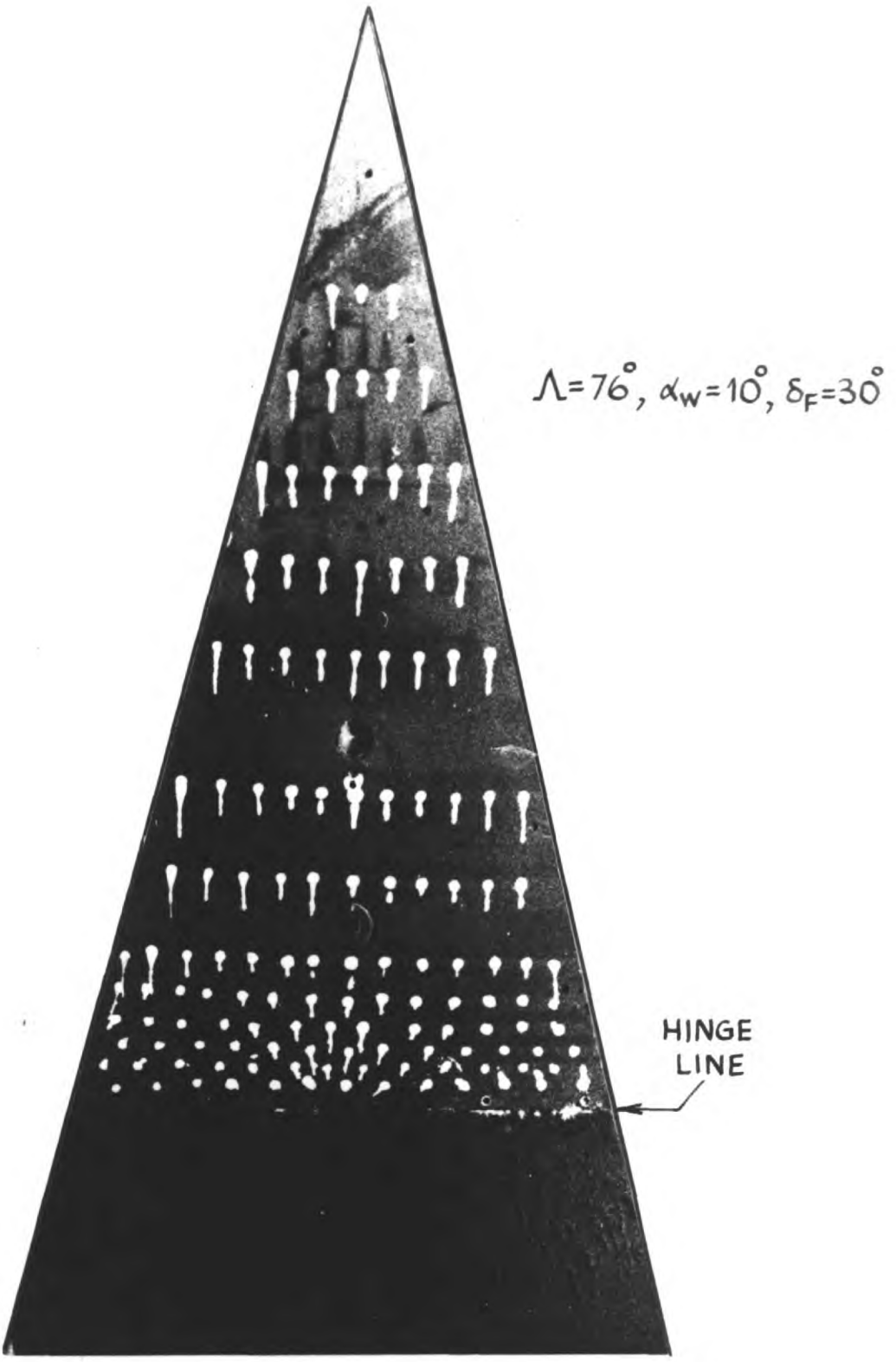

CONSTANT $C_p$ CONTOURS ON 76° DELTA WING WITH AND WITHOUT FLAP . $\alpha_W = 8°$

FIG. 40



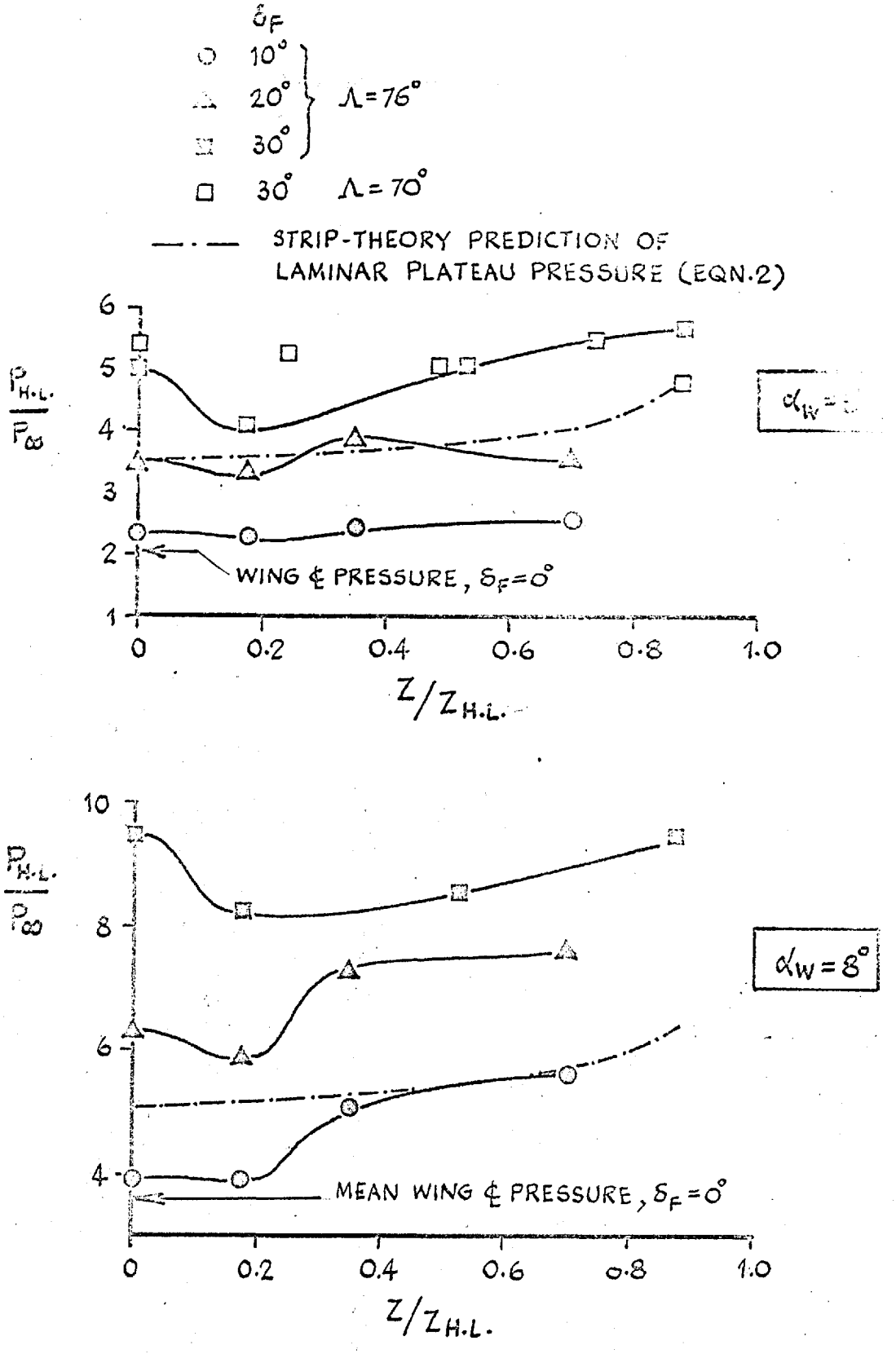

CONSTANT $C_p$ CONTOURS ON DELTA WINGS

FIG. 41



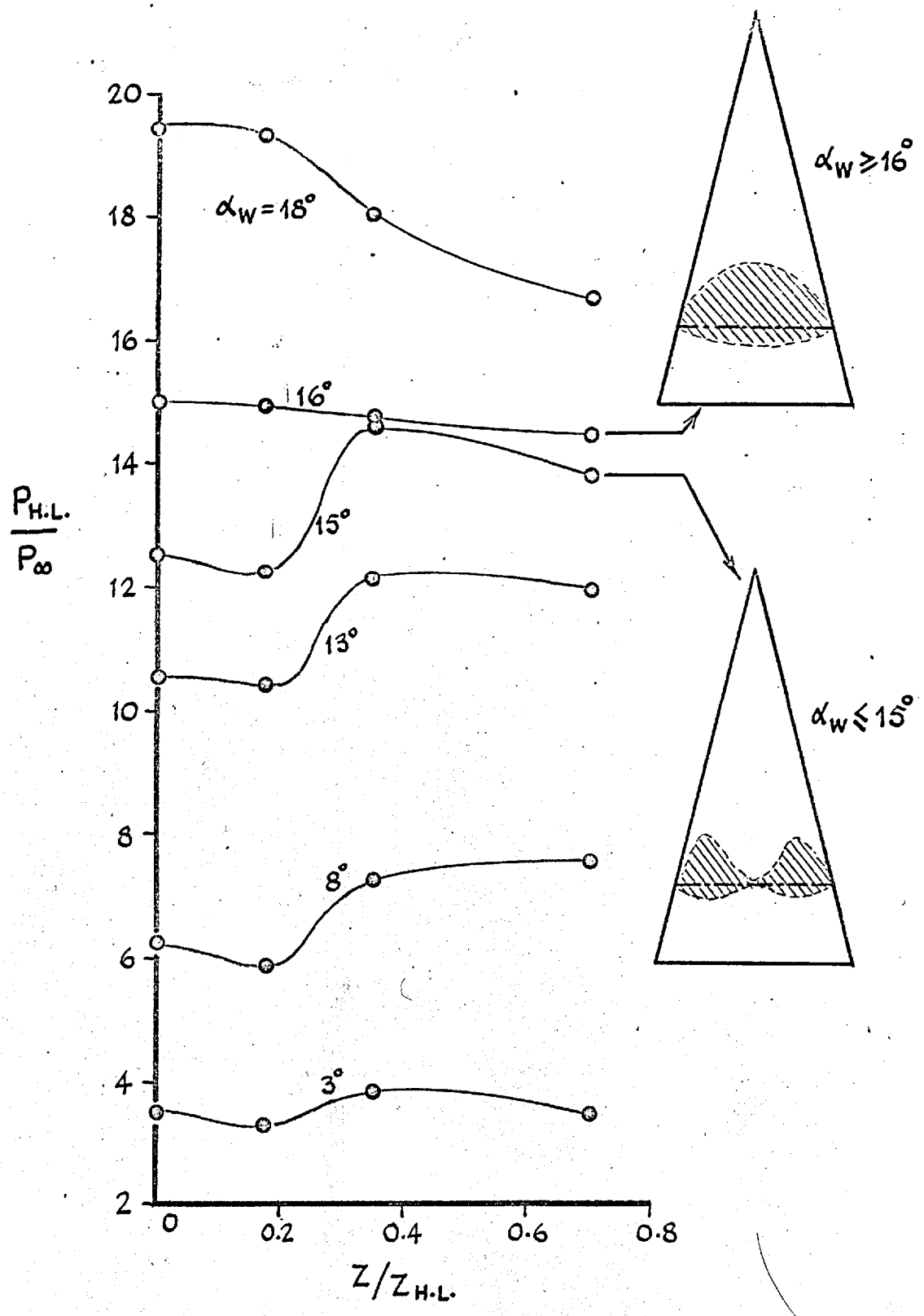

OIL-DOT VISUALISATION OF 'MIXED' SEPARATION

FIG. 42



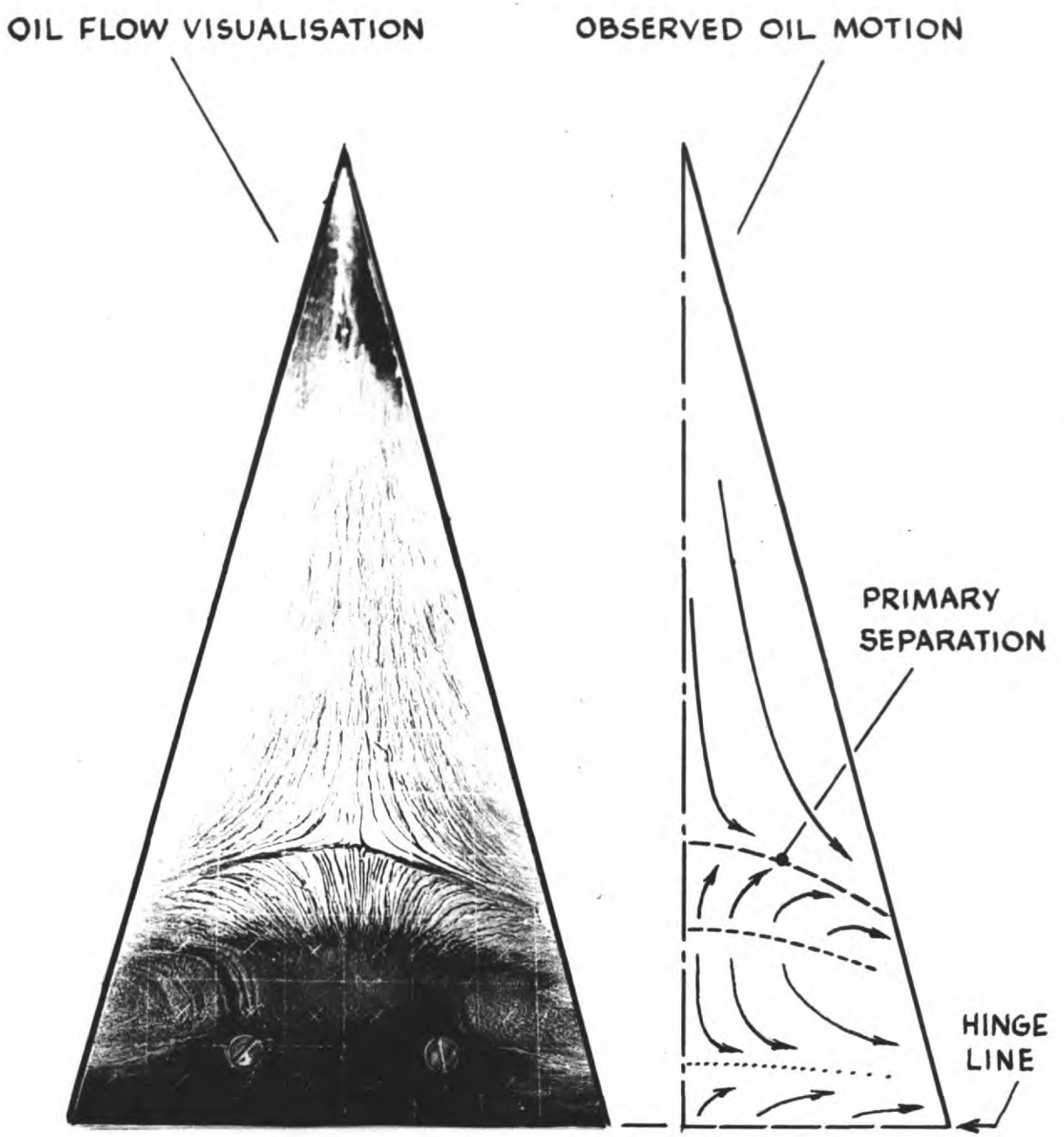

EFFECT OF FLAP DEFLECTION ANGLE ON HINGE-LINE PRESSURE DISTRIBUTION

FIG. 43




EFFECT OF INCIDENCE ON HINGE-LINE PRESSURE DISTRIBUTION . 76° DELTA . $\delta_F = 20°$

FIG. 44

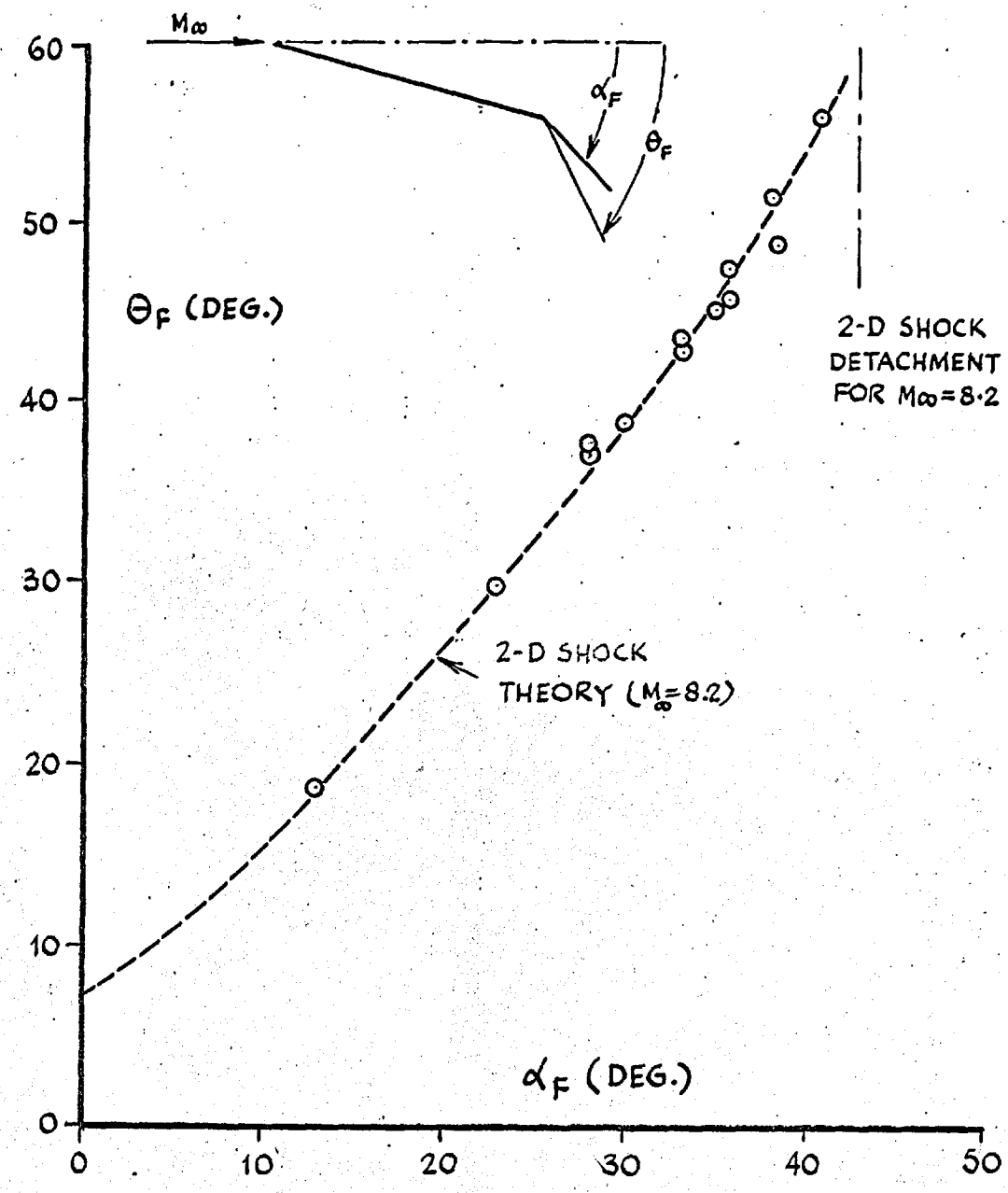



$\Lambda = 76^\circ$, $\delta_F = 40^\circ$

FLAP-INDUCED SEPARATION AT SUBSONIC SPEED

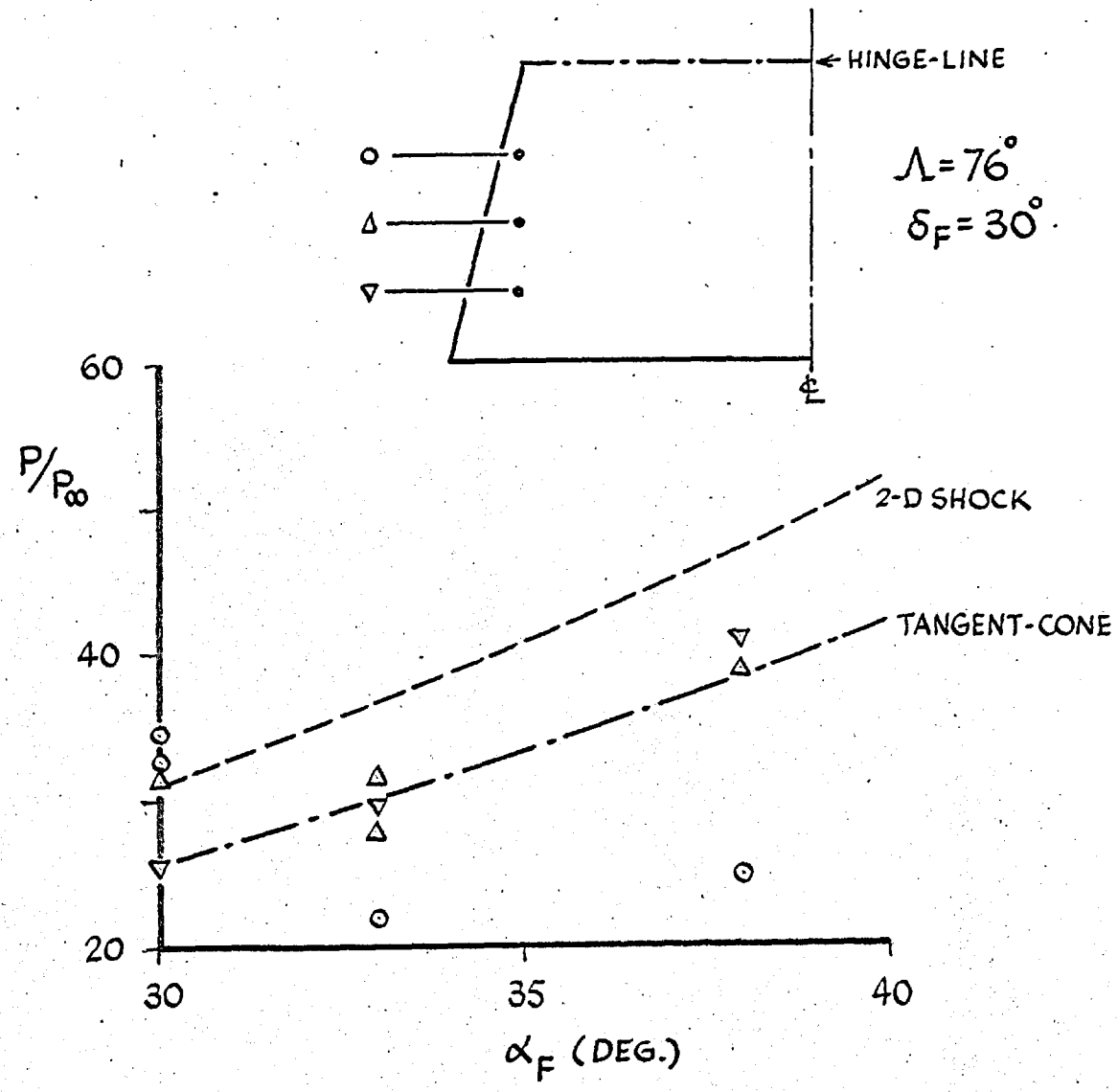
(LAMINAR FLOW. REYNOLD'S NO. $\sim 0.5 \times 10^6$)

FIG. 45



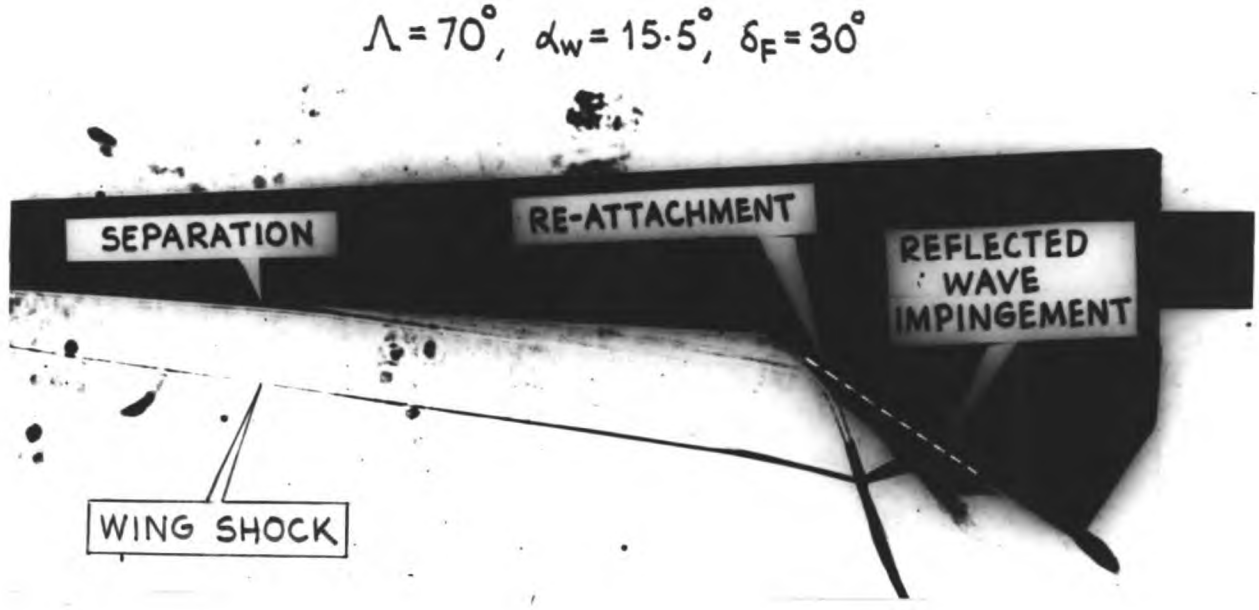

FLAP SHOCK ANGLE

FIG. 46

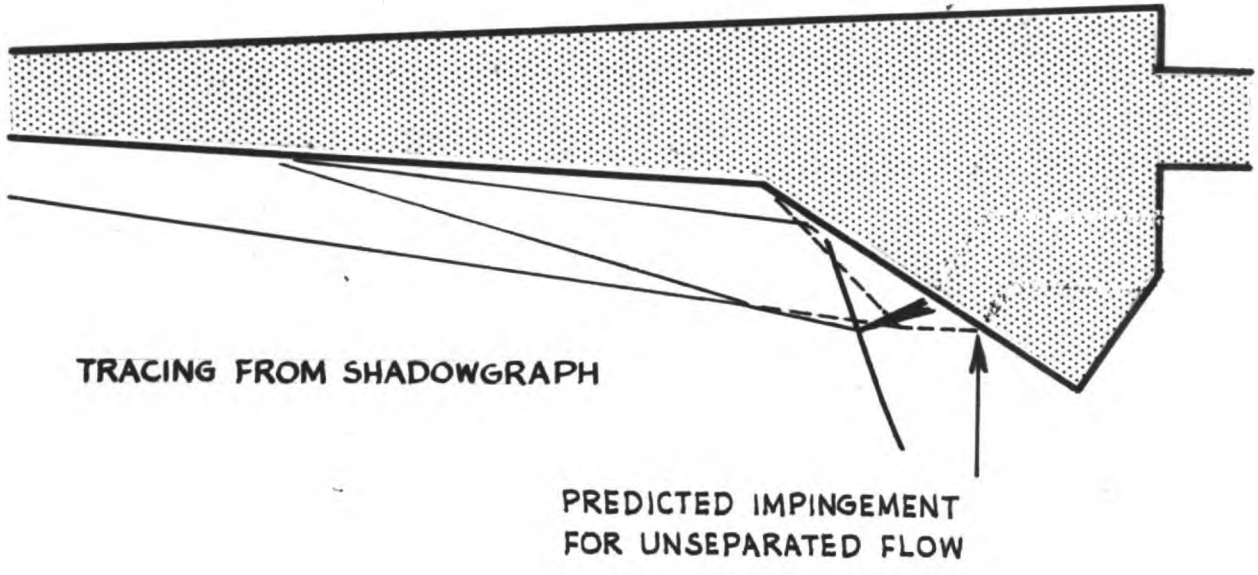



PRESSURES OVER FLAP TIP REGION

FIG. 47

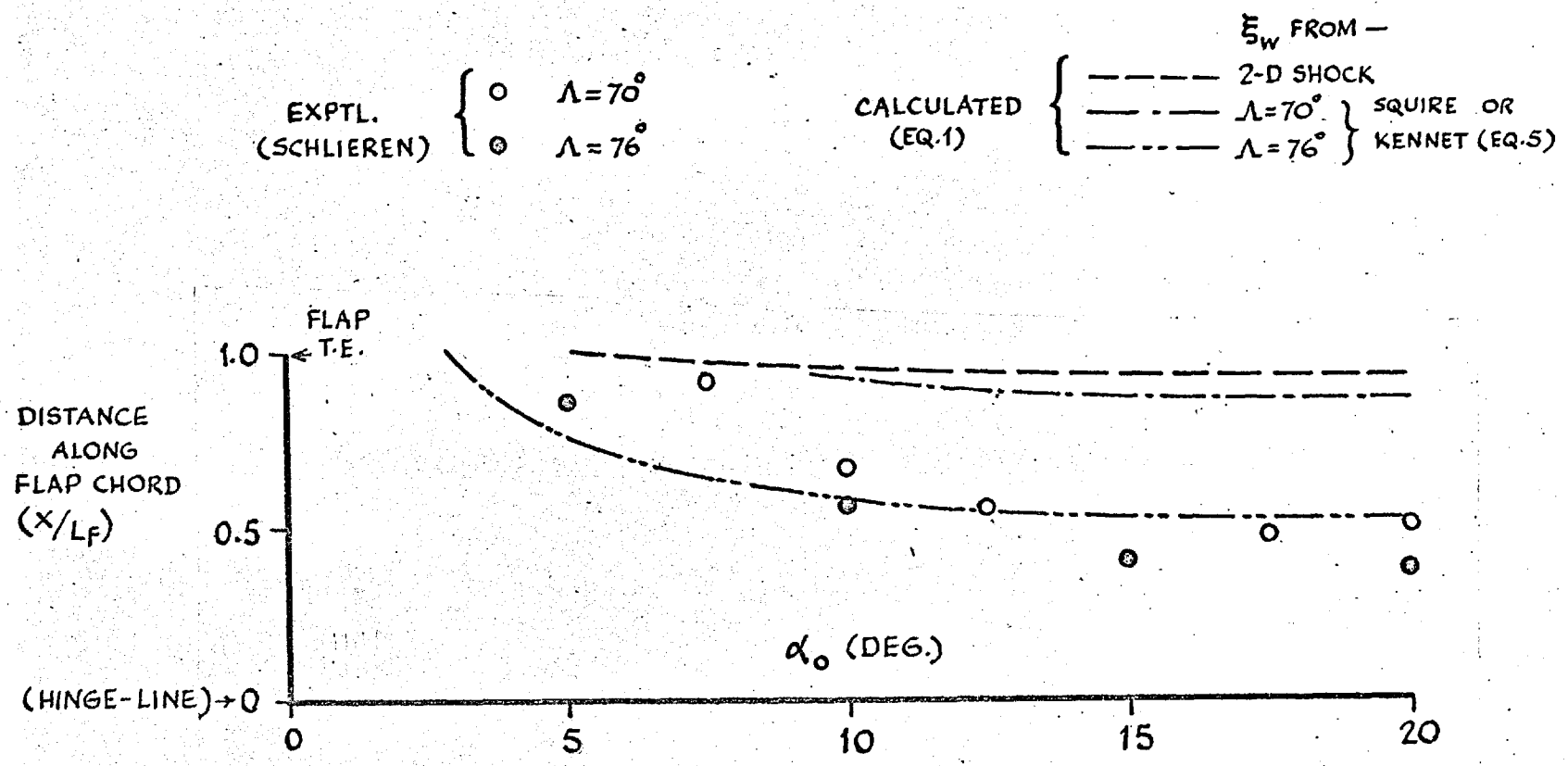



SHADOWGRAPH SHOWING WAVE INTERACTION



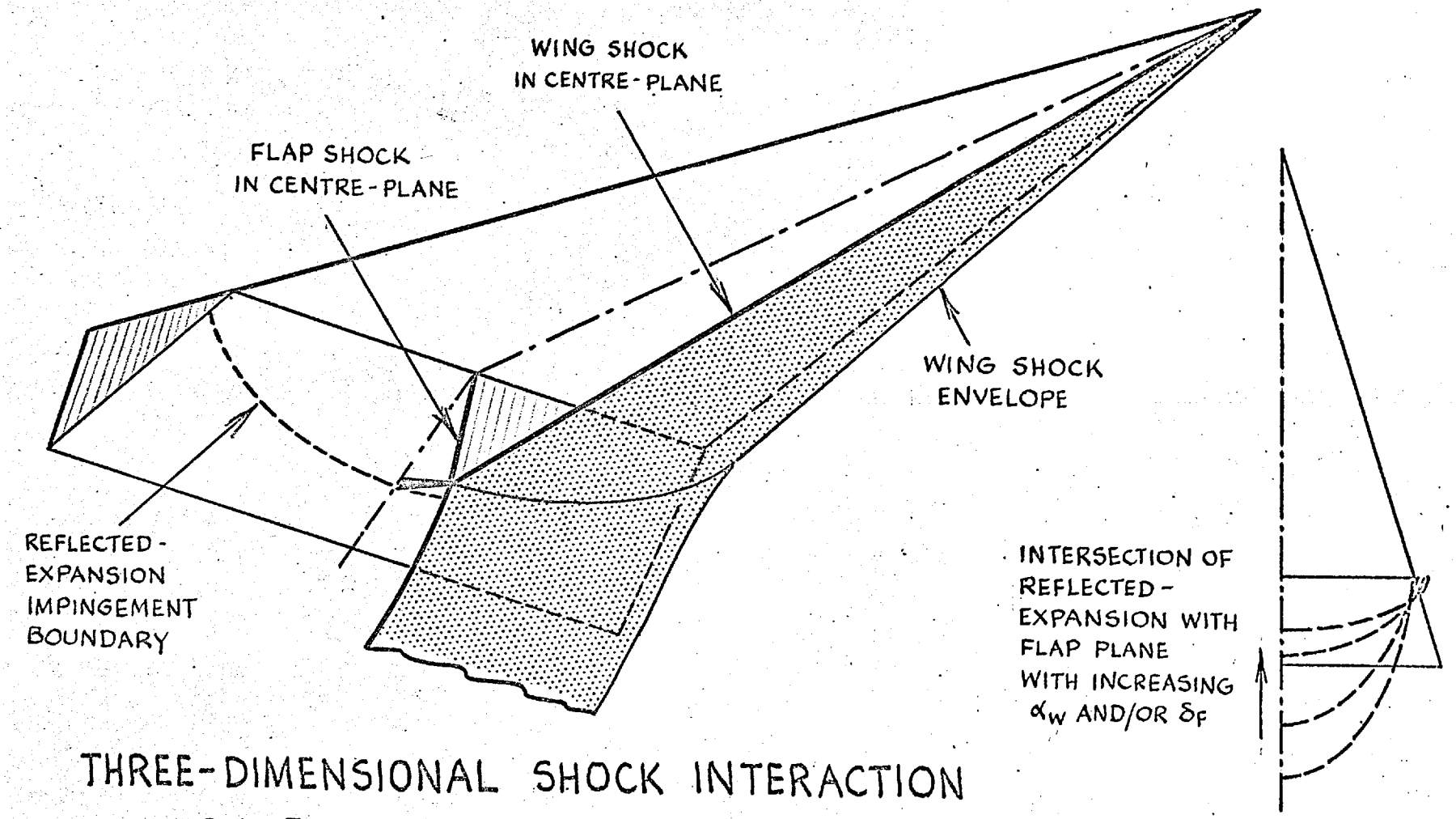

WING-SHOCK/FLAP-SHOCK INTERACTION

FIG. 48




CALCULATED AND EXPERIMENTAL IMPINGEMENT OF REFLECTED-EXPANSION ON FLAP CENTRE-LINE

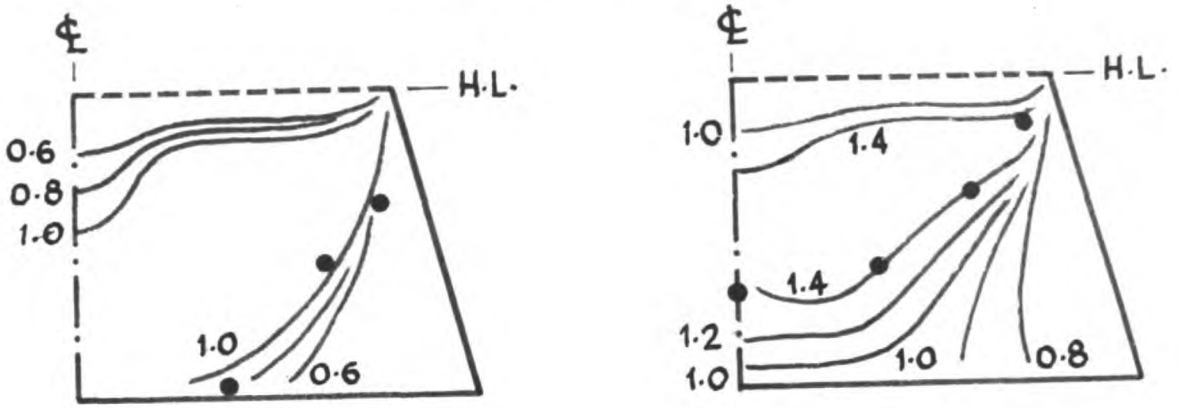
FIG. 49




THREE-DIMENSIONAL SHOCK INTERACTION
ON FLAPPED-DELTA WING

FIG. 50

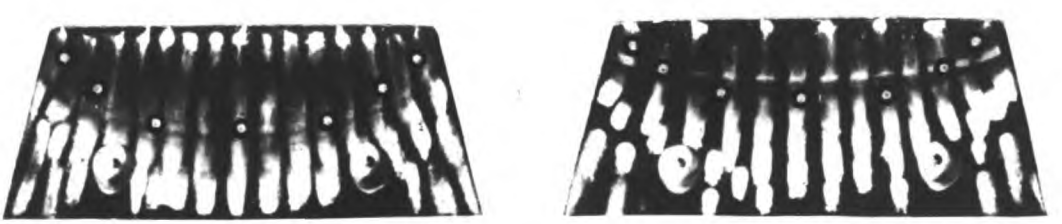
CONST. $C_p$ CONTOURS




$\alpha_w = 5°$ $\alpha_w = 8°$

$\Lambda = 76°, \delta_F = 30°$

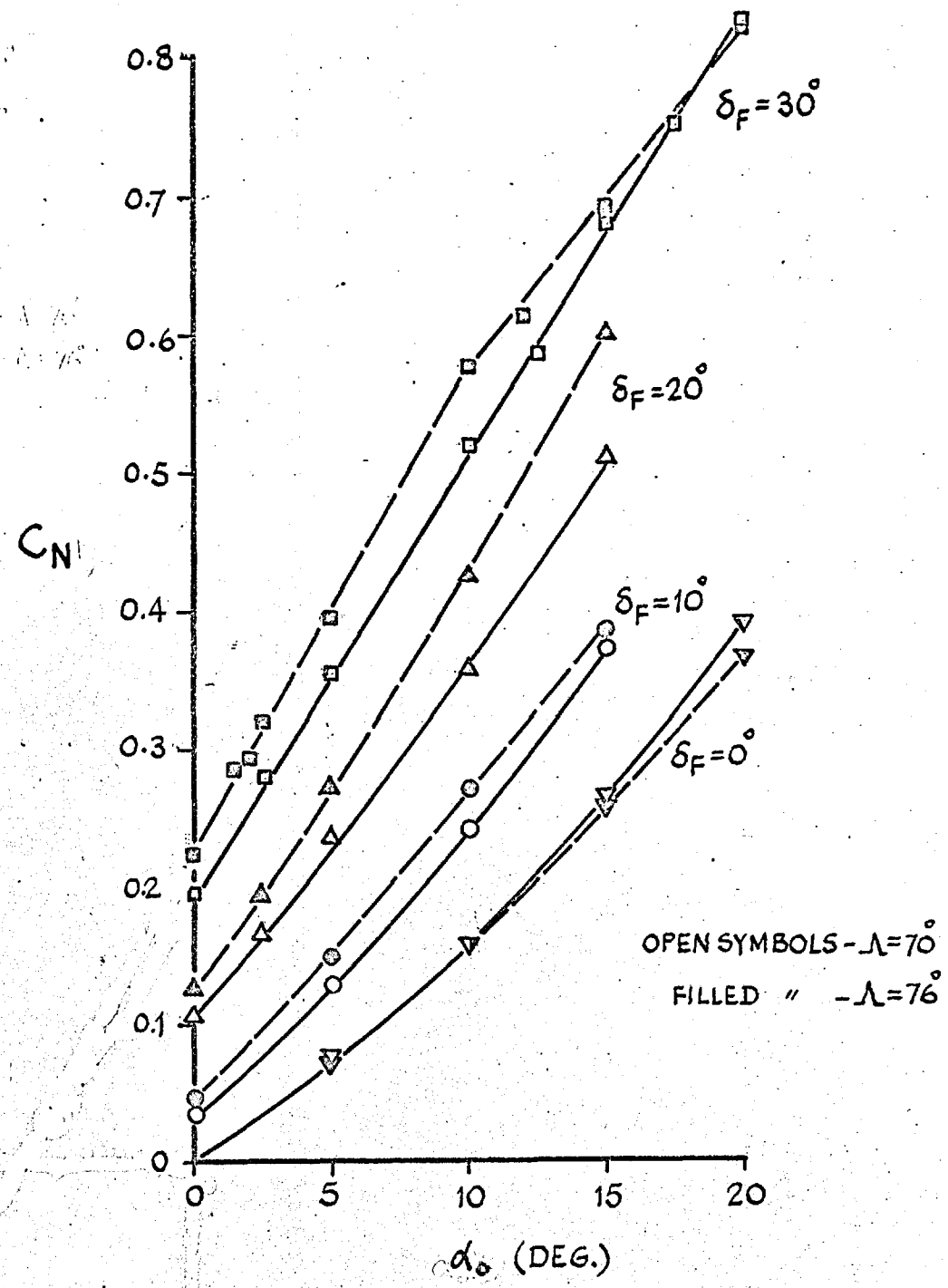
OIL-DOT VISUALISATION



$\alpha_w = 13°$ $\alpha_w = 18°$

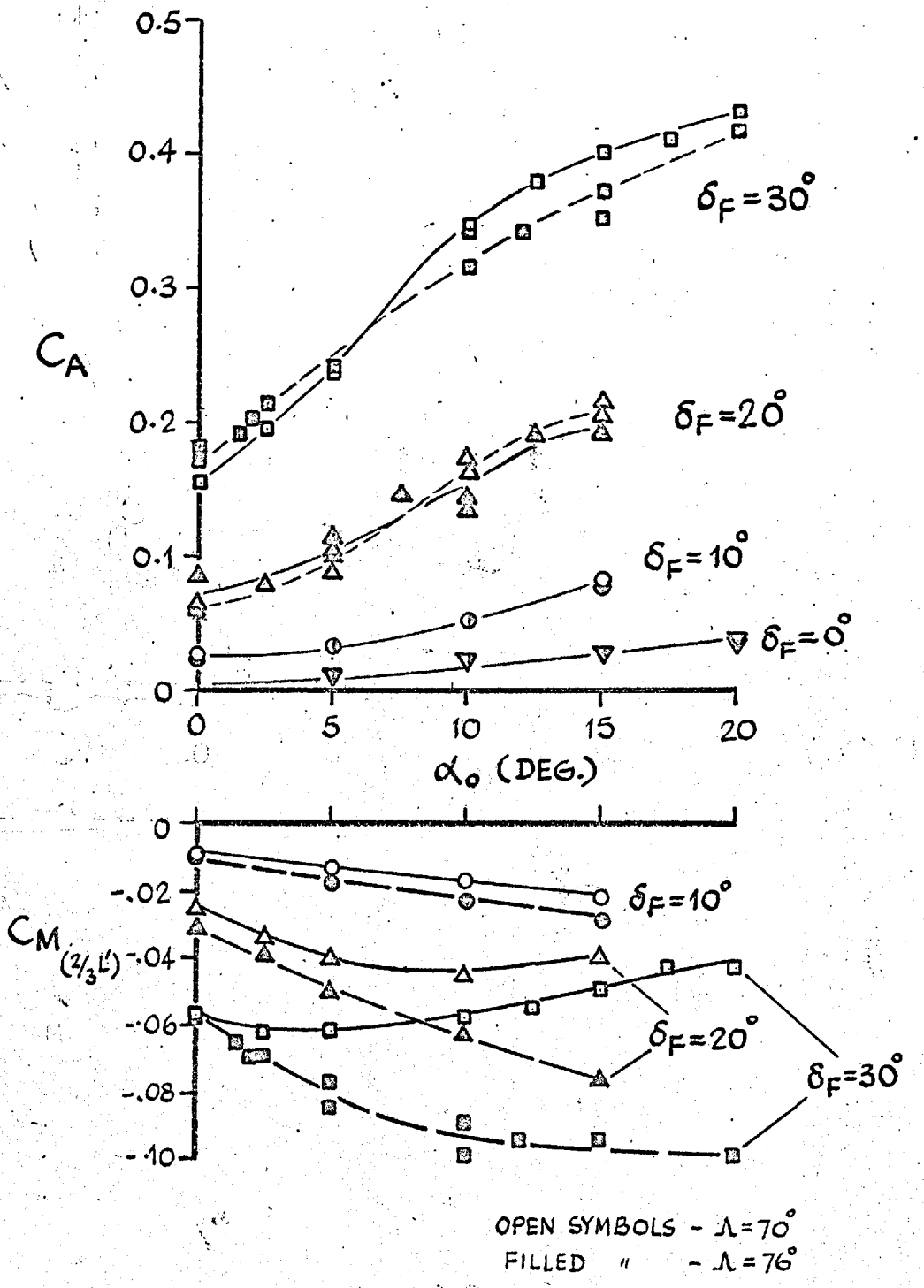
COMPARISON OF CALCULATED AND EXPERIMENTAL REFLECTED-EXPANSION IMPINGEMENT BOUNDARY

FIG. 51



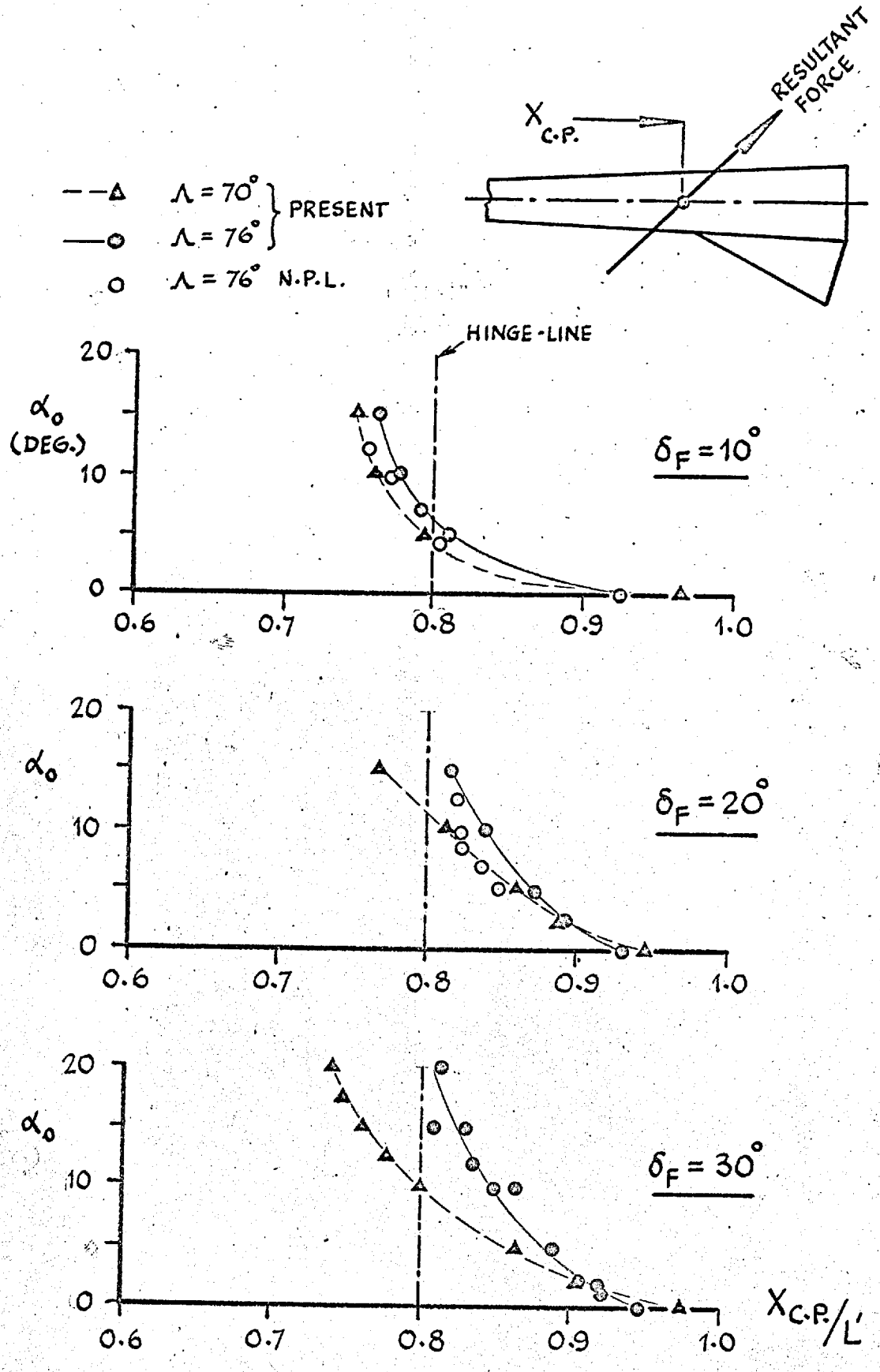

FLAPPED DELTA WINGS - NORMAL FORCE MEASUREMENTS

FIG. 52



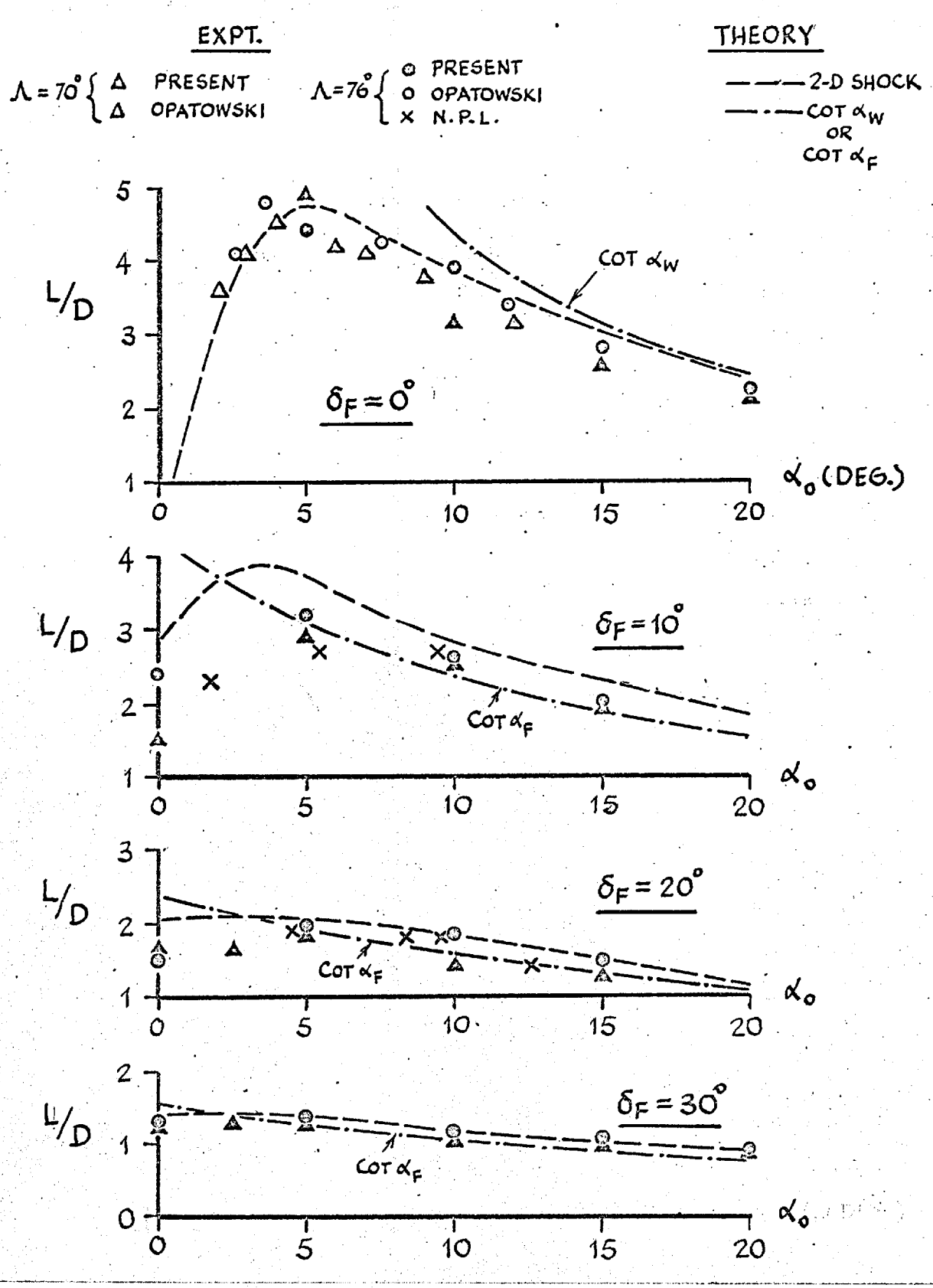

FLAPPED DELTA WINGS - AXIAL FORCE AND PITCHING-MOMENT MEASUREMENTS

FIG. 53



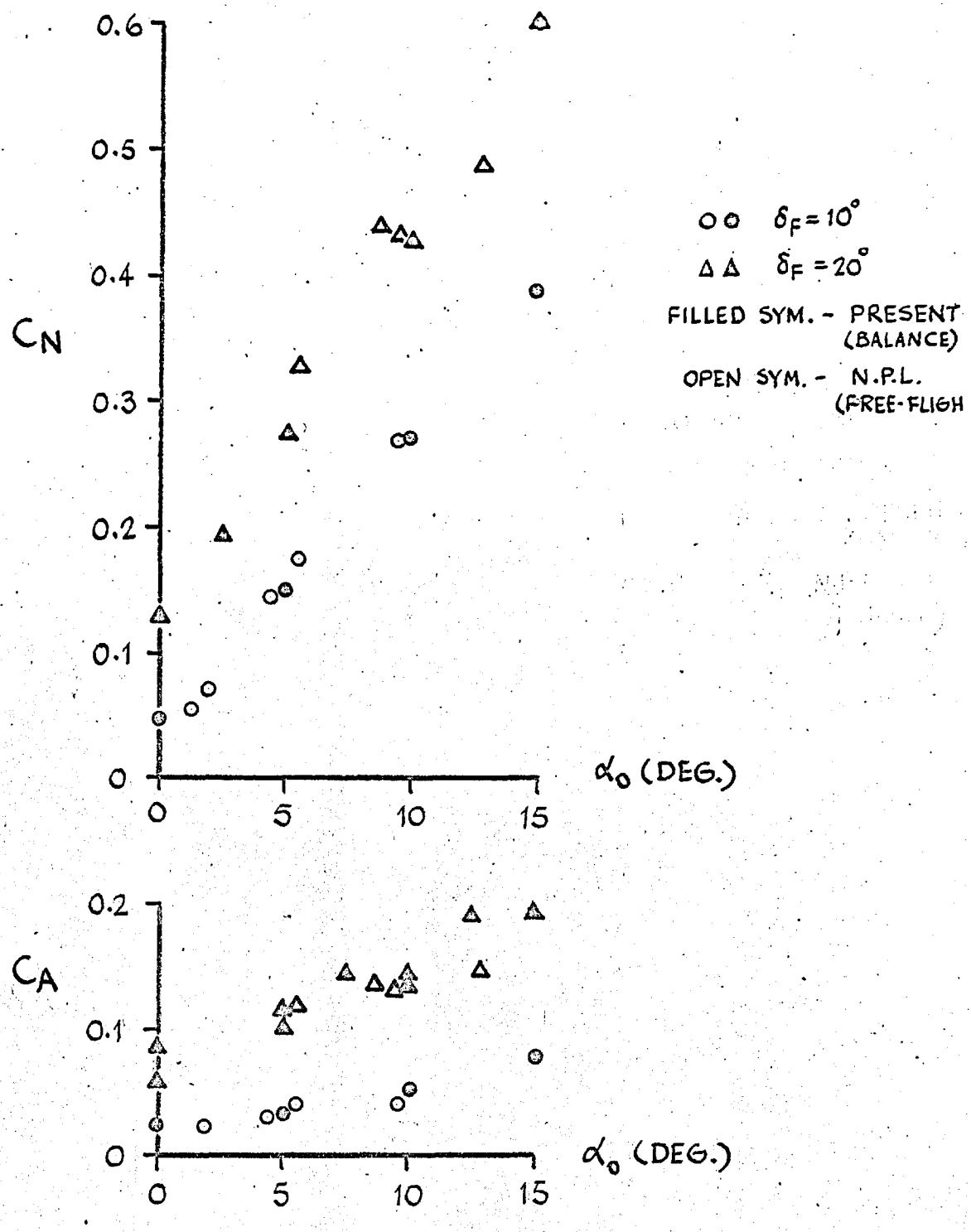

CENTRE OF PRESSURE POSITION

FIG. 54



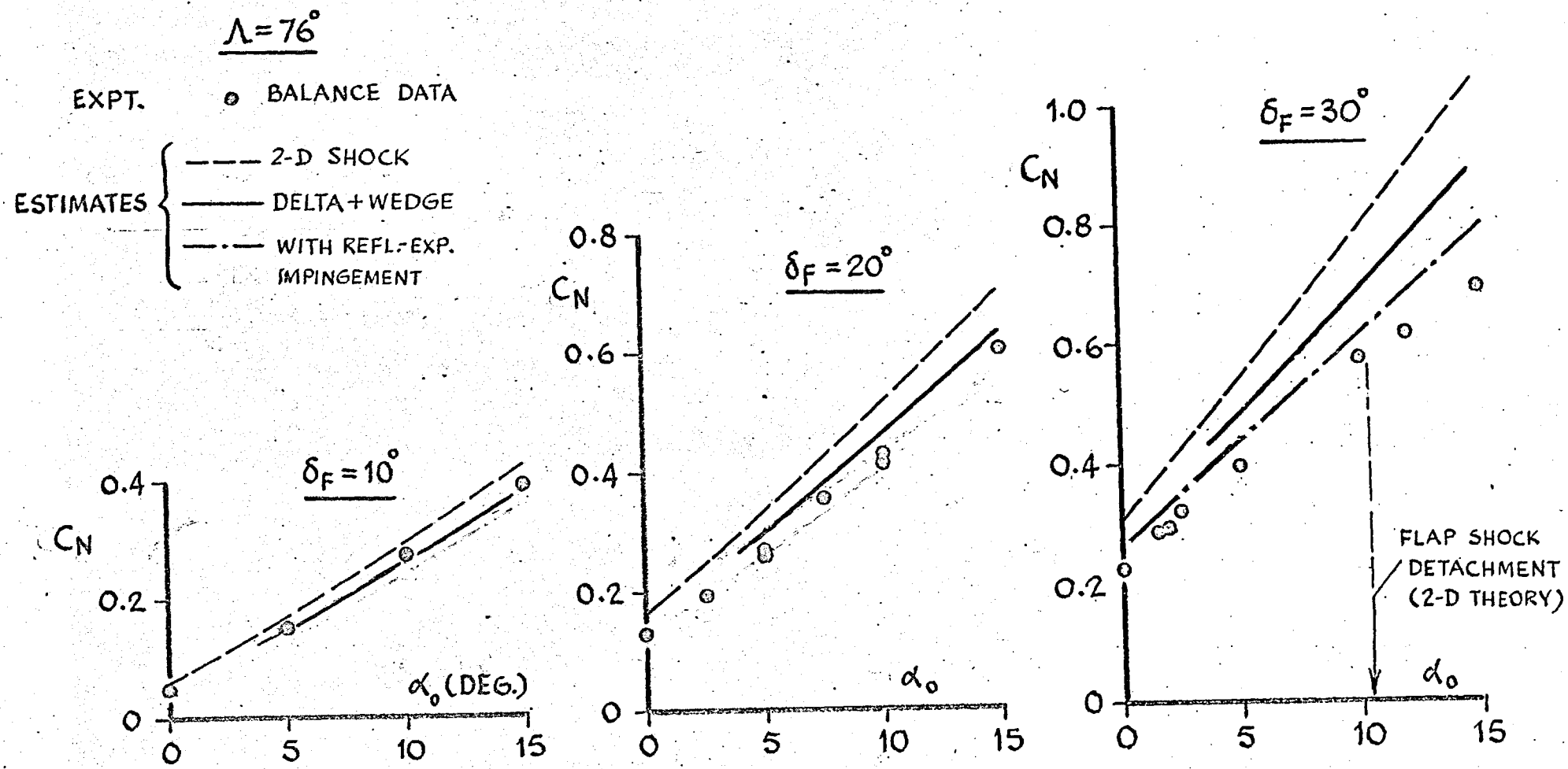

LIFT/DRAG RATIO OF DELTA WINGS WITH AND WITHOUT FLAPS

FIG. 55



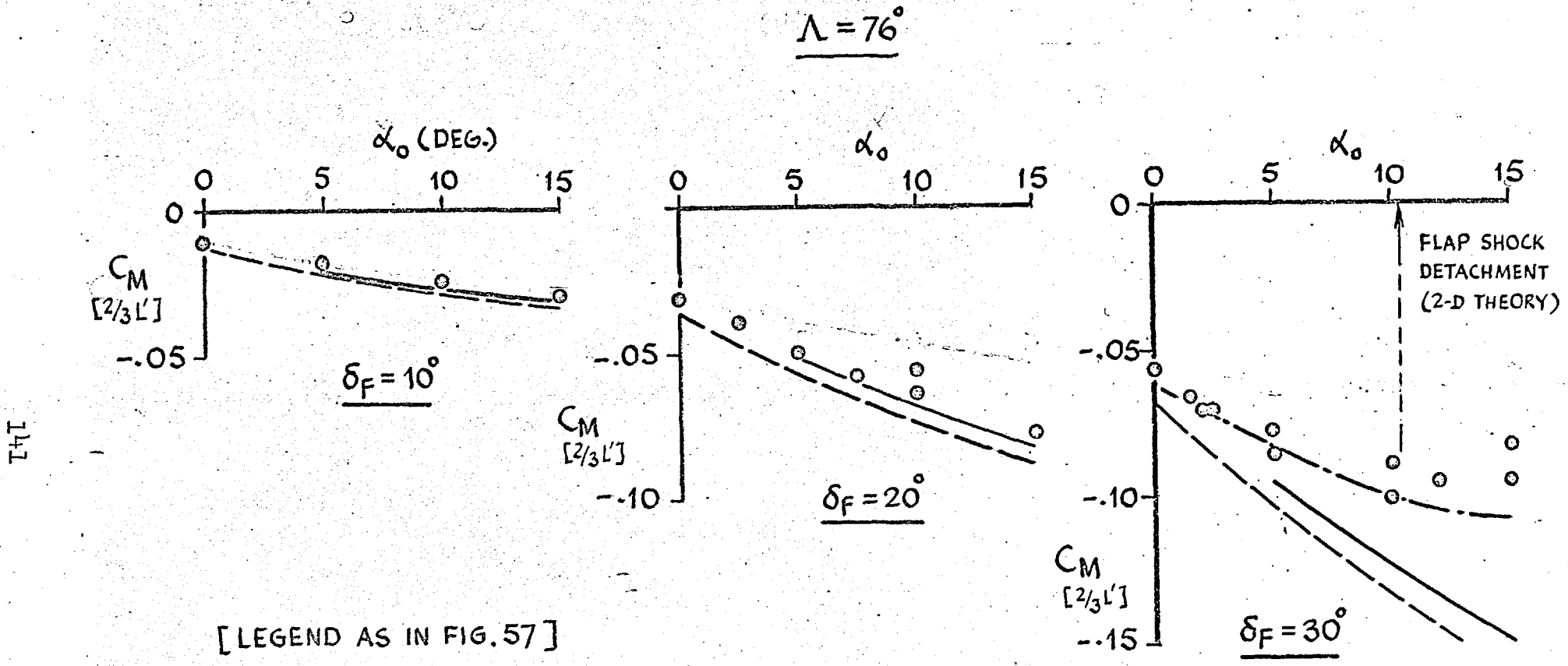

COMPARISON OF BALANCE AND FREE-FLIGHT TUNNEL (N·P·L·) DATA FOR 76° FLAPPED DELTA

FIG. 56




NORMAL FORCE COMPARISON WITH ESTIMATES

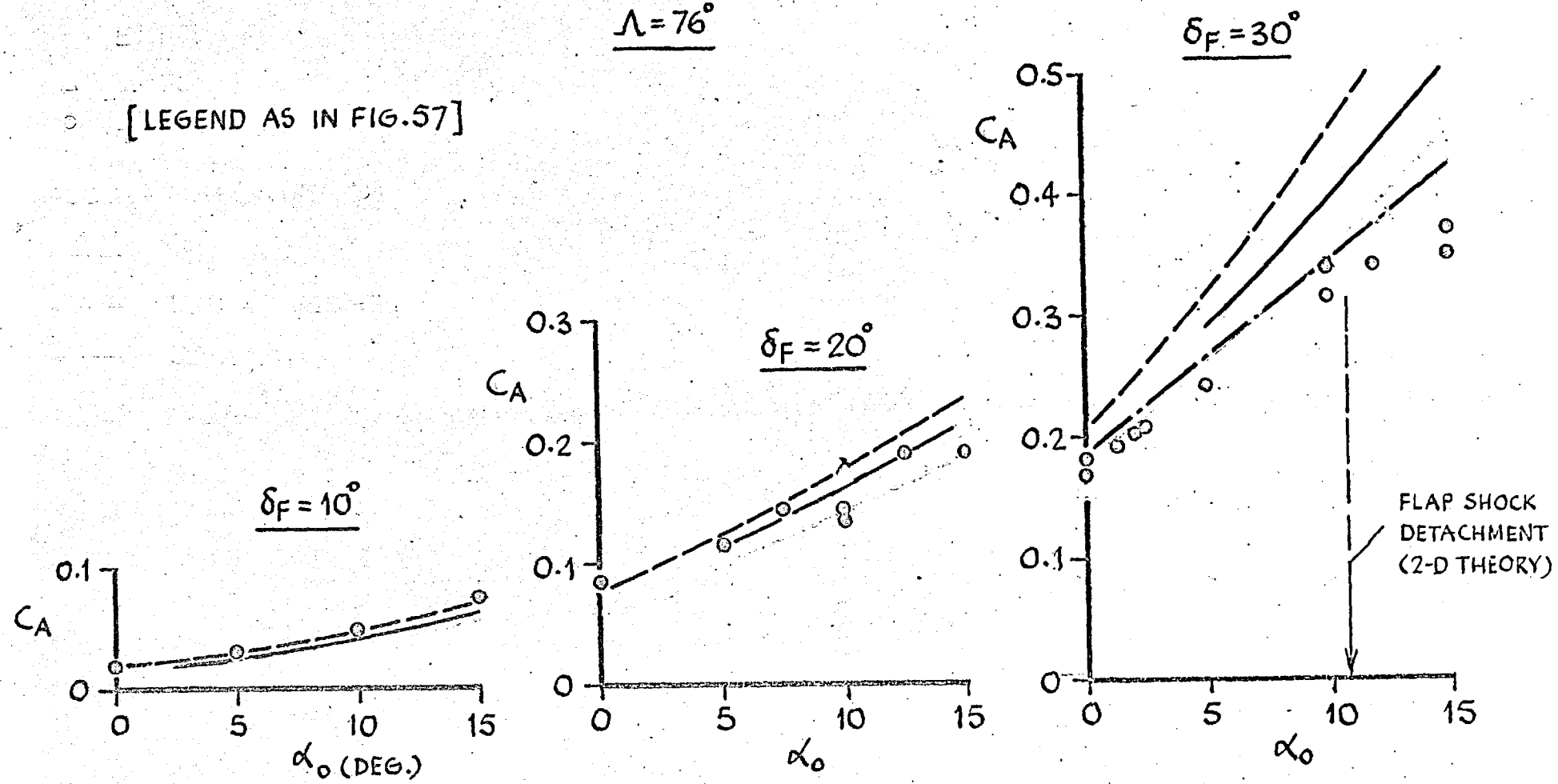
FIG. 57




[LEGEND AS IN FIG. 57]

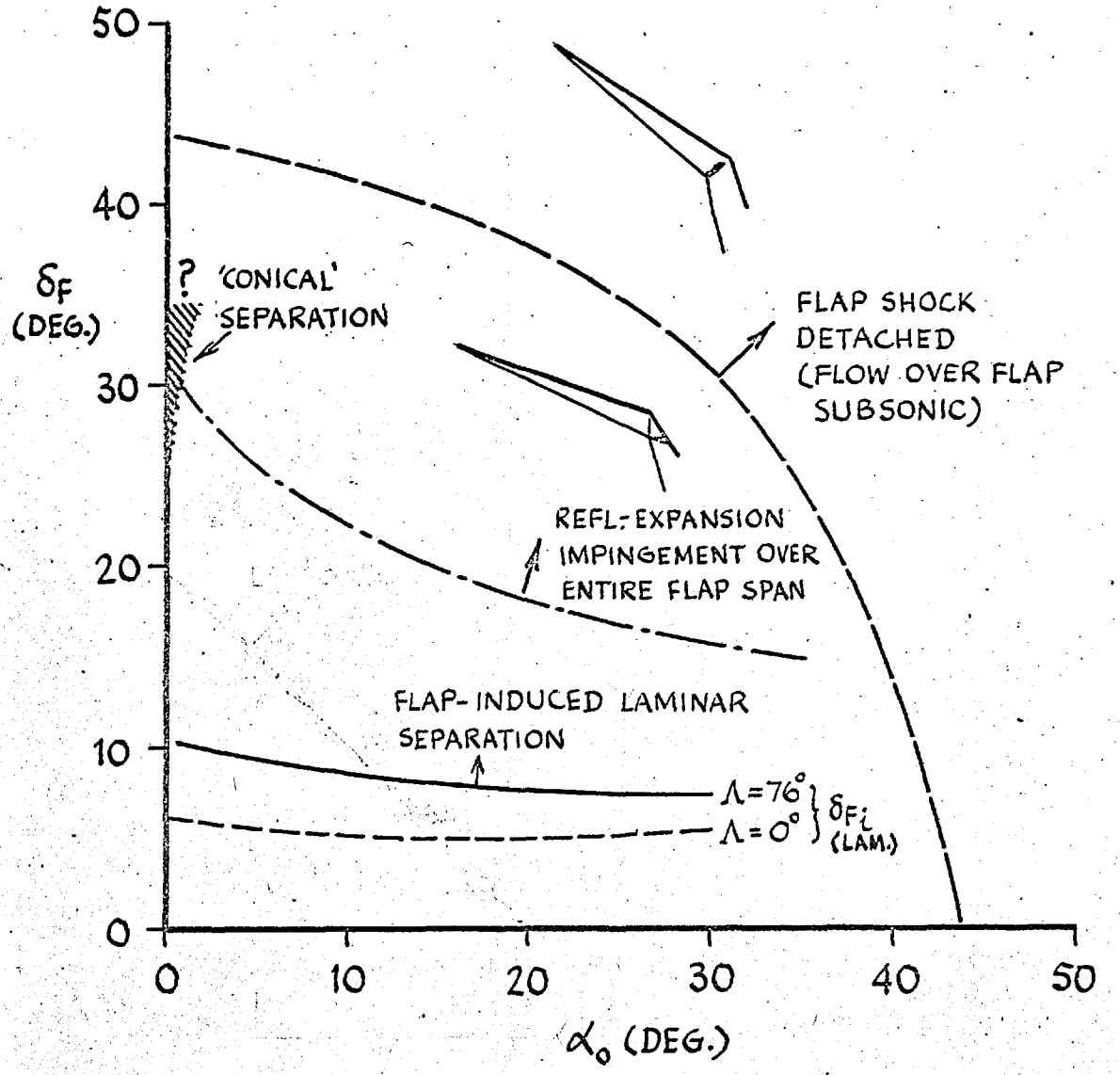
PITCHING-MOMENT COMPARISON WITH ESTIMATES

FIG. 58




AXIAL FORCE COMPARISON WITH ESTIMATES

FIG. 59




FLOW REGIMES ON 76° FLAPPED DELTA

[ $M_\infty = 8.2$ . $R_L = 0.7 \times 10^6$ ]

FIG. 60